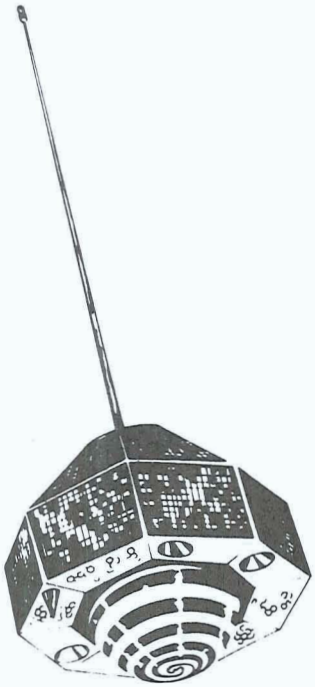

NOVEMBER 1970

PROCEEDINGS OF THE GEOS-2 PROGRAM REVIEW MEETING 22-24 JUNE 1970

VOLUME II

TRACKING SYSTEM INTERCOMPARISONS WITH GEOS-2

EDITED BY:

CSC

COMPUTER SCIENCES CORPORATION

6565 ARLINGTON BOULEVARD POST OFFICE BOX 810 FALLS CHURCH VA 22046

NATIONAL AERONAUTICS AND SPACE ADMINISTRATION

NASA

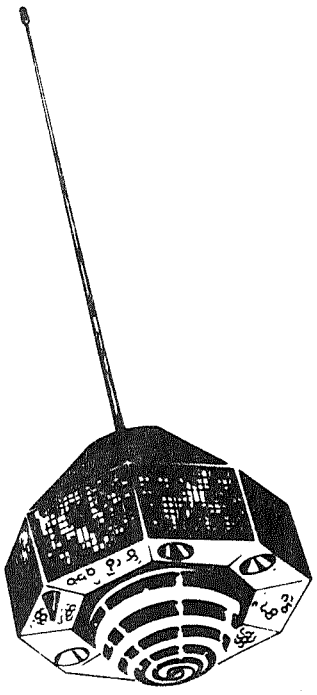

NOVEMBER 1970

PROCEEDINGS OF THE GEOS-2 PROGRAM REVIEW MEETING 22-24 JUNE 1970

VOLUME II

TRACKING SYSTEM INTERCOMPARISONS WITH GEOS-2

EDITED BY:

CSC

COMPUTER SCIENCES CORPORATION

(703) 533-8877

6565 ARLINGTON BOULEVARD POST OFFICE BOX 530 FALLS CHURCH VA 22046

NATIONAL AERONAUTICS AND SPACE ADMINISTRATION

NASA

PROCEEDINGS OF THE GEOS-2 PROGRAM REVIEW MEETING

22-24 June 1970
NASA Goddard Space Flight Center
Greenbelt, Maryland

Volume II

Tracking System Intercomparisons with GEOS-2

Edited by Computer Sciences Corporation
6565 Arlington Boulevard, Falls Church, Virginia

November 1970

TABLE OF CONTENTS

TABLE OF CONTENTS

FOREWORD

This volume (Volume II) of the proceedings of the GEOS-2 Program Review Meeting held at NASA Goddard Space Flight Center on 22-24 June 1970 presents the results to date of the Goddard Space Flight Center tracking intercomparison tests conducted with GEOS-2. The volume is composed of a series of technical papers prepared by various investigators on the tracking intercomparisons conducted using the optical and electronic subsystems on the GEOS-2 spacecraft.

John Berbert
GSFC
Principal Investigator

COMPARISON OF C-BAND, SECOR, AND TRANET WITH A COLLOCATED LASER ON 35 TRACKS OF GEOS-2

Prepared for the GEOS-2

REVIEW CONFERENCE

June 22 - 24, 1970

By

H. Parker
D. Carney
J. Berbert

COMPARISON OF C-BAND, SECOR, AND TRANET WITH A COLLOCATED LASER ON 35 TRACKS OF GEOS-2

H. Parker, D. Carney, J. Berbert

As part of the GEOS Observation Systems Intercomparison Investigation at Goddard, several of the geodetic satellite tracking systems used with GEOS-2, including the GSFC experimental Laser (GODLAS), an Army SECOR, and a Navy TRANET, were moved to the NASA Wallops Island station and located near the FPQ-6 and FPS-16 C-band radars there. Simultaneous tracking of GEOS-2 by all these systems was accomplished during April, May, and June 1968, to enable comparisons of the tracking data freed from the effects of uncertainties in survey, in the gravity field, and in systems time synchronization. Reference orbits were determined from the Laser data. Comparison of tracking data from the radio tracking systems with the 35 Laser reference orbits yielded residuals from which zero-set and timing biases were derived for each system. Preliminary results for the first 10 passes of simultaneous tracking of GEOS-2 were documented in X-514-68-458, "Comparison of C-Band, SECOR, and TRANET with a Collocated Laser on 10 tracks of GEOS-2", dated November 1968. These results were presented to the GEOS-2 C-Band Project Technical Conference at WTR in November 1968 and to the National Fall Meeting of the AGU in December 1968.

Attempts to account for the various system anomalies reported in X-514-68-458 led to the following changes to the data sets.

- The CDC-3200 Computer C-Band Preprocessing program was rewritten for the IBM 360 computer and expanded to include the computation of the calibration constants.
- All the SECOR data were corrected by the Army Map Service for a scale factor error.
- All the TRANET data were corrected by the Naval Weapons Laboratory for a Base Frequency Computation error.

The effects of these changes to the data were analyzed for the same 10 GEOS-2 passes and reported to the National Spring Meeting of the AGU in April 1969. Subsequently, all 35 coincident Laser and radio tracking system passes were analyzed with the data modifications included, and the results are the topic of this report.

The 35 Laser reference orbits were computed in the NONAME program using a priori measurement sigmas for relative data weighting of 2 meters for range and 200 arc seconds for both azimuth and elevation. The NONAME program was developed for Goddard orbital studies and operates on the IBM 360 computer. Laser tracking data are summarized in Table 1, which gives the date, the coincident data, the time span and number of Laser range measurements, and the values of range and elevation at the start, end, and at the point of closest approach (PCA) for each of the 35 passes.

The NONAME zero-set and timing bias recovery runs used tightly constrained orbital elements as determined by the Laser and assumed the a priori estimates of measurement and bias sigmas shown below. The a priori estimates of measurement sigmas were chosen to approximate the a posteriori estimates resulting from the previous 10 pass studies. The a priori bias estimates were intentionally left unconstrained, except for the TRANET time bias, which was constrained due to the high correlation between the TRANET time and zero-set biases for these relatively short passes.

MEASUREMENTS

FPQ-6 RANGE	1.0 METER
FPQ-6 AZIMUTH	30 ARC SECONDS
FPQ-6 ELEVATION	12 ARC SECONDS
FPS-16 RANGE	1.5 METERS
FPS-16 AZIMUTH	50 ARC SECONDS
FPS-16 ELEVATION	20 ARC SECONDS
SECOR RANGE	2.0 METERS
TRANET RANGE RATE	4 CM/SEC

BIAS

RANGE	1000 METERS
ANGLE	1000 ARC SECONDS
RANGE RATE	1000 CM/SEC
TRANET TIME	0.2 MILLISECOND
TIME	1 SECOND

The results of the system intercomparisons, with anomalous data removed, are summarized in Table 2, which gives the sample size (number of coincident passes), and the average RMS noise, zero-set and timing biases as well as the total RMS of the residuals about the Laser orbits for each of the radio tracking systems.

The time history of the derived zero-set biases over the duration of the experiment is given in Figure 1 for the range biases of each of the ranging systems and in Figure 2 for the TRANET range rate biases.

The AN/FPQ-6 radar is a centroid tracker, and any difference in the pulsewidth used for calibration and the pulsewidth experienced in tracking will result in a range bias error. For GEOS-2 combined beacon/skin tracks this resulted in a 30 meter error in the beacon data. For these tracks, the skin track data near the center of the pass was removed and the beacon track data was corrected by adding 30 meters. The consistent SECOR range bias is larger than expected and still not explained. However, if the bias drift indicated in Figure 1 is extrapolated linearly to earlier times, the resulting bias would be near 0 meters just prior to launch. The TRANET data is submitted to the GSDS for both a low-frequency (162:324 MHz) and a high-frequency (324:972 MHz) pair. In this study the two frequency pairs were treated as two distinct stations. After the first several weeks of operation the variations in TRANET were markedly reduced.

In summary, the results with all 35 of the WICE passes have the same general characteristics for the C-Band and SECOR data as reported earlier for the first 10 passes. The preprocessing changes noted in this report caused the C-Band bias values for a few passes to shift by several meters and caused the SECOR bias to be more negative by about 2.5 meters on all passes. The preprocessing changes in the TRANET data reduced the previous biases from 15.6 and 17.6 cm/sec to -3.4 and 1.5 cm/sec.

Table 1

THIS IS A SUMMARY FOR STATION 7052
OF MAXIMUM ELEVATION AND MINIMUM RANGE MEASUREMENTS

DATE YYMMDDHHMM	COINCIDENT DATA PRESENT	START EL (DEG)	MAX EL (DEG)	END EL (DEG)	START R (KM)	MIN R (KM)	END R (KM)	# R PTS	T SPAN (SEC)	% DATA RECV
68 4 2 121	A C6LHSO 1 3	31.50	50.92	28.31	1782.0	1342.2	1914.8	264	362	72
68 4 3 142	A C6 SOW	61.00	67.81	27.64	1217.3	1162.9	1944.2	231	273	84
68 4 5 218	A C6LHSO	36.42	69.48	27.61	1633.0	1151.5	1946.2	321	390	82
68 410 2 6	A C6LHSOW	72.13	82.60	61.00	1141.5	1105.4	1234.9	101	119	84
68 412 242	A C6LHSO	32.16	56.19	26.58	1759.9	1280.6	2014.2	285	397	71
68 413 3 2	A C6LHSO	32.30	41.35	30.18	1758.6	1528.7	1865.4	153	280	54
68 416 2 9	A C6LHSOW1	42.82	76.69	31.72	1497.1	1138.6	1851.7	263	348	75
68 417 227	A C6LHSOW 23	26.27	81.76	28.65	1981.2	1122.7	1967.6	348	466	74
68 418 250	A C6LHS	61.44	61.44	40.82	1242.1	1242.1	1583.9	37	131	28
68 420 138	A C6LHSOW	41.00	41.16	28.05	1582.0	1580.8	2020.8	95	190	50
68 426 142	A C6LHSOW 23	32.13	38.82	32.25	1843.2	1674.5	1900.3	71	241	29
68 426 331	A 6LHSO	32.24	37.12	29.87	1809.3	1684.6	1947.2	48	239	20
68 429 237	A C6LHSOW 23	31.73	85.36	27.47	1834.5	1164.8	2116.9	321	461	69
68 5 3 2 5	A C6LHSO 23	36.39	47.65	23.78	1749.6	1523.4	2340.6	248	384	64
68 5 4 224	A C6LHSO 23	34.48	62.11	29.34	1792.4	1323.6	2090.5	319	411	77
68 5 7 321	A C6 HSOW	36.32	60.38	27.81	1743.5	1343.9	2160.4	344	411	83
68 5 8 341	A C6LHS	35.44	45.35	34.39	1781.5	1572.0	1894.0	136	279	48
68 521 220	A C6L S W	31.99	40.96	28.57	2046.6	1822.0	2298.6	227	348	65
68 521 411	A 6L	35.64	41.12	27.48	1886.2	1761.1	2293.7	112	325	34
68 522 239	A 6L SOW	38.42	52.19	42.15	1843.0	1588.9	1830.3	153	274	55
68 523 259	A 6L S	54.91	66.69	39.64	1521.7	1411.6	1912.8	65	277	23
68 530 321	A C6 SO 2	29.79	79.54	24.04	2151.7	1379.5	2610.5	449	583	77
68 6 4 3 9	A C L S	40.74	59.73	39.51	1888.7	1578.4	2024.2	147	349	42
68 6 5 327	A C6 SOW 23	35.29	75.17	21.78	2029.1	1443.1	2799.3	499	582	85
68 6 6 346	A C6L SOW 23	37.12	79.45	26.97	1974.7	1416.9	2521.4	411	530	77
68 6 7 4 5	A 6L SO 3	32.92	69.75	32.49	2107.4	1480.3	2277.1	416	493	84
68 611 332	A C6L SO 2	37.60	71.14	35.33	2019.0	1510.9	2218.1	339	453	74
68 612 352	A C6L SO 2	52.65	84.97	34.51	1694.5	1447.3	2251.5	249	400	62
68 614 428	A C6 SOW 23	27.92	58.91	31.92	2357.1	1637.6	2349.3	317	522	60
68 615 3 1	A C6L SO	36.18	43.19	32.04	2142.8	1974.7	2372.3	155	331	46
68 615 450	A C6L SO	38.17	45.84	34.12	2033.1	1869.4	2253.6	167	320	52
68 621 3 5	A C6 S W	32.04	41.29	36.24	2329.4	2066.6	2245.6	112	303	36
68 621 456	A C6L SO	44.93	49.70	27.04	1913.5	1832.1	2608.9	255	378	67
68 622 325	A C6L SOW	44.89	51.35	29.38	1950.5	1835.4	2530.1	167	373	44
68 629 349	A C6L SO	43.07	60.42	33.40	2021.3	1725.3	2390.9	66	425	15

A=LASER G=GRARR C=FPS-16 6=FPQ-6 L=TRAN59 H=TRAN35 S=SECOR
O=OPTICAL OTHER THAN: W=WALLOP 1=NWIW2A 2=NWIW2B 3=NWIE3A 4=NWIE3B

Table 2

STATISTICAL SUMMARY BY STATION FOR WICE

RANGE (METERS)	SAMPLE SIZE	RMS NOISE	ZERO-SET BIAS	TIME BIAS (MILLISEC)	TOTAL RMS
LASER	35	1.3 ± 0.2	-	-	
SECOR	32	1.8 ± 0.4	-17.5 ± 4.0	-0.56 ± 0.45	18.4 ± 3.5
FPQ-6	34	1.0 ± 0.3	-1.8 ± 2.6	0.41 ± 0.33	3.2 ± 1.9
FPS-16	27	1.4 ± 0.4	5.8 ± 4.3	0.29 ± 0.34	6.7 ± 3.2
RANGE RATE (CM/SEC)					
TRANET H. F. PAIR	16	6.0 ± 7.0	-3.4 ± 7.9	0.02 ± 0.03	9.4 ± 9.6
TRANET L. F. PAIR	27	4.5 ± 2.0	1.5 ± 3.7	0.02 ± 0.05	5.6 ± 3.5
AZIMUTH (ARC SECONDS)					
LASER	35	53.2 ± 33.0	0.0 ± 0.2	-	
FPQ-6	34	20.6 ± 17.6	38.5 ± 37.0		
FPS-16	27	40.6 ± 32.9	-52.0 ± 56.5		
ELEVATION (ARC SECONDS)					
LASER	35	27.5 ± 9.7	-5.6 ± 13.0		
FPQ-6	34	10.9 ± 3.7	23.1 ± 15.5		
FPS-16	27	19.0 ± 6.9	24.0 ± 23.5		

Figure 1
LASER ORBITS
FPQ-6, FPS-16 & SECOR Range Bias

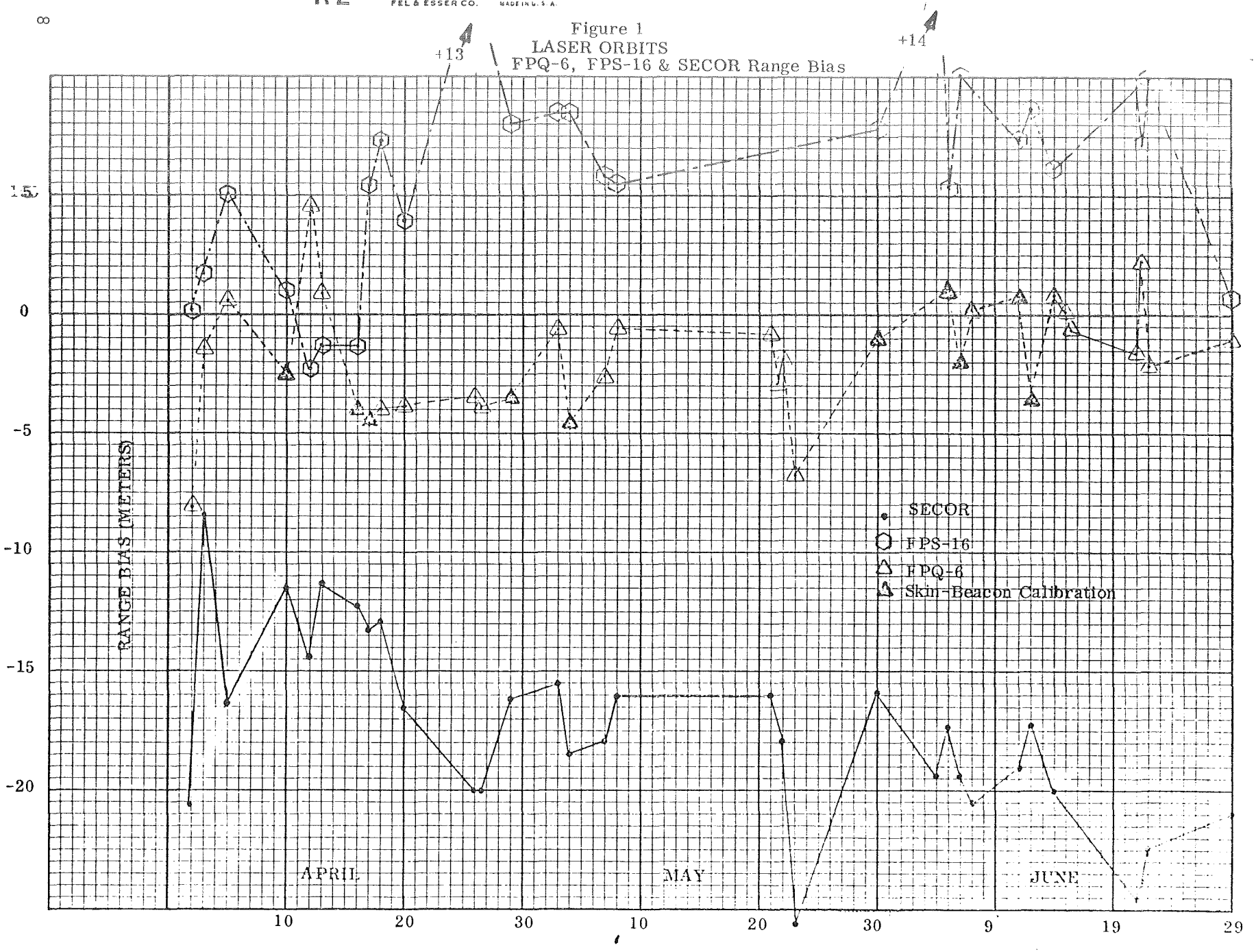

Figure 2
LASER ORBITS
TRANET RANGE RATE BIAS BY PASS

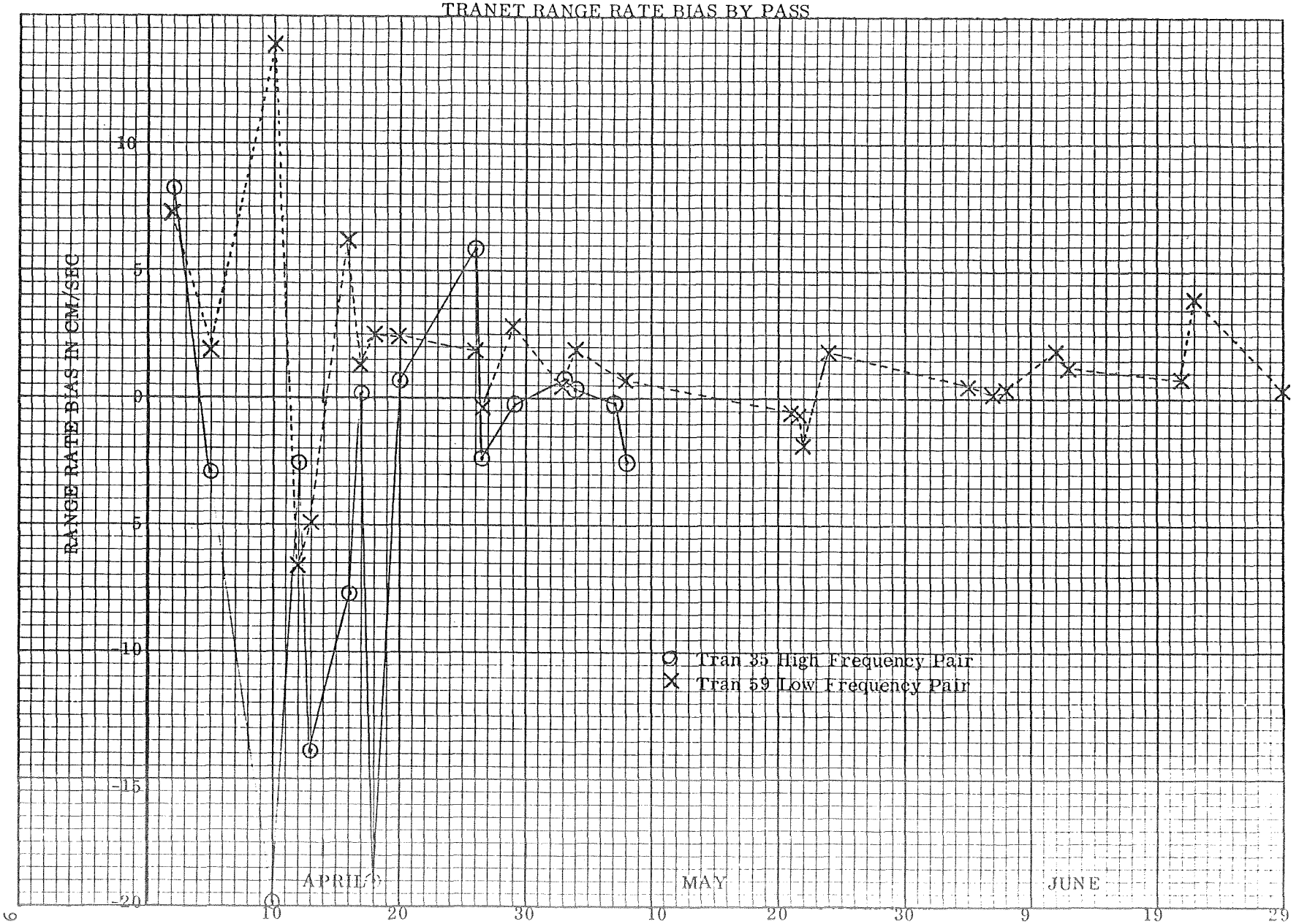

9/10

CARNARVON
LASER COLLOCATION EXPERIMENT
(CALACO)

J. M. Hlavin
RCA Service Company

J. H. Berbert
Goddard Space Flight Center

Prepared for the

GEOS-2 REVIEW CONFERENCE

JUNE 1970*

GODDARD SPACE FLIGHT CENTER
GREENBELT, MARYLAND

*Previously presented to the National Fall AGU Meeting in San Francisco, December, 1969.

CARNARVON
LASER COLLOCATION EXPERIMENT
(CALACO)

J. H. Berbert
J. M. Hlavin

INTRODUCTION

In December, 1968, the Goddard mobile laser was shipped to Carnarvon, Australia, for the purpose of evaluating the accuracy of the Goddard Range and Range Rate (GRARR) System and the FPQ-6 C-band radar. An earlier laser/GRARR intercomparison at the Rosman, North Carolina, station using GEOS-1 resulted in several recommendations for improving the GEOS-2 GRARR data.[1] This second laser/GRARR test was needed to evaluate the improved GRARR data and to establish that the laser could support both day and night tracking at a remote site. At Carnarvon, the station code for the mobile laser was CRMLAS, and for the GRARR site it was CARVON.

The laser arrived at the Carnarvon site in January, 1969. Setup operations were started immediately after arrival, and the first track was made on February 6, 1969.

The laser tracking system placed at Carnarvon uses an intense, highly collimated, short-duration light beam for illuminating the spacecraft being tracked. At the spacecraft, the beam is reflected back towards the ground station by an array of cubical corner reflectors. The returning light is photoelectrically detected, and its travel time is measured to yield the range data. The data rate for the laser was 1 measurement per second in range, azimuth, and elevation.

The GRARR system is a precision spacecraft-tracking system that determines range using sidetone ranging techniques. The range rate is determined using coherent Doppler principles. Each GRARR station uses an S-band system in conjunction with a 1-, 2-, or 3-channel transponder on the spacecraft being tracked. The data rate for the GRARR was 1 sample per second in range and range rate.

Data from the C-band radar system were not available for this report.

TRACKING DATA

During the period from February 6 to May 16, 1969, 94 laser tracking passes were made. However, the data from only 84 of these passes were available for this report. The additional data from the other passes will be included in a later report.

Of the 84 laser tracking passes investigated, 54 occurred during the day (sun elevation angle above -10°) and 30 occurred at night. These acquired data demonstrated that the laser could be regularly used for both day and night tracking when STADAN Minitrack data are used for initial spacecraft acquisition.

There were 57 simultaneous GRARR/laser tracking passes during the test period. During the preprocessing and validation of the GRARR data, it was found that the range data taken April 29, 1969, contained a systematic error due to an intermittent hardware failure. The range time interval decade counter which counted hundreds of nanoseconds failed in that it indicated a zero whenever a seven should have been indicated. Therefore, approximately 10% of the range measurements contained a 700-nanosecond error, equivalent to a 105-meter bias. The remaining 90% of the range data and all of the range rate data did not appear to be affected by the failure. However, since there was a known hardware problem, data from the 13 GRARR passes after April 29, 1969, were discarded, and a set of 44 GRARR tracking passes were considered in this investigation. The analysis of the additional GRARR passes will be included in a later report.

The GEOS-2 spacecraft has a 2-channel S-band transponder that is used in conjunction with the ground equipment. During the course of this experiment, both transponder channels were used and evaluated; transponder channel A (1.4 MHz) was used for 12 GEOS-2 passes, and transponder channel C (3.2 MHz) was used for 32 GEOS-2 passes. Channels A and C of the GRARR operate on up-link frequencies of 2271.9328 MHz and 2270.1328 MHz, respectively.

DATA ANALYSIS

The raw laser data were preprocessed by the Optical Systems Branch at GSFC and deposited in the Goddard data center. The following systematic corrections were applied to the laser data.

a. Range and elevation data were corrected for refraction.

b. Range zero-set system delay correction was added.

c. Outliers were removed at the five sigma level.

The GRARR station clock was synchronized to the cesium time standard, and the laser station time was maintained by the rubidium secondary time standard. The difference between these two standards was less than 0.1 millisecond for the passes considered in this report.

For data comparison purposes, it was assumed that there were no systematic errors in the laser range measurements. However, there may be a bias of up to 2 meters in the laser data [2], and this should be taken into account in evaluating the test results.

The raw GRARR data were preprocessed with the following systematic corrections applied [3].

a. Range and range rate data were corrected for refraction.

b. Range zero-set transponder delay correction was added.

c. Range and range rate data were corrected for antenna offset.

d. Range outliers were removed at the 10 sigma level.

e. Station range zero-set bias was removed electronically by the station operator prior to each pass by matching survey and measured range.

A careful check was maintained on the GEOS-2 transponder and GRARR ground station master oscillators. A small long-term (6 month) drift was noted in the onboard transponder oscillator. However, a preliminary analysis of the transponder oscillator drift indicates that it would not be detectable in the measurements taken during this experiment.

The procedure used to evaluate the GRARR data was to fit a short-arc orbit to the laser range, azimuth, and elevation measurements using a weighted least squares criterion. GRARR and laser residuals from the short-arc orbit were then computed and their statistics were tabulated. The GSFC NONAME [4] orbit determination program was used in this analysis. The a priori relative weight assigned to the orbital elements and the range, azimuth, and elevation measurements in forming the short-arc orbit are given in Table 1. The weights shown leave the orbital elements essentially unconstrained, allowing them to adjust to fit the laser data.

The GRARR range and range rate, and laser range, azimuth, and elevation residuals about the laser reference orbit were computed for each short-arc. Because the GRARR data were edited such that they were within the laser time span, there was no extrapolation of the short-arc orbit used in determining the GRARR residuals. The

direct result of this procedure is to minimize any error contributed by the short-arc orbit.

Table 1
Orbital Element and Laser Measurements Weight Factors

Parameter		Weight Factor
Elements	Position (X, Y, Z)	$\pm 10^5$ meters
	Velocity ($\dot{X}$, $\dot{Y}$, $\dot{Z}$)	$\pm 10^3$ meters/second
Measurements	Laser range	±2 meters
	Laser azimuth	±200 arc seconds
	Laser elevation	±200 arc seconds
	GRARR range	Not used in orbit formation
	GRARR range and range rate	Not used in orbit formation

The mean and rms values of the residuals were calculated on a per pass basis. The rms values derived in the above runs are about the laser orbit and are indicative of the total error in the GRARR System (systematic errors plus noise). The detailed per pass statistics of the range and range rate measurements are shown in Tables 2 and 3. The first column in Tables 2 and 3, EPOCH, gives the year, month, day, and hour of the pass under consideration. The second column, ID, indicates a day or night pass by D or N, respectively, and indicates the GRARR transponder channel, A or C, used when simultaneous data were taken.

Average values and their variations for the rms and mean values of the range, range rate, azimuth, and elevation residuals with respect to the laser orbits for the 44 GRARR passes and the 84 laser passes were calculated and are listed in Table 4.

An examination of the laser data given in Table 4 indicates that there was no essential difference in the laser residual statistics between day and night tracking.

An examination of the GRARR statistics in Table 4 indicates an average range total rms value of 7.3 meters and an average range rate total rms value of 1.7 centimeters per second was established for the 44 passes. The variation in the range rate rms value between the two transponder channels is not considered significant. However, a significant difference in range rms values between the two transponder channels is indicated. It should again be noted that the average GRARR range and range rate rms values are from residuals about the laser orbit, contain systematic errors, and are representative of the total unmodeled uncertainty in the GRARR measurements.

Table 2
NONAME Range Measurement Residual
Mean and rms Values in Meters

NONAME RANGE MEASUREMENT RESIDUAL MEAN AND RMS VALUES
(VALUES IN METERS)

EPOCH	ID*	CRMLAS MEAN	CARVON MEAN	NCARVN MEAN	CRMLAS RMS	CARVON RMS	NCARVN RMS
69020623	D	0.0			1.053		
69020709	D	0.002			1.301		
69020723	D	-0.0			1.199		
69020810	D	0.0			1.343		
69021510	D	0.004			1.773		
69021611	D	0.0			1.235		
69021622	D	0.001			1.243		
69021711	D	-0.0			0.893		
69021723	D	0.001			1.589		
69021823	DC	0.004	-2.324		1.445	5.595	
69021910	DC	-0.0	-9.118		1.200	9.853	
69021923	DC	-0.001	-6.769		1.411	7.566	
69022010	DC	-0.004	1.743		1.508	3.400	
69022100	D	0.0			1.043		
69022110	DC	0.001	-4.455		1.545	5.295	
69022323	DC	0.002	-1.681		1.745	3.264	
69022510	DC	0.0	-1.239		1.070	3.681	
69022523	DC	0.002	-5.075		1.387	7.756	
69022610	DC	0.001	0.698		1.354	5.252	
69022700	DC	0.001	-10.134		1.081	11.268	
69022710	DC	-0.001	-7.753		1.401	9.445	
69022800	DC	-0.0	-16.072		1.283	16.515	
69022811	DC	0.001	-6.283		1.116	9.738	
69030223	DC	0.0	-9.933		0.980	10.578	
69030310	DC	-0.0	-1.250		1.222	3.524	
69030510	D	0.001			1.627		
69030600	DA	0.0	-3.657		1.138	5.005	
69030611	D	0.005			1.273		
69030910	DC	0.0	-5.635		0.953	6.911	
69031010	D	-0.0			1.220		
69031100	DC	-0.001	0.019		0.930	5.600	
69031111	DC	-0.003	-11.387		1.482	12.512	
69031211	NC	-0.0	-15.839		1.232	16.349	
69031311	NC	0.003	-4.771		1.217	5.601	
69031323	DC	0.0	-7.101		1.041	7.649	
69031411	NC	-0.0	-12.944		1.144	13.453	
69031700	DA	-0.001	-1.517		1.274	3.457	
69031711	NA	-0.002	-4.961		1.540	6.017	
69031800	DA	0.001	-4.671		1.130	5.729	
69031811	NA	-0.006	0.566		1.540	3.290	
69031901	DC	0.0	0.703		1.107	3.015	
69031911	N	0.001			1.249		
69031923	D	0.0			1.212		
69032023	DC	-0.0	-10.637		1.230	11.184	
69032200	DC	-0.001	-8.710		1.604	9.201	
69032411	NC	0.0	-4.986		1.461	5.868	
69032501	DC	-0.0	-7.762		1.402	8.272	
69032511	NC	-0.0	2.917		1.240	4.613	
69033111	N	0.006			1.416		
69040112	N	-0.002			1.874		
69040501	D	0.002			1.376		
69040511	N	-0.0			1.555		
69040601	D	0.0			1.078		

Table 2
NONAME Range Measurement Residual Mean and rms Values in Meters (Cont.)

NONAME RANGE MEASUREMENT RESIDUAL MEAN AND RMS VALUES
(VALUES IN METERS)

EPOCH	ID*	CRMLAS MEAN	CARVON MEAN	NCARVN MEAN	CRMLAS RMS	CARVON RMS	NCARVN RMS
69040611	NC	-0.003	-0.248		1.485	2.630	
69040812	NC	-0.0	-10.325		1.464	11.449	
69040911	NC	0.0	-12.870		1.314	13.174	
69041000	D	0.0			0.987		
69041011	NC	0.001	-8.074		1.341	9.173	
69041101	D	-0.0			1.057		
69042100	DA	-0.0	8.716		1.149	9.175	
69042111	NA	0.0	-5.825		1.086	6.628	
69042113	NA	0.0	-3.776		0.977	4.707	
69042211	NA	-0.001	-4.660		1.407	5.677	
69042311	NA	-0.0	-2.617		1.072	4.162	
69042512	NA	-0.004	0.637		1.366	3.045	
69042801	DA	0.0	1.169		1.161	3.299	
69042912	N	-0.0			1.048		
69043001	D	-0.0			1.019		
69043012	N	-0.001			0.981		
69050102	D	-0.0			0.986		
69050112	N	-0.0			1.240		
69050212	N	-0.001			1.306		
69050411	N	0.0			1.073		
69050501	D	-0.0			1.116		
69050512	N	0.0			1.020		
69050601	D	-0.001			1.139		
69050612	N	0.002			1.027		
69051001	D	0.0			1.168		
69051112	N	0.0			1.383		
69051201	D	-0.001			1.190		
69051212	N	-0.0			1.285		
69051402	D	0.0			1.162		
69051513	N	0.0			1.557		
69051601	D	-0.001			1.125		

	CRMLAS MEAN	CARVON MEAN	NCARVN MEAN	CRMLAS RMS	CARVON RMS	NCARVN RMS
AVERAGE	0.000	-4.952		1.258	7.263	
ST. DEV.	0.002	5.194		0.210	3.652	
NO. OF PASSES	84	44				

* ID : TIME OF PASS; D-DAY, N-NIGHT
GRARR TRANSPONDER CHANNEL - A OR C

Table 3
NONAME Range Rate Measurement Residual
Mean and rms Values in Centimeters per Second

NONAME R RATE MEASUREMENT RESIDUAL MEAN AND RMS VALUES
(VALUES IN CMS/SEC)

EPOCH	ID*	CARVON MEAN	CARVON RMS
69021823	DC	1.605	2.700
69021910	DC	0.336	1.149
69021923	DC	0.639	1.403
69022010	DC	0.836	1.222
69022110	DC	2.626	2.905
69022323	DC	0.367	1.044
69022510	DC	1.757	2.097
69022523	DC	0.888	1.902
69022610	DC	1.312	2.458
69022700	DC	0.222	1.020
69022710	DC	0.466	1.635
69022800	DC	1.287	1.616
69022811	DC	0.821	1.786
69030223	DC	0.821	1.810
69030310	DC	1.179	1.973
69030600	DA	1.402	1.795
69030910	DC	0.338	0.953
69031100	DC	0.304	1.227
69031111	DC	0.731	1.343
69031211	NC	0.814	1.468
69031311	NC	0.303	1.225
69031323	DC	0.433	1.187
69031411	NC	0.643	1.062
69031700	DA	0.301	1.173
69031711	NA	-0.229	1.725
69031800	DA	0.287	0.810
69031811	NA	-0.118	1.245
69031901	DC	0.107	0.866
69032023	DC	0.505	0.997
69032200	DC	-0.639	2.683
69032411	NC	1.443	2.127
69032501	DC	1.659	2.158
69032511	NC	-3.240	4.731
69040611	NC	0.865	1.294
69040812	NC	0.146	3.179
69040911	NC	0.467	1.109
69041011	NC	0.952	1.420
69042100	DA	-0.205	0.714
69042111	NA	-0.008	1.373
69042113	NA	1.486	2.080
69042211	NA	0.352	1.740
69042311	NA	0.687	1.514
69042512	NA	0.760	2.235
69042801	DA	0.695	1.410

	CARVON MEAN	CARVON RMS
AVERAGE	0.600	1.672
ST. DEV.	0.854	0.749
NO. OF PASSES	44	

* ID : TIME OF PASS: D-DAY, N-NIGHT
GRARR TRANSPONDER CHANNEL - A OR C

Table 4
Summary of Laser and GRARR Statistics About Laser Orbit

	Measurement	84 Track Average	54 Daylight Track Average	30 Nighttime Track Average
LASER	Range rms	1.3 ± 0.2 m	1.2 ± 0.2 m	1.3 ± 0.2 m
	Range mean	0.0 ± 0.1 m	0.0 ± 0.1 m	0.0 ± 0.1 m
	Azimuth rms	31. ±17. arc sec	32. ±16. arc sec	29.0 ±18. arc sec
	Azimuth mean	0. ± 1. arc sec	0. ± 1. arc sec	0. ± 1. arc sec
	Elevation rms	22. ±11. arc sec	23. ±10. arc sec	20. ±11. arc sec
	Elevation mean	-9. ±14. arc sec	-8. ±16. arc sec	-10. ±11. arc sec
	Measurement	44 Track Average	Channel A (12 Track) Average	Channel C (32 Track) Average
GRARR	Range rms (total)	7.3 ± 3.7 m	5.0 ± 1.8 m	8.0 ± 3.8 m
	Range mean	-5.0 ± 5.2 m	-1.7 ± 4.0 m	-6.1 ± 5.0 m
	Range rate rms (total)	1.7 ± 0.8 cm/sec	1.5 ± 0.5 cm/sec	1.7 ± 0.8 cm/sec
	Range ratemean	0.6 ± 0.9 cm/sec	0.5 ± 0.6 cm/sec	0.7 ± 0.9 cm/sec

An inspection of the GRARR residuals plots indicates that small systematic errors existed within the GRARR data. An error model consisting of range and range rate zero-set biases and a common station timing bias was selected to explain the observed systematic error. The GRARR data were evaluated for a second time against the laser-determined short-arc orbits using the weighted least squares technique and the above error model to determine the true rms noise and bias values of the range and range rate measurements. The relative weights used in these regression runs are listed in Table 5.

Table 5
Weight of Orbit Elements, GRARR Measurements, and GRARR Biases Used in Regression Analysis

	Parameter	Weight
Orbital Elements	Position (X, Y, Z)	$\pm 1 \times 10^{-3}$ meters
	Velocity ($\dot{X}$, $\dot{Y}$, $\dot{Z}$)	$\pm 1 \times 10^{-6}$ meters/second
Measurements	GRARR range	±5 meters
	GRARR range rate	±0.05 meters/second
Bias	GRARR range	±1000 meters
	GRARR range rate	±10 meters/second
	GRARR time	±1 second

The range rms noise, range bias, range rate rms noise, range rate bias, and station timing bias were computed for each pass.

Average values and their variations for the GRARR noise and bias parameters determined in the regression runs for the 44 passes were calculated and are listed in Table 6.

Table 6
Regression Analysis Results

GRARR Measurement	44 Track Average	Channel A (12 Track) Average	Channel C (32 Tracks) Average
Range rms	2.9 ± 0.2 m	3.0 ± 0.2 m	2.9 ± 0.2 m
Range bias	-4.3 ± 6.0 m	-2.0 ± 4.0 m	-5.2 ± 6.5 m
Range rate rms	1.3 ± 0.6 cm/sec	1.3 ± 0.4 cm/sec	1.3 ± 0.6 cm/sec
Range rate bias	1.2 ± 2.3 cm/sec	0.0 ± 0.7 cm/sec	1.7 ± 2.5 cm/sec
Time bias	-0.4 ± 1.1 msec	0.2 ± 0.4 msec	-0.6 ± 1.2 msec

The results of the error model regression runs listed in Table 6 could account for the difference in the GRARR range rms values between the two channels. Here it is noted that the range noise rms values for both channels were the same (approximately 3 meters). However, the channel A transponder had a -2.0-meter bias and the channel C transponder had a -5.2-meter bias. The difference between the two transponder biases is probably due to drift in the transponder electronics since its prelaunch calibration.

The regression values of average range rate rms noise given in Table 6 display no significant difference between the two transponder channels.

Both the time bias average values in Table 6 and the variations about these values are unbelievably large. As noted earlier, a very tight control was maintained between the station clocks and on the GRARR system master oscillators. The results of this careful control should limit the pass-to-pass time biases to less than 0.2 millisecond. It was noted that for these short-arc passes, the time biases were determined primarily by the range data and thus may be the result of some other systematic error in the range data incorrectly modeled as a time bias.

The range rate biases as determined in the regression show a substantial difference between the two transponder channels. However, it should be pointed out that there is a high correlation between time bias and range rate bias for the short-arc

geometry used in this intercomparison and that the extracted range rate bias for channel C may be the result of the unlikely channel C time bias. The negative average time bias shown is in the correct direction and has about the right magnitude to account for most of the positive average range rate bias that is given.

CONCLUSIONS

It was concluded that the laser could support scheduled tracking, both day and night, at a remote site, and the laser measurement statistics show no significant difference between day and night tracking. The basic laser measurement statistics were:

- Laser range rms value . . . . . 1.3 meters
- Laser azimuth rms value . . . . . 31. arc seconds
- Laser elevation rms values . . . . . 22. arc seconds

In addition, it was concluded that the Carnarvon GRARR data had the following uncertainties:

- Total range uncertainty of ±7.3 meters consisting of:
  - Zero-set bias of -2.0 meters for channel A
  - Zero-set bias of -5.2 meters for channel C
  - Measurement noise level of 2.9 meters
  - Plus other systematic errors (such as time bias, refraction, etc.).
- Total range rate uncertainty of ±1.7 cm/sec consisting of:
  - Measurement noise level of 1.3 cm/sec
  - Systematic errors (such as zero-set bias, time bias, refraction, etc.).

The above results are in substantial agreement with the earlier Rosman test, where the Rosman GRARR showed a range bias of -5.3 ± 12.4 meters, a systematic S-shaped variation in the range rate residuals between ±6 cm/sec, and a 2.1-ms time bias.

The range measurement shows a small negative bias in both tests, with variations in the Carnarvon basis being substantially smaller. The systematic component of the range rate residuals and the time bias errors determined by the regression runs are also substantially smaller for the Carnarvon test than those determined at Rosman. The S-shaped variation in the Carnarvon range rate residuals was absent in most of the passes and, when present, the effect was smaller than that documented in the Rosman test. The above results were probably due to the better control exerted over the station clock and over the transponder down-link oscillator as recommended in the Rosman test results.

The above results augmented with the additional laser, GRARR, and the Carnarvon C-band data will be published in more detail in a future report.

REFERENCES

1. J. Berbert, P. Maresco, and R. Reich; Intercomparison of Collocated Laser Optical and GRARR Radio Ranging System Track on GEOS-A, September 1970, X-514-67-447.

2 J. Berbert, J. Hlavin, R. Reich; Laser/Laser Comparisons from the GORF, ARLACO, and GOLACO Tests. GEOS-II Review Conference, June 22—24, 1970.

3. Final on GRARR/GEOS-A Data Validation. June 1968, I-514-68-111. pp C1 to C8.

4. O'Neill, Brian: NONAME, Volumes I, II, III, and IV. NASA Contract Number NAS 5-9756-71D. August 1968.

LASER/LASER COMPARISONS FROM THE GORF, ARLACO, AND GOLACO TESTS

J.H. Berbert
Goddard Space Flight Center

J.M. Hlavin
RCA Service Company

R.F. Reich
RCA Service Company

Prepared for the

GEOS-2 REVIEW CONFERENCE

JUNE 1970

GODDARD SPACE FLIGHT CENTER
GREENBELT, MARYLAND

LASER/LASER COMPARISONS FROM THE GORF, ARLACO, AND GOLACO TESTS

J. Berbert, M. Hlavin, R. Reich

INTRODUCTION

The Goddard Experimental Laser (GEL) has been used since 1966 for participation in geodetic data observation campaigns and for intercomparison with other geodetic tracking systems (References 1, 2, and 3). In late 1968, the Goddard Mobile Laser (GML) became available. This afforded an opportunity to collocate and intercompare the GEL and the GML to help determine whether systematic errors were apparent in the data from either one. Since the GML was developed, it has participated in three such laser/laser intercomparison tests: twice with the GEL at Goddard and once with the SAO laser at Mt. Hopkins, Arizona (see Figure 1).

This paper summarizes preliminary results from all three tests. The GML data were used for forming the reference short-arc orbits, since the GML data were common to all three tests. The resulting reference orbits were tightly constrained and used to determine SAO or GEL measurement residuals from which the relative range biases and bias uncertainties were determined (see Figure 2). The a priori weights of the orbital elements and the GML range, azimuth, and elevation measurements, used in forming the short-arc orbits, are given in Figure 3. The a priori GEL measurement and bias weights are given in Figure 4.

In these tests, relative time biases were not derived because the laser system clocks were known to be synchronized to within 0.05 millisecond.

RESULTS

A chronological plot of range bias of the GEL or SAO laser, relative to the GML, is plotted for each pass of the three intercomparison tests: GORF 1 (see Figure 5), ARLACO - Phases 1 and 2 (see Figures 6 and 7), and GOLACO (see Figure 8). A summary of the average range noise and average relative bias over all passes within each intercomparison test is given in Figure 9.

GORF-1

The large GEL rms noise value of 1.86 meters in the first laser intercomparison test (GORF-1) was attributed to using an older refurbished ruby rod at least an inch

shorter than the optimum 6 inches. The shorter rod results in a longer pulse, which increases the rms noise. All the GEL 6-inch ruby rods had been provided to the GML.

The large and relatively stable 4.09-meter bias between the GEL and the GML exhibited in the five GORF-1 passes was an order of magnitude larger than had been expected. A review of the calibration techniques revealed that the GML boresight tower calibrations had been done near the threshold levels of the return pulse energy; whereas, the GEL calibrations were done near the expected return-pulse signal level from the satellite. This would cause the GML system to trigger earlier on the higher-energy return pulses from the satellite than on the calibration pulses, thus leading to short GML range measurements on the satellite and a positive relative range bias for the GEL with respect to the GML as observed (Reference 4).

This explanation was proposed and accepted after the conclusion of the GORF-1 test. The GML calibration procedures were changed accordingly, so that subsequent boresight tower calibrations used a return-pulse signal level that approximated that of the average satellite return. Unfortunately, no test data were collected under the new procedures before the GML was shipped to Carnarvon.

ARLACO

The next laser intercomparison test (ARLACO) took place at Mt. Hopkins, Arizona, where the GML was collocated with the SAO laser. This test was run in two phases. The GML position was shifted approximately 10 meters between phases 1 and 2 to provide data for evaluation of laser survey recovery capability.

Some difficulties were experienced in preparing for this test. The narrow road to the Mt. Hopkins site had to be improved in 52 places to transport the GML system to the site. Also, the GML system initially suffered from arcing due to the 8000-foot altitude.

During the ARLACO test, it was planned to measure the return-pulse signal level of both the GML and SAO lasers. However, for the GML system, it was not possible to measure both the range and the return pulse levels simultaneously, because the signal-level measuring devices interfered with the range measurements.

For this test, preparations were made to analyze the results of the first few passes as soon as possible in order to determine and correct any deficiencies. These precautions proved worthwhile, since quick-look analysis of the first pass data uncovered a 100-millisecond time bias and a 5.5-meter range bias between the two lasers

(not shown in Figure 6). The time bias was determined to be due to an intentional offset in the time tag of the SAO data which was overlooked in the preprocessing of the data. A large part of the range bias, 4.8 meters, was due to a change in the SAO system internal delay since the previous calibration. These errors were detected, verified, and corrected by the end of the second pass.

At the conclusion of the ARLACO test, SAO preprocessed their laser data and submitted them to the National Space Science Data Center (NSSDC) at GSFC These are the data denoted by the crosses in Figures 6 and 7 and averaged in Figure 9. No satisfactory explanation is presently available for the apparent 3.3-meter shift in bias between phases 1 and 2, or for the large outliers near the ends of both phases.

The data denoted by crosses within circles in Figures 6 and 7, and also averaged in Figure 9, are the SAO data that were corrected for refraction. These data had to be corrected, since discussions with SAO indicated that the data in the NSSDC were not corrected for refraction (contrary to the refraction code indicator in the data format). Refraction corrected data subsequently were submitted by SAO to the NSSDC in June 1970, after these analyses were done.

The data denoted by triangles in these figures are the refraction-corrected SAO data compared with GML data using a constant 102.2-nanosecond internal-delay calibration rather than the delay value measured for each pass. The 102.2-nanosecond value is the average measured GML internal delay for all the GOLACO passes, applied after the fact to the GML data from the ARLACO passes. As can be seen, this constant value increases the fluctuations in the bias for the first few passes of phase 1 and decreases the fluctuations for the last few passes of phase 2. The motivation for using a constant value of internal delay for the GML data arises from the GOLACO test results which are explained below.

The decrease in the GML (MOBLAS) rms noise from 1.23 meters in the GORF-1 test to 0.99 to 1.06 meters in the ARLACO and GOLACO tests is thought to be due to correction of an instability in the receiver circuit shortly after the GORF-1 test.

GOLACO

The results of the third laser intercomparison test (GOLACO) are given in Figures 8 and 9.

The decrease in the GEL (GODLAS) rms noise from 1.86 meters in the GORF-1 test to 1.00 meter in the GOLACO test is attributed to replacing the shorter refurbished ruby rod with an optimum length 6-inch rod and to various other circuit improvements.

It is interesting to note what appears to be a correlation between bias results and the training of the operator responsible for the GML boresight tower calibration, indicating the somewhat subjective nature of the calibration. For the first three GOLACO passes, the GML calibrations were done by a member of the crew who had not previously had that responsibility. On about April 5th, the crew was retrained in the calibration procedures that were established at the conclusion of the GORF-1 test. This coincided with a noticeable decrease in the bias for the next several weeks. From about April 25th through the end of the test, the newly trained calibration operator was replaced by another operator. This coincided with a noticeable increase in the bias and bias fluctuations.

A related but more specific effect is illustrated in Figure 10. Here, the derived range bias between the lasers is plotted against the GML internal delay measured prior to each pass during the boresight tower calibration. The systematic nature of the bias, when plotted in this manner, indicates the high correlation between the range bias and the calibration measurement of internal system delay. In fact, a straight line with a slope of 1.5 meters per 10 nanoseconds (1.0 meter per 1.0 meter) and an intercept of 106.2 nanoseconds provides a good least squares fit to the data in Figure 10. The rms of the bias variations about this line is only 0.71 meter compared to an rms of 1.25 meters about the best fitting horizontal line. Thus, using a constant internal delay of 106.2 nanoseconds, rather than the measured internal delay, reduces the bias variations.

A reasonable physical interpretation of this result is that the GML internal system delay is more stable than the calibration measurements of it. For example, an increase of say 10 nanoseconds (1.5 meters) in the GML internal-delay measurement (not accompanied by a real change in GML internal delay) would produce GML range measurements to the satellite shorter by 1.5 meters. Consequently, the bias of the GEL relative to the GML would be larger by 1.5 meters. Difficulties in matching the calibration return-pulse signal level to the satellite return-pulse signal level could cause such an effect.

If the 106.2-nanosecond intercept of the fitted line is chosen as the constant value for the GML internal system delay, then the average bias for the GOLACO data

is zero, with variations in bias of 0.71 meter, as shown by the variations about the fitted line. This 106.2-nanosecond value of internal system delay probably corresponds to the delay for a calibration return-pulse signal level equal to the average satellite return-pulse signal level for the GOLACO data. However, the GML system was not able to precisely measure or correct for return-pulse signal level during the GOLACO test. The return-pulse level, used in each prepass calibration, could be adjusted only in 10-db steps and at best was only an estimate of the expected average satellite return for that pass. Furthermore, considerable signal strength fluctuations are to be expected from pulse to pulse within a pass. Because of this, the return signal should be measured or compensated for on every pulse.

In Figure 11, the same range bias values are plotted against the GEL internal-delay measurements. In this case, the points appear randomly scattered, so that correlation between these parameters is not apparent. This is probably due to the use of an experimental GEL device to measure the return-pulse level of each pulse during GOLACO passes. Using this device, a prepass boresight tower calibration of delay versus pulse level was applied to the measured satellite return pulses to correct for systematic errors in delay due to pulse level.

CONCLUSIONS

1. The relative bias between the GEL and the GML system was reduced from 4.09 to -1.19 meters from the GORF-1 to the GOLACO test. The rms noise of the GEL was reduced from 1.86 meters to 1.00 meter, and the rms noise of the GML was reduced from 1.23 to 1.06 meters. These improvements are attributed to several factors:
   - The better GML calibration procedure established after the GORF-1 test, which approximately matches the calibration return-pulse signal level to the average satellite return-pulse signal level.
   - The GEL pulse-level measurement and correction techniques.
   - The improved system hardware in both the GEL and the GML (receiver upgrading, longer ruby rod, etc.)
2. In ARLACO phases 1 and 2, the SAO system exhibited average pulse-to-pulse rms range measurement noises of 1.4 and 1.1 meters and average biases relative to the GML of -1.4 meters and +1.8 meters.

3. All 3 independent laser systems, involved in the ARLACO and GOLACO tests, were in agreement to better than 2 meters. This supports the hypothesis that these systems, at the time of the tests, had an absolute accuracy of better than 2 meters. Furthermore, all three laser systems are undergoing signal processing developments which are anticipated to improve their accuracy by almost an order of magnitude.

1. GODDARD SIDE BY SIDE — TEST 1
   10/08/68 TO 11/01/68
   GODDARD MOBILE LASER VS GODDARD EXPERIMENTAL LASER

2. ARIZONA COLLOCATION EXPERIMENT (ARLACO)
   10/06/69 TO 11/07/69 PHASE I
   12/12/69 TO 1/31/70 PHASE II
   GODDARD MOBILE LASER VS SAO LASER

3. GODDARD SIDE BY SIDE TEST 2
   3/26/70 TO 5/14/70
   GODDARD MOBILE LASER VS GODDARD EXPERIMENTAL LASER

Figure 1. Laser/Laser Tests

- FORM SHORT ARC ORBITS USING ALL THE MOBILE LASER RANGE, AZIMUTH, AND ELEVATION DATA

- SOLVE FOR RANGE BIAS BETWEEN STATION BASED ON MOBLAS SHORT ARC ORBITS & SAO OR GEL DATA WITHIN THE MOBLAS DATA SPAN

Figure 2. Range Measurement Intercomparison

ORBITAL ELEMENTS	WEIGHTING FACTOR
POSITION	$\mp 10^5$ METERS
VELOCITY	$\mp 10^3$ METERS/SEC
MOBILE LASER	
RANGE	$\mp$ 2 METERS
AZIMUTH	$\mp$ 200 ARC SEC
ELEVATION	$\mp$ 200 ARC SEC

Figure 3. A priori Weighting of GML Data Used in Forming Short-Arc Orbits

SAO AND GEL LASERS	WEIGHTING FACTOR
RANGE	∓ 2 METERS
RANGE BIAS	∓ 1000 METERS

Figure 4. A Priori Weighting of SAO and GEL Data Used in Bias Recovery

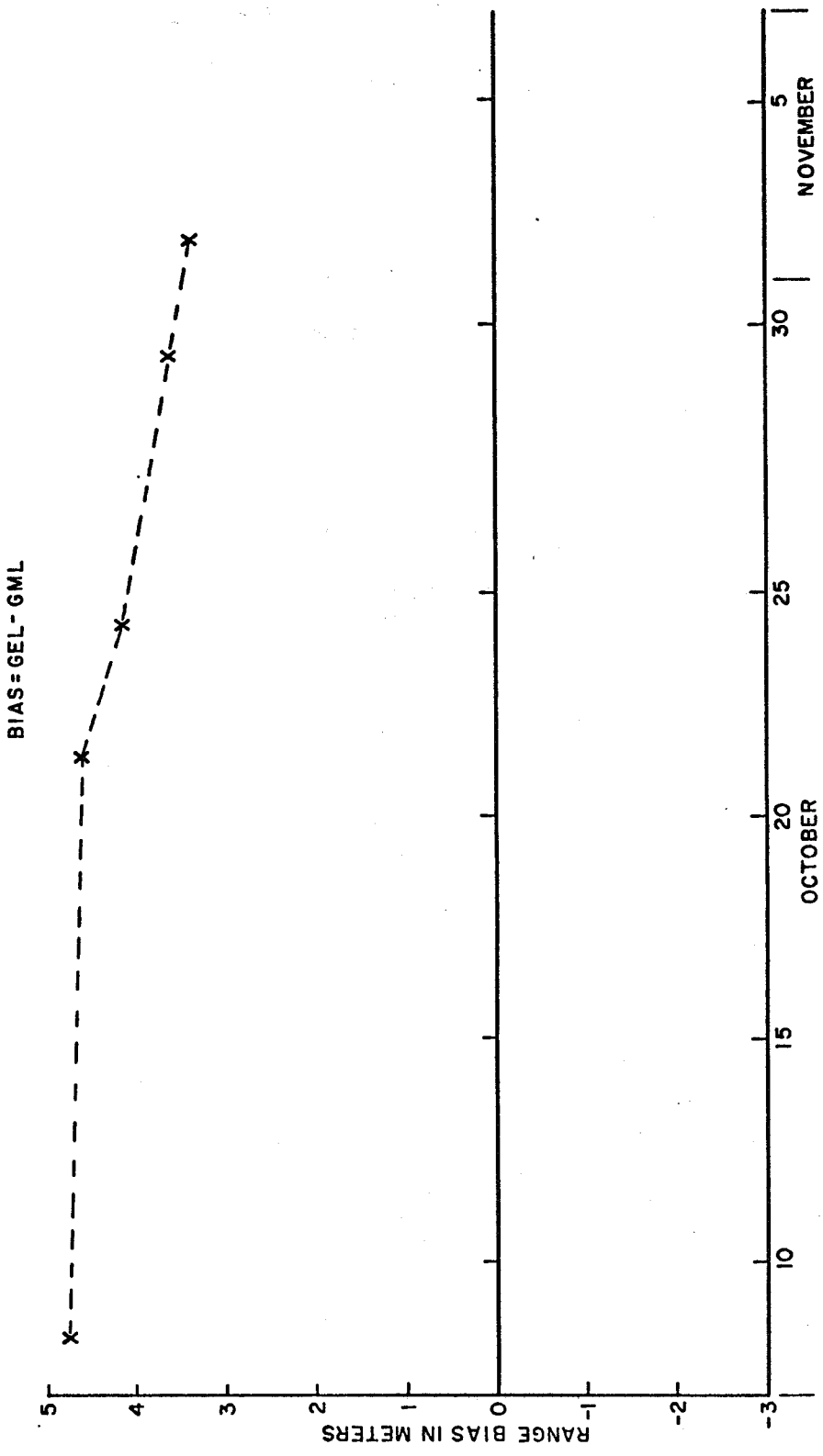

Figure 5. GORF-1, R-Bias vs Date, October—November 1968

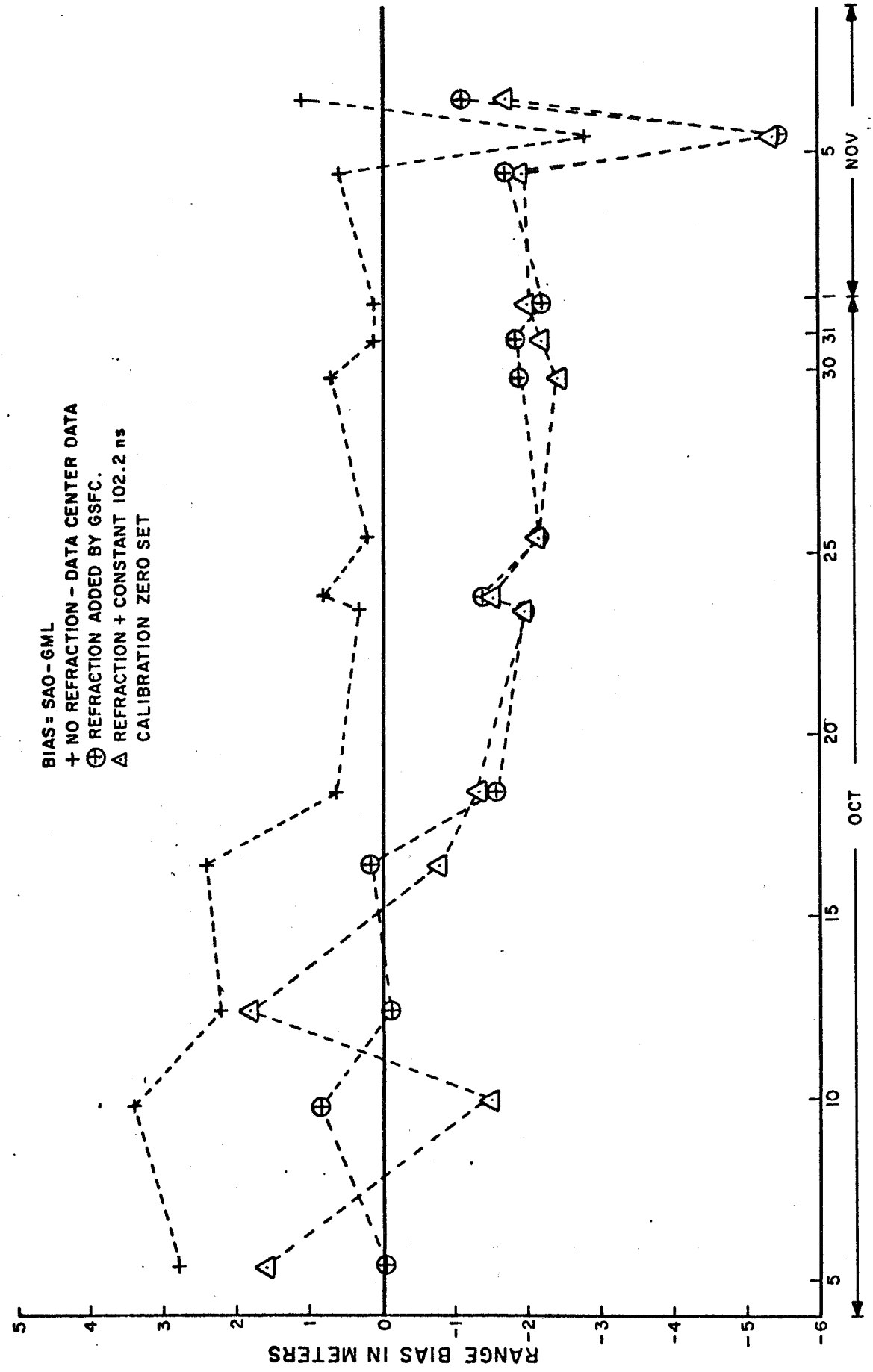

Figure 6. ARLACO, Phase 1, Range Bias vs Date, October—November 1969

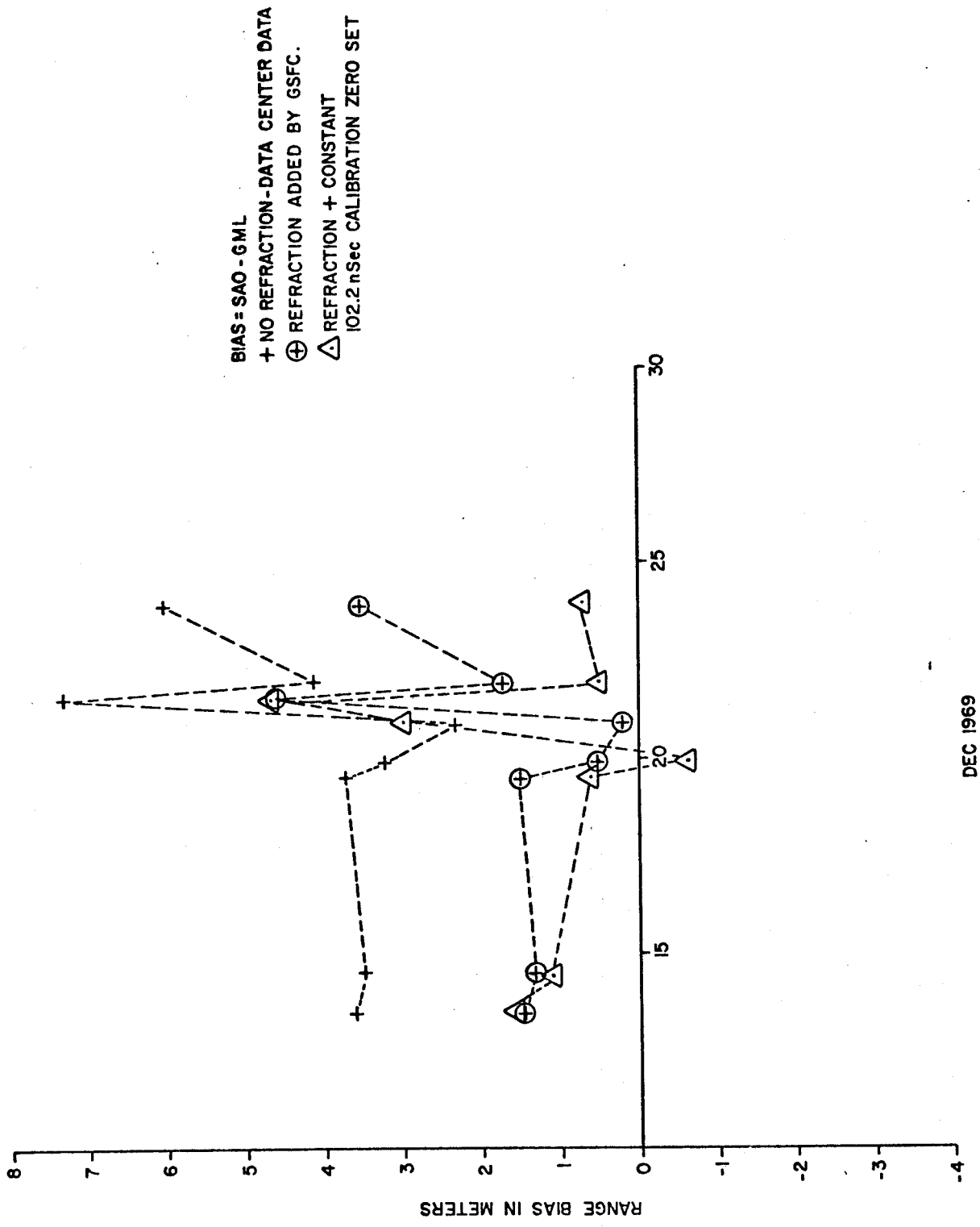

Figure 7. ARLACO, Phase 2, Range Bias vs Date, December 1969

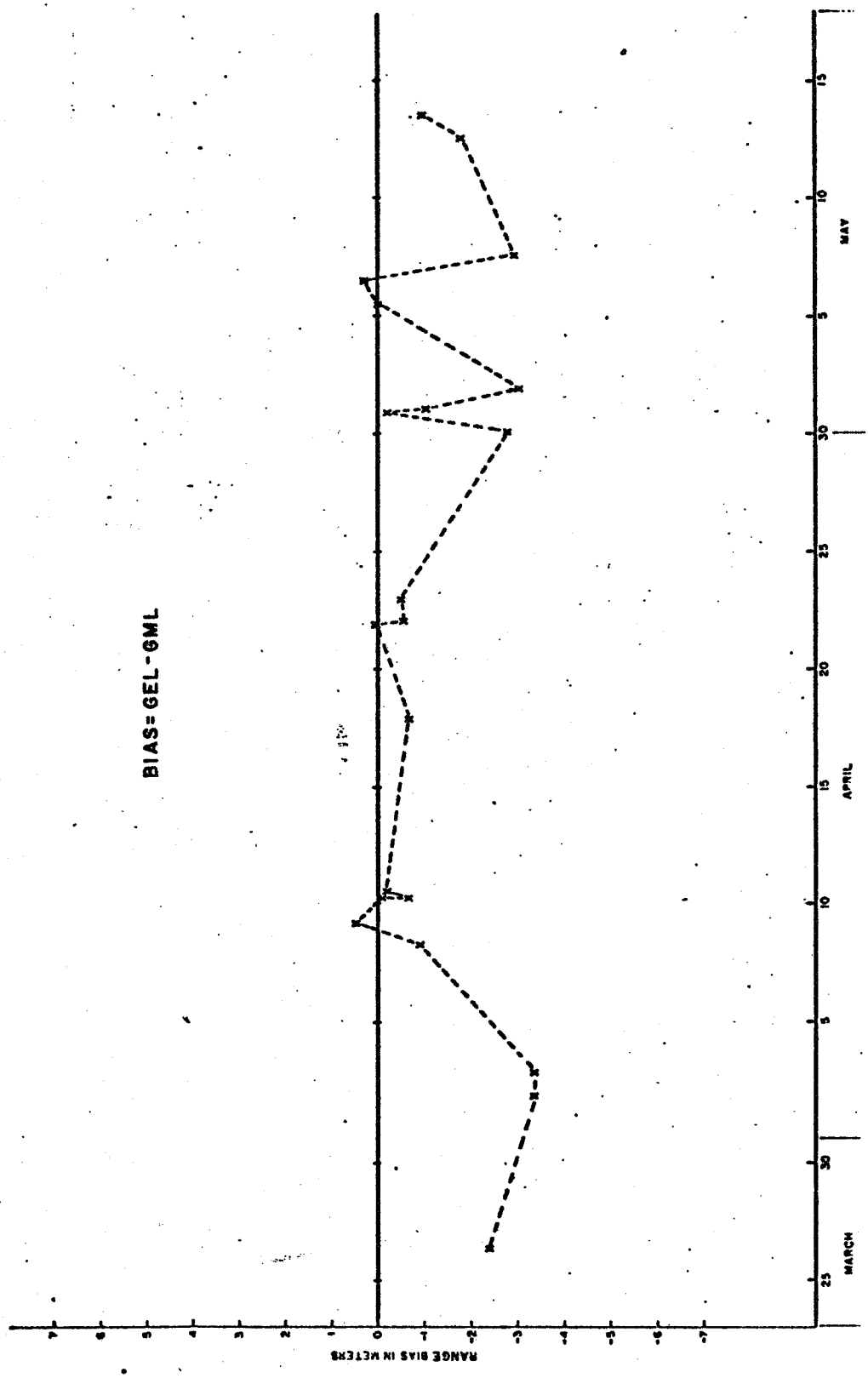

Figure 8. GOLACO, Range Bias vs Date, March—May 1969

EXPERIMENT	NUMBER OF PASSES	R-RMS (METERS)				R-BIAS (METERS)		
		GML (MOBLAS)	SAO		GEL	SAO		GEL
			NSSDC	REFR CORR		NSSDC	REFR CORR	
GODDARD SIDE BY SIDE 1 (GORF-1)	5	1.23	—	—	1.86	—	—	4.09 ± 0.59
ARLACO PHASE 1	14	1.04	1.52	1.37	—	0.90 ± 1.51	-1.43 ± 1.43	—
ARLACO PHASE 2	8	0.99	1.18	1.09	—	4.22 ± 1.61	1.82 ± 1.49	—
GODDARD SIDE BY SIDE 2 (GOLACO)	21	1.06	—	—	1.00	—	—	-1.19 ± 1.25

Figure 9. Statistical Summary

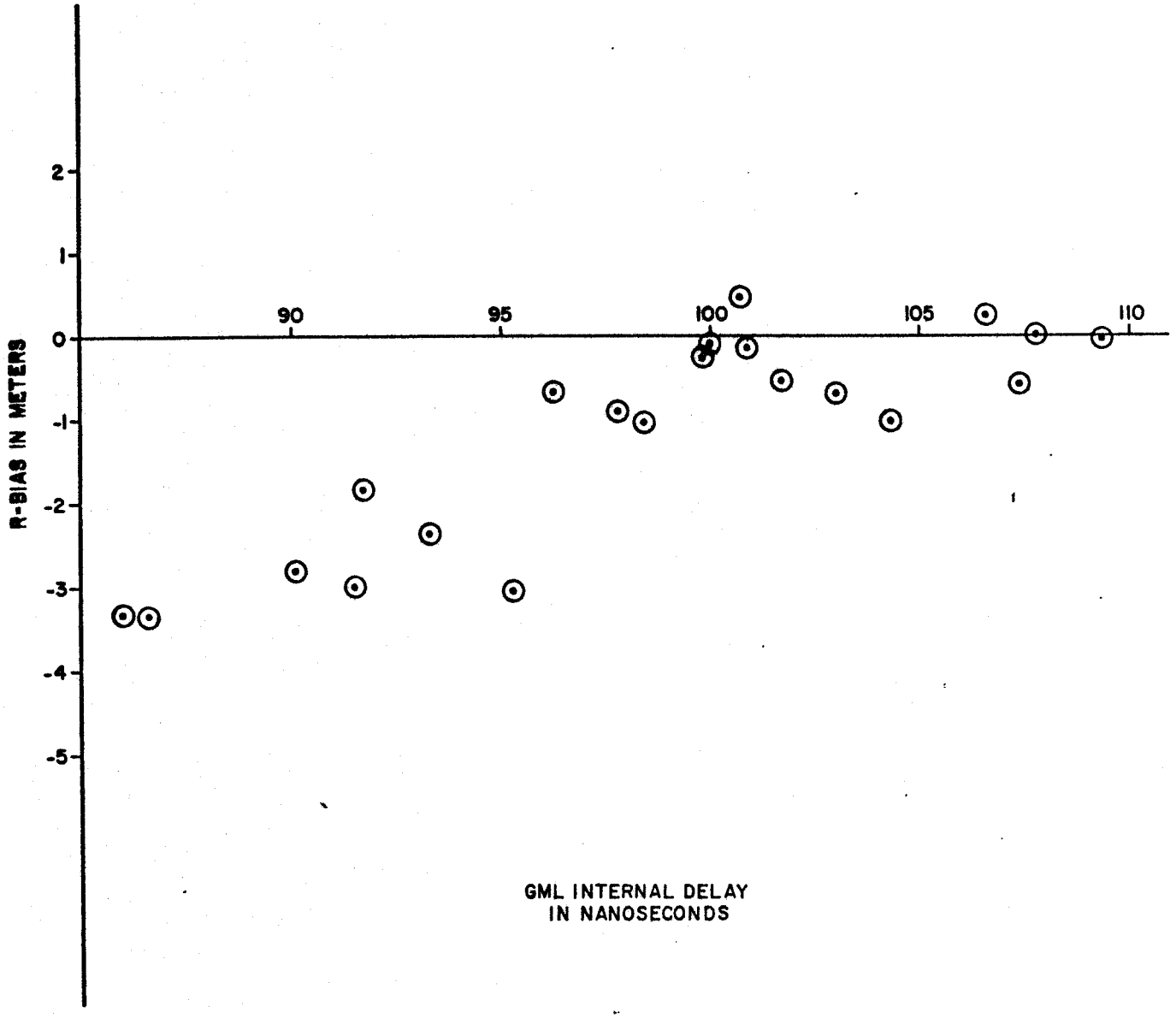

Figure 10. Plot of Range Bias Between GEL and GML vs GML Internal Delay

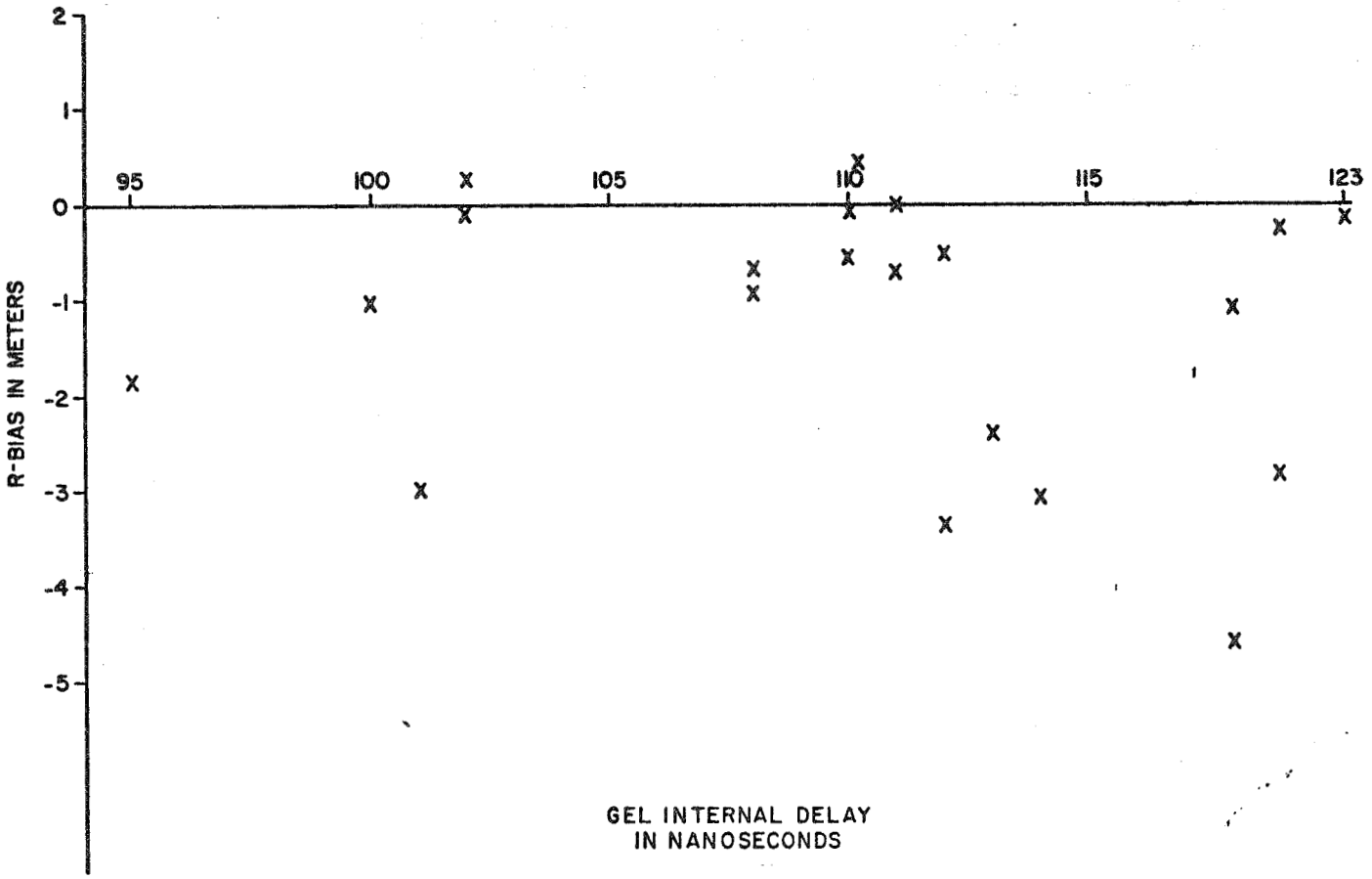

Figure 11. Plot of Range Bias Between GEL and GML vs GEL Internal Delay

REFERENCES

1. Intercomparison of Collocated Laser Optical and GRARR Radio Ranging System Tracks on GEOS-A, September 1967, X-514-67-447

2. Comparison of C-Band, SECOR, and TRANET with a Collocated Laser on 10 Tracks of GEOS-2, John H. Berbert and Horace C. Parker, November 1968. X-514-68-458

3. Geodetic Systems Intercomparisons Based on 35 GEOS-2 Tasks Taken During the W.I.C.E., H. Parker, D. Carney, J. Berbert; presented at the GEOS-2 Review Conference, June, 1970

4. A Comparison of Satellite Range Measurements Taken by the GSFC Experimental and Mobile Laser Systems, Brian O'Neill, November, 1968

REFRACTION STUDIES USING THE WICE DATA

Prepared for the GEOS-2

REVIEW CONFERENCE

June 22 - 24 1970

by

J. Mallinckrodt
H. Parker
J. Berbert

REFRACTION STUDIES USING THE WICE DATA

J. Mallinckrodt, H. Parker, J. Berbert

During the first few months of GEOS-2, Goddard sponsored the Wallops Island Collocation Experiment (WICE) as part of the GEOS Observation Systems Intercomparison Investigation. The availability in the WICE experiment of a large number of collocated redundant metric sensors experiencing predictably different degrees of refraction affords a unique opportunity to compare various methods of refraction correction. This paper will discuss the progress of refraction studies based on the WICE data.

Figure 1 indicates the principal objectives of the study. The first objective involves formula comparisons. Since most practical refraction correction formulas involve varying degrees of approximation in themselves, irrespective of any errors in the external data inputs, a considerable effort has been made first to compare various refraction correction formulations under idealized common input data assumptions in order to become quite aware of their differences and to spot any gross deficiencies in some of the formulations. Within the GEOS program the refraction correction formulas in use by various agencies for correcting various data sources are not standardized. For the troposphere alone 4 such distinct formulations have been identified for elevation angle, 9 for range, and 7 for range rate. In addition to these, the comparisons have included the CRPL Standard Atmosphere calculations and a highly refined ray tracing integral program. The discrepancies have been found to be highly significant at low elevation angles and significant in some cases at all elevation angles. Figure 2 is presented to give an idea of the variability between various formulations. The report on this study has been written and is available (Ref. 1).

The second main source of variation in the refraction corrections is in the data source. For example, in the case of the ionosphere, options include ionospheric soundings, multi-frequency measurements such as with SECOR and TRANET, or a priori predictions. Figure 3 indicates the WICE data sources permitting refraction comparisons for the tropospheric and ionospheric errors.

Recent effort has concentrated on the ionospheric comparisons and includes the following parts.

Ref. 1: Berbert, J. H. and Parker, H. C., "GEOS Satellite Tracking Corrections for Refraction in the Troposphere", GSFC X-514-70-55, February, 1970.

1. Composite Ionospheric Profiles

Figure 4 illustrates the problem of synthesizing a composite profile from available bottomside and topside (ALOUETTE) sounder data. Coincidences in time and position between ALOUETTE and GEOS were, of course, dependent on their different orbital parameters. Nevertheless, some 46 near coincidences during April-June, 1968 were identified. These were ranked quantitatively for degree of coincidence by evaluating a semi-empirical expression for ionospheric correlation as a function of spatial and temporal separation and from this and consideration of the availability of other data such as TRANET, SECOR and Laser for intercomparisons, the list was reduced to 17 candidate passes for extensive analysis. The ALOUETTE data have been obtained for most of these cases, scaled and reduced to electron density profiles vs true height, as have the coincident Wallops Island bottomside sounder records. From these, and using appropriate interpolation between records, a composite best-estimate electron density profile has been formulated applicable to the point of closest approach on the GEOS trajectory for 16 of the 17 selected passes.

2. Comparisons Between Profiles and 2-Frequency SECOR Corrections

Ray tracing calculations have been carried out on the 16 composite profiles using the REEK program and implicitly assuming a spherically stratified ionosphere with no variation in electron density with latitude or longitude. These results have been compared with the two-frequency SECOR derived ionospheric corrections (see Figures 5 and 6).

The SECOR correction at the maximum elevation point generally agrees within about 10% with the ray traced composite profile correction. However, initial results of these comparisons have shown that at times there is a considerably greater degree of North-South or rise-set assymetry than had been anticipated.

In Figure 5 the SECOR determinations show as much as 100% difference in range corrections at 35^{o} elevation on the rise and set. Two possible explanations suggest themselves for this phenomenon.

- Actual horizontal gradients of total electron content in the GEOS-2 orbital plane. Sunset line effects seem the most likely explanation although preliminary studies indicate that even these would not normally be expected to induce more than a 30-40% change in electron content in a 700 mile span.

- Magneto-Ionic effects. However, preliminary estimates do not explain the observed magnitude of assymetry.

3. Comparisons Between SECOR and TRANET Multi-Frequency Corrections

Comparisons of differentiated SECOR with TRANET corrections and integrated TRANET with SECOR corrections have been made on several passes with excellent agreement.

4. Geographical Variation Predictions

In pursuit of this question several approaches to predicting spatial variations or actual electron content horizontal gradients are being studied. All of these utilize the published "Ionospheric Predictions" or actually the harmonic expansion coefficient representation thereof as a basis for spatial scaling according to the computed latitude and longitude of each height point along the line-of-sight ray to each of several representative points along the GEOS trajectory.

5. ALOUETTE Determination of Spatial Variations

Additionally, the ALOUETTE topside reductions are being carried out at several points along the trajectory, representing roughly the rise to set trajectory above 30° elevation. This will permit a rough check of the gradients predicted as described above. If the discrepancies warrant, it may be advisable to attempt estimation of the electron content gradients on the basis of the ALOUETTE observations, however, this is still only being considered on a contingency basis.

In summary, the preliminary results show that, as expected, the NBS predicted ionosphere is unrealistic for determining tracking systems refraction corrections in the VHF/UHF band. Using a composite electron density profile, based on bottomside and topside ionograms, for determining the SECOR ionospheric refraction corrections, provides agreement with the 2-frequency SECOR refraction corrections to within 10% at high elevation angles near the sounding station, but fails at low elevation angles, far removed from the area where the soundings were obtained.

Acknowledgement

The authors wish to acknowledge the contributions of the many participants in this refraction study as indicated in Figure 7. J. Spurling of Wallops provided the ground index and radiosonde profiles for the troposphere. G. Trimble of ETR provided the "REEK" ray trace program used in these analyses. J. Jackson of GSFC is contributing his unique and invaluable guidance and computer programs in scaling the topside and bottomside ionograms and forming the composite profiles.

C. Mamekos has conscientiously assisted Mr. Jackson in scaling the ionograms. Dr. A. Tucker of the University of Texas has provided expertise on TRANET and has calculated predicted electron contents using the NBS harmonic expansion coefficients. In addition, discussions with R. Reich, P. Schmid, B. Rosenbaum, and Dr. S. Rangaswamy, of GSFC, with J. Wright of the ESSA Laboratory in Boulder, and with AMS personnel associated with the SECOR data processing, have greatly aided the progress of this study.

WICE REFRACTION STUDIES

OBJECTIVES

- COMPARISON OF REFRACTION CORRECTION FORMULATIONS IN USE IN GEOS PROGRAM, (X-514-70-55)
- DATA SOURCE COMPARISON; SOUNDINGS, MULTI-FREQUENCY, PREDICTIONS, ETC.
- ESTIMATES OF RESIDUAL ERROR

Figure 1

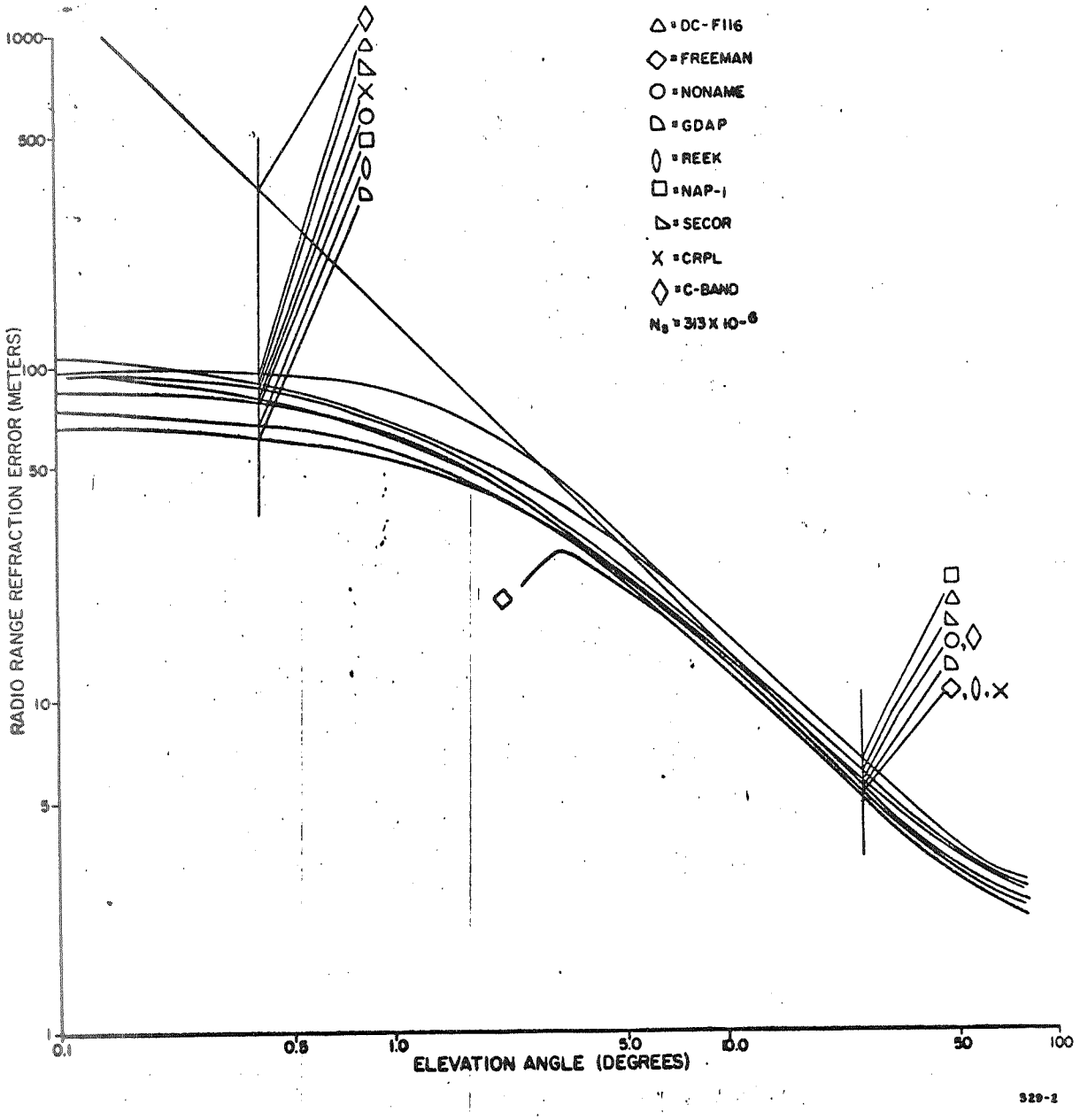

Figure 2. Range Error Due to Tropospheric Refraction

REFRACTION DATA SOURCES

TROPOSPHERE

- GROUND INDEX MEASUREMENTS
- RADIOSONDE MEASUREMENTS
- ORBIT, OPTICAL, AND RADIO INTERCOMPARISONS

IONOSPHERE

- BOTTOMSIDE SOUNDINGS
- TOPSIDE SOUNDINGS (ALOUETTE)
- SECOR 2-FREQUENCY DETERMINATIONS
- TRANET 3-FREQUENCY DETERMINATIONS
- PREDICTIONS
- ORBIT, OPTICAL, AND RADIO INTERCOMPARISONS

Figure 3

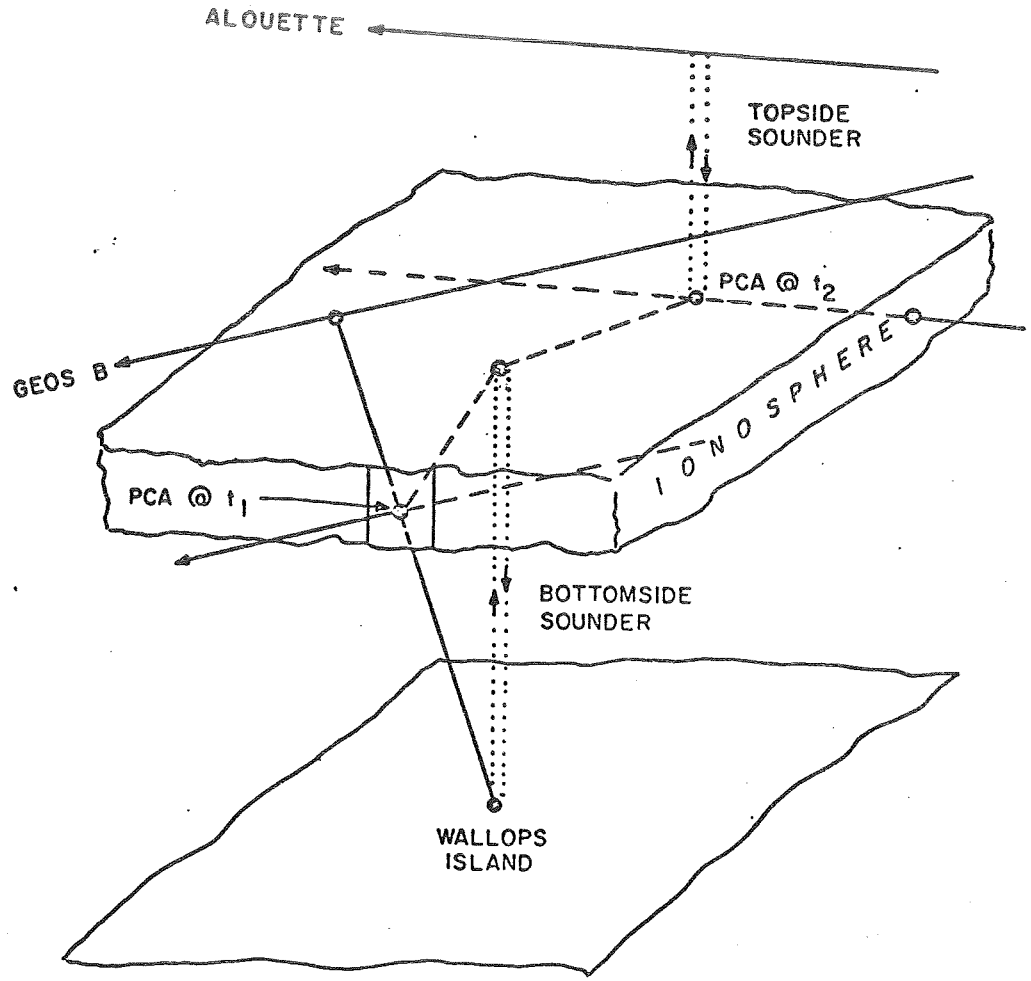

COMPOSITE IONOSPHERIC PROFILES

Figure 4

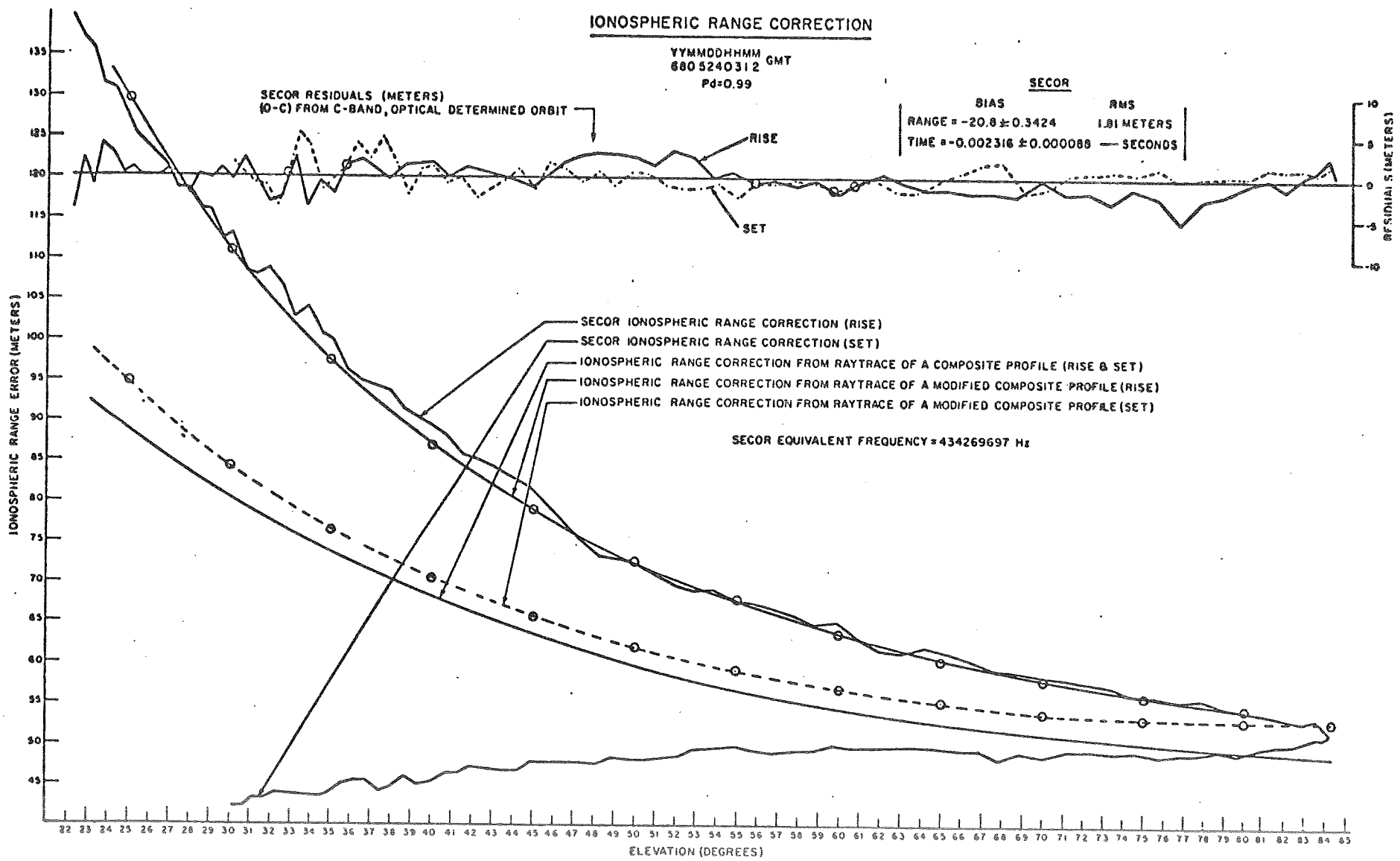
IONOSPHERIC RANGE CORRECTION
YYMMDDHHMM GMT
6805240312
Pd=0.99
SECOR RESIDUALS (METERS)
(O-C) FROM C-BAND, OPTICAL DETERMINED ORBIT
RISE
SET
SECOR
BIAS
RMS
RANGE = -20.8 ± 0.3424
1.81 METERS
TIME = -0.002316 ± 0.000088
SECONDS
SECOR IONOSPHERIC RANGE CORRECTION (RISE)
SECOR IONOSPHERIC RANGE CORRECTION (SET)
IONOSPHERIC RANGE CORRECTION FROM RAYTRACE OF A COMPOSITE PROFILE (RISE & SET)
IONOSPHERIC RANGE CORRECTION FROM RAYTRACE OF A MODIFIED COMPOSITE PROFILE (RISE)
IONOSPHERIC RANGE CORRECTION FROM RAYTRACE OF A MODIFIED COMPOSITE PROFILE (SET)
SECOR EQUIVALENT FREQUENCY = 434269697 Hz
IONOSPHERIC RANGE ERROR (METERS)
RESIDUAL (METERS)
ELEVATION (DEGREES)

Figure 5

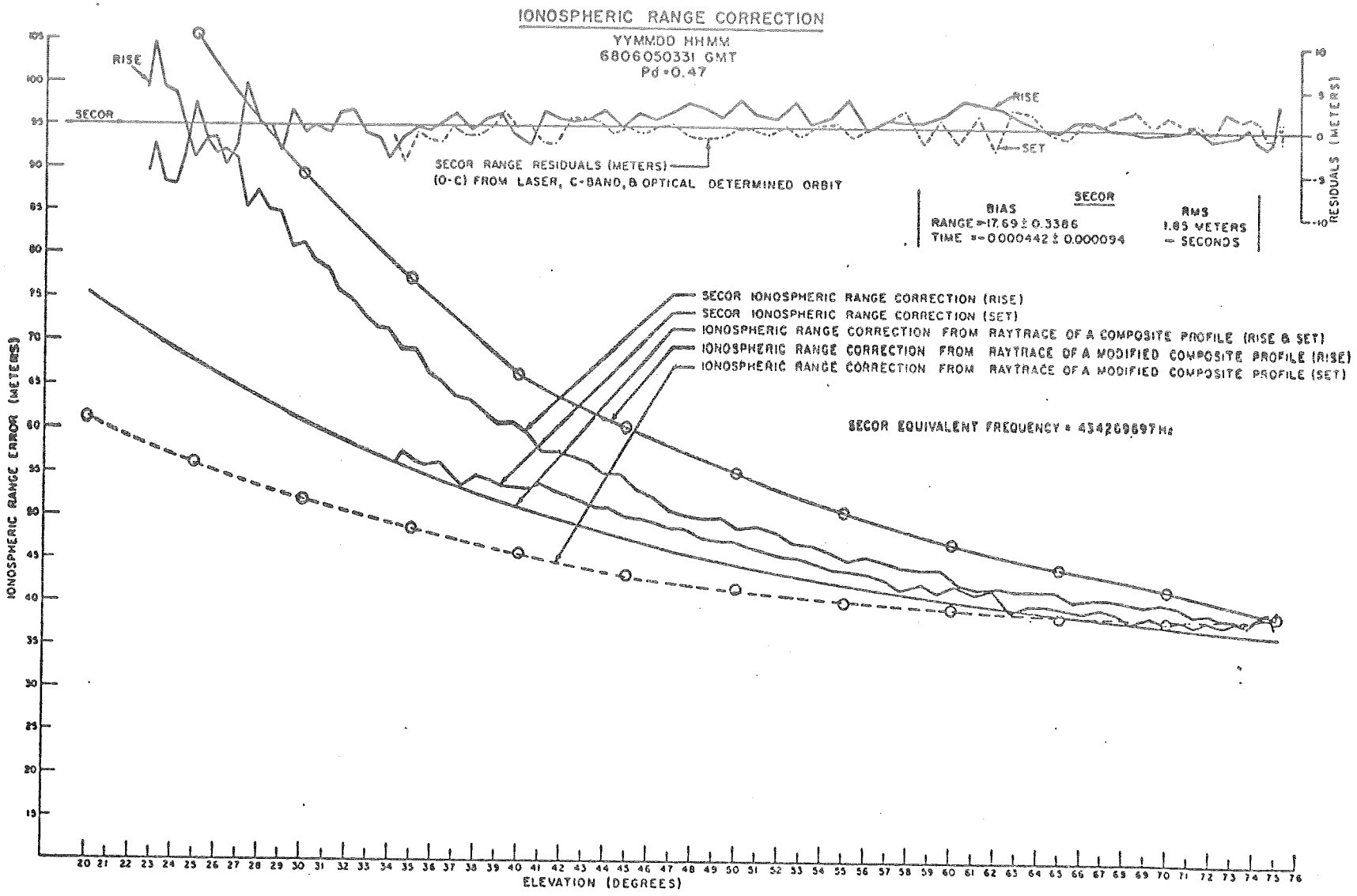
IONOSPHERIC RANGE CORRECTION
YYMMDD HHMM
6806050331 GMT
Pd=0.47
RISE
SECOR
SECOR RANGE RESIDUALS (METERS)
(O-C) FROM LASER, C-BAND, & OPTICAL DETERMINED ORBIT
RISE
SET
RESIDUALS (METERS)
SECOR
BIAS
RANGE =-17.69 ± 0.3386
TIME =-0.000442 ± 0.000094
RMS
1.85 METERS
= SECONDS
SECOR IONOSPHERIC RANGE CORRECTION (RISE)
SECOR IONOSPHERIC RANGE CORRECTION (SET)
IONOSPHERIC RANGE CORRECTION FROM RAYTRACE OF A COMPOSITE PROFILE (RISE & SET)
IONOSPHERIC RANGE CORRECTION FROM RAYTRACE OF A MODIFIED COMPOSITE PROFILE (RISE)
IONOSPHERIC RANGE CORRECTION FROM RAYTRACE OF A MODIFIED COMPOSITE PROFILE (SET)
SECOR EQUIVALENT FREQUENCY = 4342698971Hz
IONOSPHERIC RANGE ERROR (METERS)
ELEVATION (DEGREES)

Figure 6

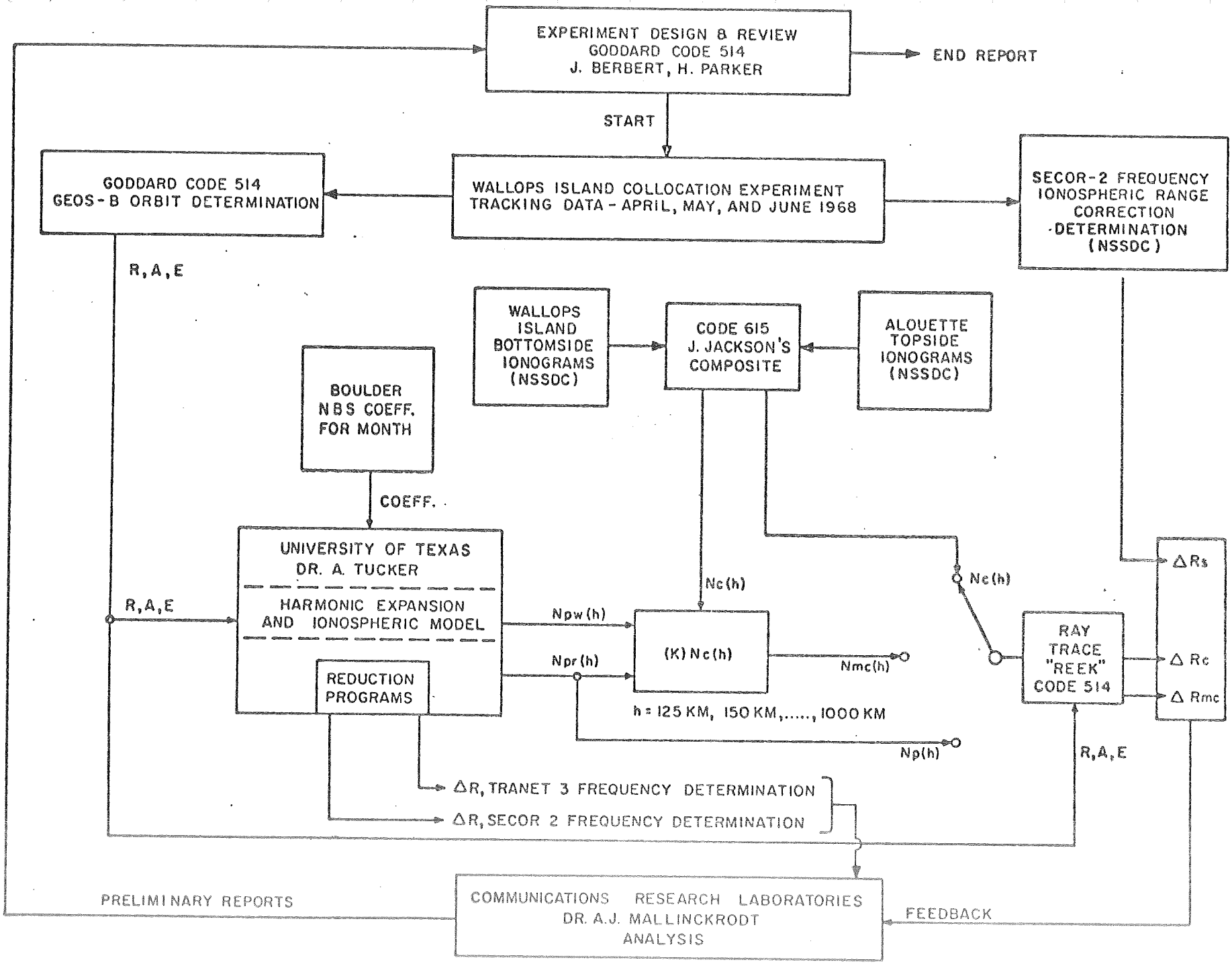
EXPERIMENT DESIGN & REVIEW
GODDARD CODE 514
J. BERBERT, H. PARKER
END REPORT
START
GODDARD CODE 514
GEOS-B ORBIT DETERMINATION
WALLOPS ISLAND COLLOCATION EXPERIMENT
TRACKING DATA - APRIL, MAY, AND JUNE 1968
SECOR-2 FREQUENCY
IONOSPHERIC RANGE
CORRECTION
-DETERMINATION
(NSSDC)
R,A,E
WALLOPS
ISLAND
BOTTOMSIDE
IONOGRAMS
(NSSDC)
CODE 615
J. JACKSON'S
COMPOSITE
ALOUETTE
TOPSIDE
IONOGRAMS
(NSSDC)
BOULDER
NBS COEFF.
FOR MONTH
COEFF.
UNIVERSITY OF TEXAS
DR. A. TUCKER
HARMONIC EXPANSION
AND IONOSPHERIC MODEL
REDUCTION
PROGRAMS
R,A,E
Nc(h)
Nc(h)
Npw(h)
Npr(h)
(K) Nc(h)
Nmc(h)
h = 125 KM, 150 KM,....., 1000 KM
Np(h)
RAY
TRACE
"REEK"
CODE 514
ΔRs
Δ Rc
Δ Rmc
R,A,E
ΔR, TRANET 3 FREQUENCY DETERMINATION
ΔR, SECOR 2 FREQUENCY DETERMINATION
PRELIMINARY REPORTS
COMMUNICATIONS RESEARCH LABORATORIES
DR. A.J. MALLINCKRODT
ANALYSIS
FEEDBACK

Figure 7

GEOS-II QUALITY ASSURANCE AND DATA VALIDATION

Prepared for the GEOS-2

REVIEW CONFERENCE

June 22 - 24 1970

By

J. Casto
M. Hlavin
R. Reich
J. Berbert

GEOS-II QUALITY ASSURANCE AND DATA VALIDATION

J. Casto, M. Hlavin, R. Reich, and J. Berbert

1.0 INTRODUCTION

The GEOS-II spacecraft was supported by several types of tracking systems within the STADAN. The data collected by those systems which are of geodetic quality are validated and submitted to the Space Sciences Data Center at GSFC, where they are made available to other agencies. This paper describes the current status of the validation effort for information collected by the Goddard Range and Range Rate (GRARR) systems and by the Minitrack Optical Tracking System (MOTS). Also contained is a brief description of the utilization of data from these systems for quality assurance on the tracking performance of the STADAN.

2.0 OPTICAL VALIDATION

The optical validation techniques used are basically those employed during the GEOS-I program. They are fully documented in the document GSFC X-514169-83, GEOS-I MOTS OPTICAL VALIDATION REPORT. The current status of the GEOS-II data is contained in Figure 1.

3.0 QUALITY ASSURANCE AND GRARR VALIDATION

These two tasks, although separate, are quite closely related. The quality assurance effort was performed using the GRARR data both as the subject of evaluation and as a reference for analysis of less precise tracking systems. Both functions were accomplished by forming precision orbits, the arc lengths being 2 - 4 days. The scheduling of the GRARR was oriented to this end throughout the GEOS-II lifetime.

Having formed the orbit, data from the several GRARR stations were then evaluated and any inconsistencies noted. In those cases where operational problems were evident, corrective action was taken. The orbit accuracy was not being evaluated; the orbit determination process was simply used as a tool to ensure that the 4 operational GRARR stations produced consistent data. This same evaluation technique is being used for validation of the GRARR data. The GRARR determined orbits were also used as a reference for evaluation of the performance of the Minitrack stations.

3.1 GRARR DATA PREPROCESSING

The preprocessing of the GRARR data consists of those items done during GEOS-I, along with 4 additional corrections. The GEOS-I corrections are contained in GSFC I-514-68-111, FINAL REPORT ON GRARR/GEOS-A DATA VALIDATION, Section 3.1.1. The additional corrections for GEOS-B are as follows:

1. X-Y axis offset corrections to measured range and range rate

2. Tropospheric and Ionospheric Refraction corrections to range and range rate (ref. Private communication; Parker to Berbert, Fall 1969), based on orbit determined elevation

3. Range correction based on measured range rate and prelaunch calibration of spacecraft transponder

4. Time synchronization corrections (as received).

3.2 GRARR DATA REDUCTION

The orbit determination program used edits the tracking data based on the value of the measurement residuals from the orbit. The editing criteria employed are 90 meters for range, 25 cm/sec for range rate and 1 degree for X-Y angle. The final orbits contain from 8 - 20 spacecraft passes.

3.3 QUALITY ASSURANCE RESULTS

Several GRARR data errors were discovered and corrected as a result of the GEOS-II quality assurance program. Some of these are listed below.

On approximately one half of the supported passes, the ALASKA GRARR exhibited a one second time error in the range rate information. The cause was found to be in the equipment turn on procedure.

The Carnarvon station exhibited an abnormally large noise content in the range data when compared to other stations. The cause was found to be a faulty circuit board in one of the mixers; the symptoms could only be detected on targets possessing satellite dynamics.

A procedural error in equipment turnoff was discovered at Rosman.

Several cases of X-Y angle encoder slippage were detected at Carnarvon. A severe RF axis misalignment problem was also discovered at this station.

3.4 GRARR VALIDATION STATUS

Figure 2 contains the current status of the validation effort. The operational dates of each station are shown in Figure 3.

MOTS OPTICAL DATA VALIDATION STATUS

TECHNIQUE USED	GSFC X-514-69-83 GEOS-I MOTS OPTICAL VALIDATION REPORT
DATA COLLECTION PERIOD	FEB 1968 - DEC 1969
NUMBER OF PLATES TAKEN	7971
NUMBER OF PREOPERATIONAL PLATES	41
PLATES BROKEN OR NON-REDUCIBLE	2468
PLATES REDUCIBLE	5642
PLATES REQUESTED FOR REDUCTION	3571
PLATES VALIDATED	2643
PLATES REJECTED	35
PLATES IN PROCESSING	222
PLATES TO BE REDUCED	671
PERCENT OF TASK COMPLETED	74.9%
SPEOPTS NETWORK CLOSED	JAN 1969

Figure 1

GRARR DATA VALIDATION STATUS

- NUMBER OF PASSES TAKEN 2024
- NUMBER OF PASSES VALIDATED 1140
- PERCENT DATA PASSING VALIDATION CRITERIA 94%
- TIME PERIOD VALIDATED FEB 1968-APRIL 1969

Figure 2

STATION OPERATIONAL DATES

• TOTAL TIME PERIOD	FEB 1968 - SEPT 1969
• MADGAR	FEB 1968 - MAY 1968 SEPT 1968 - JAN 1969
• ROSMAN	FEB 1968 - SEPT 1968
• CARVON	FEB 1968 - JUNE 1969
• ALASKA	FEB 1968 - SEPT 1969

Figure 3

IONOSPHERIC CORRECTIONS BASED ON VHF RANGE AND RANGE RATE MEASUREMENTS

P. E. Schmid
Goddard Space Flight Center

S. Rangaswamy
Nat'l Acad of Science

C. W. Murray, Jr.
Goddard Space Flight Center

Prepared for
GEOS-2 Review Conference

June 22-24, 1970

ABSTRACT

The interpretation of radio tracking data will lead to bias in range and range rate computed from these data if one assumes that the radio signals travel with freespace velocity - that is, the speed of light in a vacuum. This propagation bias due to the ionospheric plasma is directly proportional to the number of electrons along the ray path linking the vehicle and tracking station. Consideration of appropriate equations for GEOS-2 ionospheric corrections led to the conclusion that the integrated electron content can be extracted directly from VHF tracking data. This paper outlines the theoretical aspect of this unique ionospheric correction scheme and presents experimental verification based on analysis of Goddard Range and Range Rate VHF tracking data.

INTRODUCTION

A careful review of the biasing effect of the Earth's ionosphere on GEOS-2 tracking data led to the conclusion that the integrated electron content required for ionospheric corrections is inherent, at least at VHF (nominal 150 MHz), in range, range rate, and angle tracking data. By refining the analysis procedure this technique may prove useful during spacecraft tracking at frequencies as high as 2GHz even though at 2GHz the ionospheric effect is reduced by a factor of approximately 20 0. At this point it is worth recalling the reasons why VHF tracking is still widely used by NASA and others, even though based solely on radiowave propagation considerations, the higher frequencies 1GHz and above are much more desirable (reference 1). The two distinct advantages of the lower frequencies such as used by the VHF Goddard Range and Range Rate tracking system (uplink 148.260 MHz, downlink 136.140 MHz) are ease of signal acquisition and simplicity in spacecraft antenna design. Ease in signal acquisition is especially important during near-Earth passes of spin stabilized unmanned spacecraft in highly elliptical orbits where lunar distance as well as near-Earth tracking is desired without antenna electronic or mechanical despinning and/or switchover. Such spacecraft are included in Goddard's Explorer Series and this paper will be concerned with one of these spacecraft, namely, Explorer 34 (also termed IMP-4, Interplanetary Monitoring Platform).

Spacecraft antenna simplicity (i.e., no mechanical or electronic beam steering) and ease of acquisition by the ground tracking station at VHF both result from the following basic antenna principles:

1. Antenna conical beamwidth is inversely proportional to the square-root of antenna power gain.

2. For a given effective antenna aperture, as frequency increases beamwidth decreases.

OVERALL TRACKING DATA HANDLING

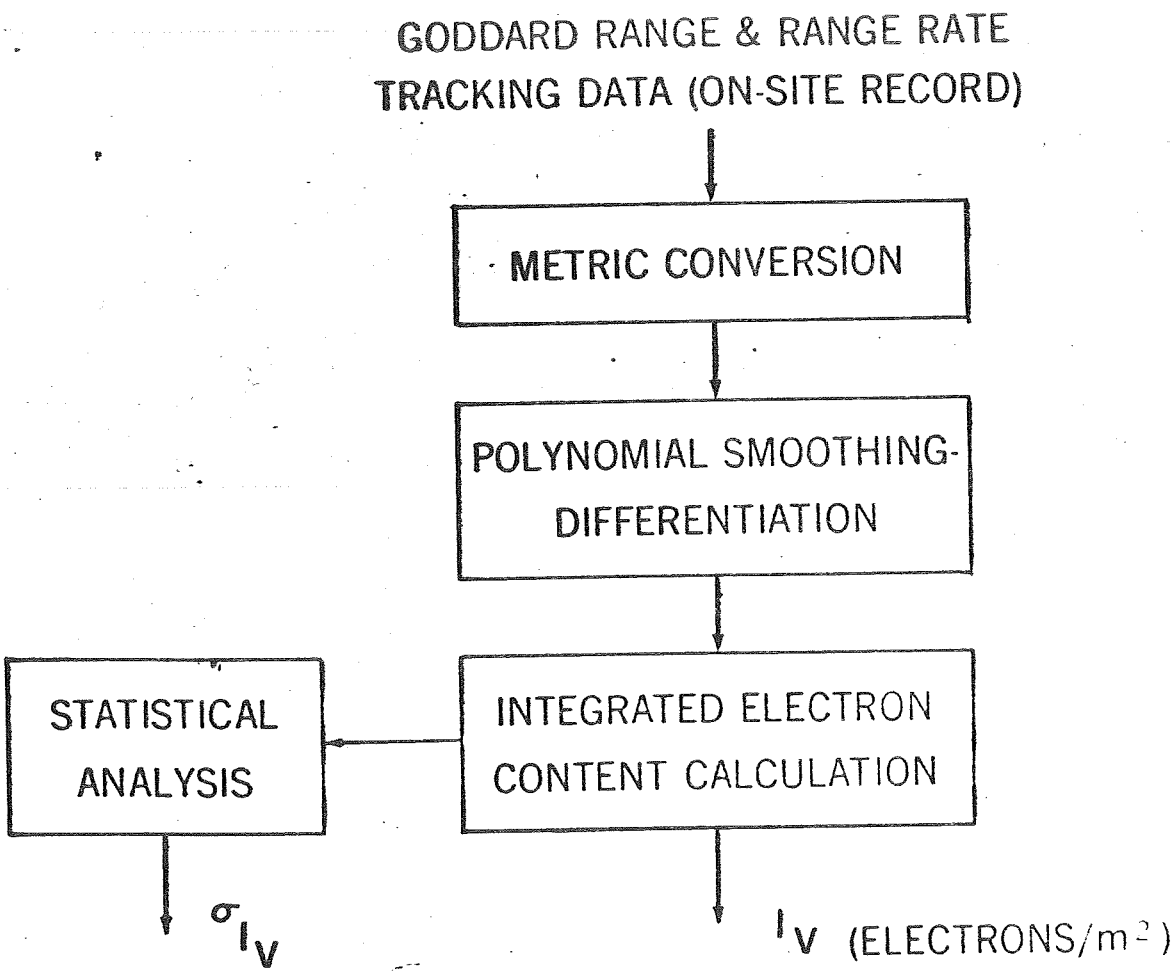

NASA GSFC T&DS
MISSION & TRAJECTORY ANALYSIS
BRANCH 551 DATE 10 June 70
BY P. SCHMID PLOT NO 1279

FIGURE 1

3. Effective aperture is closely linked to physical aperture or cross-section.

4. Energy transfer between an omnidirectional antenna and a fixed aperture antenna is independent of frequency providing the omnidirectional pattern falls within the beamwidth of the latter (reference 2).

Thus, the motivation for the analysis presented in this paper is two fold, namely:

1. The experimental verification of GEOS-2 ionospheric correction equations as applied to range tone delay and carrier Doppler phase, and

2. Investigation of a possible procedure for real-time ionospheric corrections to VHF Goddard Range and Range Rate tracking data such as associated with the forthcoming RAE-B (Radio Astronomy Explorer) scheduled for launch in late calendar 1972.

The basic tracking data handling for such electron content extraction is indicated in figure 1. Metric conversion is the conversion of time delays, Doppler count times and X and Y angles to the desired quantitities range, range rate, aximuth angle and elevation angle. The polynomial smoothing and differ-ententiation leads to those quantities used in the calculation of integrated electron content (elevation angle, elevation angle rate, range rate, and differentiated range). It also provides an estimate of the noise on each of these parameters which in turn is used to calculate the one-sigma uncertainty associated with the calculated integrated electron content at the mid-point of the selected data arc.

The midpoint of the data arc is selected because:

1. Calculation of the one-sigma uncertainty is easier to compute at the center and,

2. For uncorrelated noise and odd-ordered polynomials fit to the data, the uncertainty is a minimum at the center. For uncorrelated noise and even-ordered polynomials, the uncertainty is not a minimum at the exact data span center. However for any reasonable data stretch the difference between the ratio of the integrated electron content one-sigma uncertainty to the value of the integrated electron content as calculated at the center and as calculated as the exact point of minimum uncertainty is negligible.

TRACKING SYSTEM AND GEOMETRY

Since the experimental verification of the GEOS-2 ionospheric correction equations is based on Goddard VHF tracking data from the Explorer 34 spacecraft, a brief description of Explorer 34 orbit parameters and Goddard Range and Range Rate (GRARR) tracking system characteristics is in order.

ORBIT PARAMETERS:

Explorer 34, a spin stabilized 160 pound spacecraft, was launched on May 24, 1967 into the highly elliptical four-day period orbit indicated in figure 2. The vehicle reentered on May 3, 1969. This spacecraft was also known as IMP-4 or IMP-F. Currently another vehicle, IMP-G, is collecting scientific data in an orbit quite similar to that employed by IMP-F. This affords the opportunity of collecting tracking data during passes which accentuate the biasing effect of the ionosphere while minimizing data noise. As will be discussed more fully later, the best results in terms of low variance and repeatibility in extracting electron content from VHF GRARR data have been during near-Earth (i.e., perigee) passes. It is expected that use of the 100 kHz tone (instead of the usual 20 kHz) and the use of 10 second Doppler integration times (instead of 1 second) will lead to satisfactory electron content calculations at lunar distances. The effect of spacecraft spin on range rate derived from carrier Doppler measurements is a most important consideration which is discussed in detail in reference 3, 4, and 5. This will not be elaborated upon at this time other than to state that the bias due to spacecraft spin has been completely modeled out in this analysis. In terms of magnitude, the spin bias for IMP-4 is on the order of 3 cm/sec whereas the bias due to the ionosphere during perigee passes is on the order of 30 cm/sec corresponding to night time values of integrated content measured as 10^{17} electrons/m^2. The absolute magnitude for the spin induced bias in a phase modulated tracking system is (from reference 4):

EXPLORER 34 ORBIT PARAMETERS

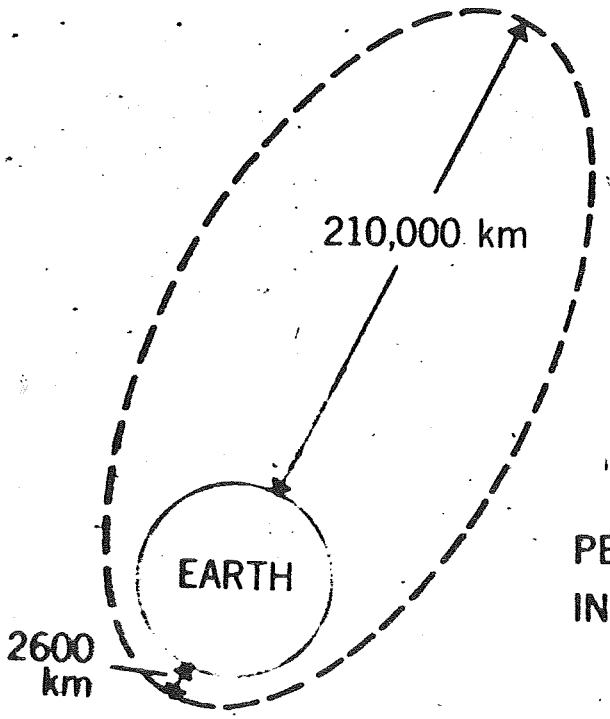

EXPLORER 34 = IMP-F = IMP-4
13 DECEMBER 1968

PERIOD ≐ 4 DAYS
INCLINATION ≐ 66°

LAUNCHED 24 MAY 1967
RE-ENTERED 3 MAY 1969

UP-LINK CARRIER FREQUENCY = 148.260 MHz
DOWN-LINK CARRIER FREQUENCY = 136.140 MHz

SPACECRAFT RF POWER 4 WATTS PHASE MODULATED (30% IN CARRIER)

FIGURE 2

$$|\Delta f| = \frac{\left|1 \pm \frac{1}{k}\right|}{2} f_s \lambda_t \qquad (1)$$

where

k = spacecraft transponder turnaround ratio

λ_t = up link transmission wavelength

f_s = spacecraft spin rate.

The $\pm$ sign for a given spin sense depends upon relative spacecraft transponder receive-transmit polarizations. Note that the result is independent of the aspect angle.

The absolute sign of the spin bias is positive if the transmit polarization is in the same sense as the spin (IMP-4), negative if opposite sense. For the VHF GRARR system k = 12/13, $\lambda_t \doteq 2$ m. For IMP-4 $f_s \doteq 0.4$ revolutions per second and the minus spin in equation (1) is appropriate.

The VHF GRARR tracking sites are listed in figure 3. Each site also has S-Band GRARR capability such as used to track GEOS-2. At present simultaneous VHF and S-band tracking is not possible because of shared subsystems.

VHF TRACKING SYSTEM PERFORMANCE:

The GRARR tracking system, like many similar schemes, employs range tones narrow band phase modulated (modulation index less than unity) onto a carrier. This signal is transmitted from ground station to spacecraft where it is translated by an onboard oscillator and re-transmitted to the ground site. The downlink carrier is derived from the onboard translation oscillator. Sidebands proportional to the Doppler shifted uplink frequency are phase modulated onto this carrier. After ground receiver combining and detection of

GODDARD VHF RANGE AND RANGE RATE TRACKING SITES

SITE	LATITUDE	LONGITUDE
FAIRBANKS, ALASKA	64.97°	-147.51°
ROSMAN, NORTH CAROLINA	35.19°	-82.87°
SANTIAGO, CHILE	-33.15°	-70.67°
CARNARVON , AUSTRALIA	-24.90°	113.72°
TANANARIVE, MADAGASCAR	-19.02°	47.30°

NOMINAL ANTENNA GAIN=20dB

TRANSMIT POWER=10kw (cw)

FIGURE 3

carrier and sidebands a Doppler output is obtained which corresponds to the result which except for spacecraft spin bias, would also have been obtained had a coherent (i.e., phase locked) transponder of turn-around ratio of k = 1 been employed.

The key to the ionospheric data derived from raw VHF tracking data is the different manner in which the electron plasma affects the range tone (group delay) and carrier Doppler range rate (phase delay). This will be discussed more fully in the next section. However, the important point, in terms of required tracking system performance is low random noise for angle, angle rate, range rate, and range measurements. The systematic range bias, as will be shown, is of no consequence since it is differentiated out. Also there is no reason to expect systematic range rate offsets (other than due to spacecraft spin and ionosphere) since the Doppler comparisons are made in real time with two-way radiowave propagation time short relative to local and reference oscillator short term stabilities (reference 6).

Figure 4 shows the expected range noise related to slant range from the tracking site. The calculation is based upon an assumed omnidirectional (0dB) spacecraft antenna, 1 watt radiated power and no radio frequency system losses. IMP-4 radiated 4 watts (reference 7) via a turnstile antenna (nominal 0dB gain relative to isotropic) and the measured range noise levels during perigee passes range typically from 3 to 10 meters. This is considered reasonable agreement since the radio frequency losses plus variations in antenna gain versus aspect angle can easily add 5 to 10 dB fluctuations. Three important points are to be noted regarding GRARR VHF ranging - first, the range tone jitter becomes thermal noise limited at approximately 20,000 km for the assumed parameters - second, the entire noise level can be reduced by a factor of 5 by switching in the 100kHz range tone and finally the thermal limited noise can be reduced by a factor of 3 by switching in the 0.1 Hz (instead of 1.0 Hz) tracking filter. The range measurement noise is linked to range tone phase measurement noise by:

VHF RANGE NOISE

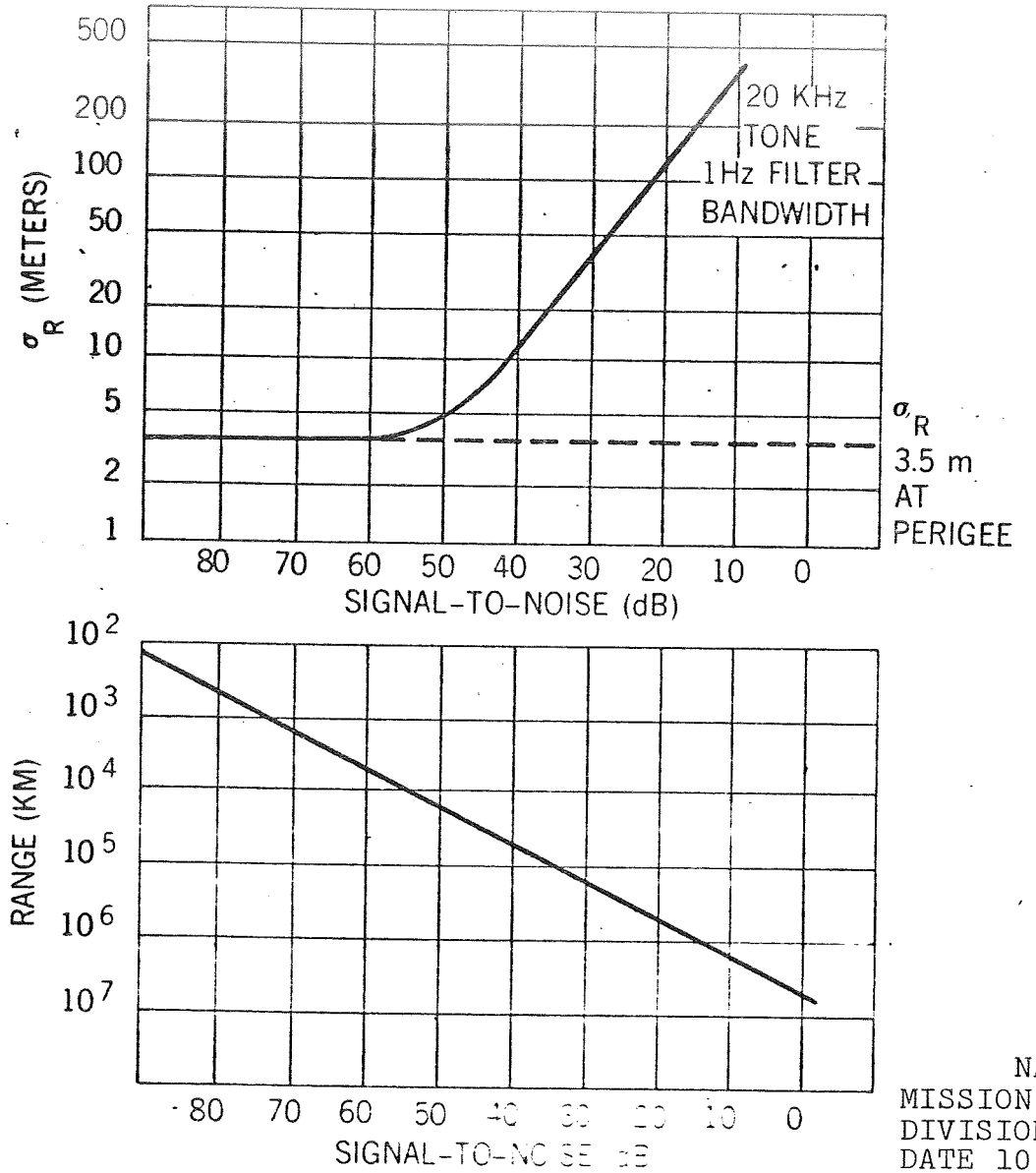

NASA GSFC-T&DS
MISSION & TRAJECTORY ANALYSIS
DIVISION BRANCH 551 DATE
DATE 10 JUNE 70, P. SCHMID
PLOT NO. 1280

FIGURE 4

$$\Delta R = \left(\frac{\Delta\Phi}{2\pi}\right) \left(\frac{\lambda m}{2}\right) \qquad (2)$$

where

$\Delta\Phi$ = phase jitter (radians)

λ_m = tone wavelengths (reference 7)

Using analogous link parameters one obtains the range rate noise characteristics indicated in figure 5. Usual near-Earth operation (i.e., unless otherwise requested) corresponds to 1 per second data at a 1 kHz loop bandwidth. Measured noise in this case, however, exceeds the 6 cm/sec indicated in figure 5, due to the cyclic component to the Doppler measurement introduced by the non-uniform phase pattern of the rotating spacecraft antenna. If this harmonic component (typically 30 cm/sec amplitude sinusoid) is modeled out range rate noise values corresponding to figure 5 are achieved. However, at present only the spin induced Doppler bias is modeled out while the sinusoidal variation is taken out by means of the polynomial smoothing (figure 1).

Finally, the integrated electron content measurement while not a critical function of elevation angle (figure 6), is quite sensitive to angle rates. Thus, boresight pointing biases are again differentiated out; however, it appears that monopulse angle data taken below 20° elevation begins to become corrupted in harmonic fashion by multipath propagation as a result of the relatively broad ground site antenna beamwidth (nominally 15°). In the data used for this paper, one sigma noise over a one to three minute data time span for angle data ranges from 0.01° to 0.07°

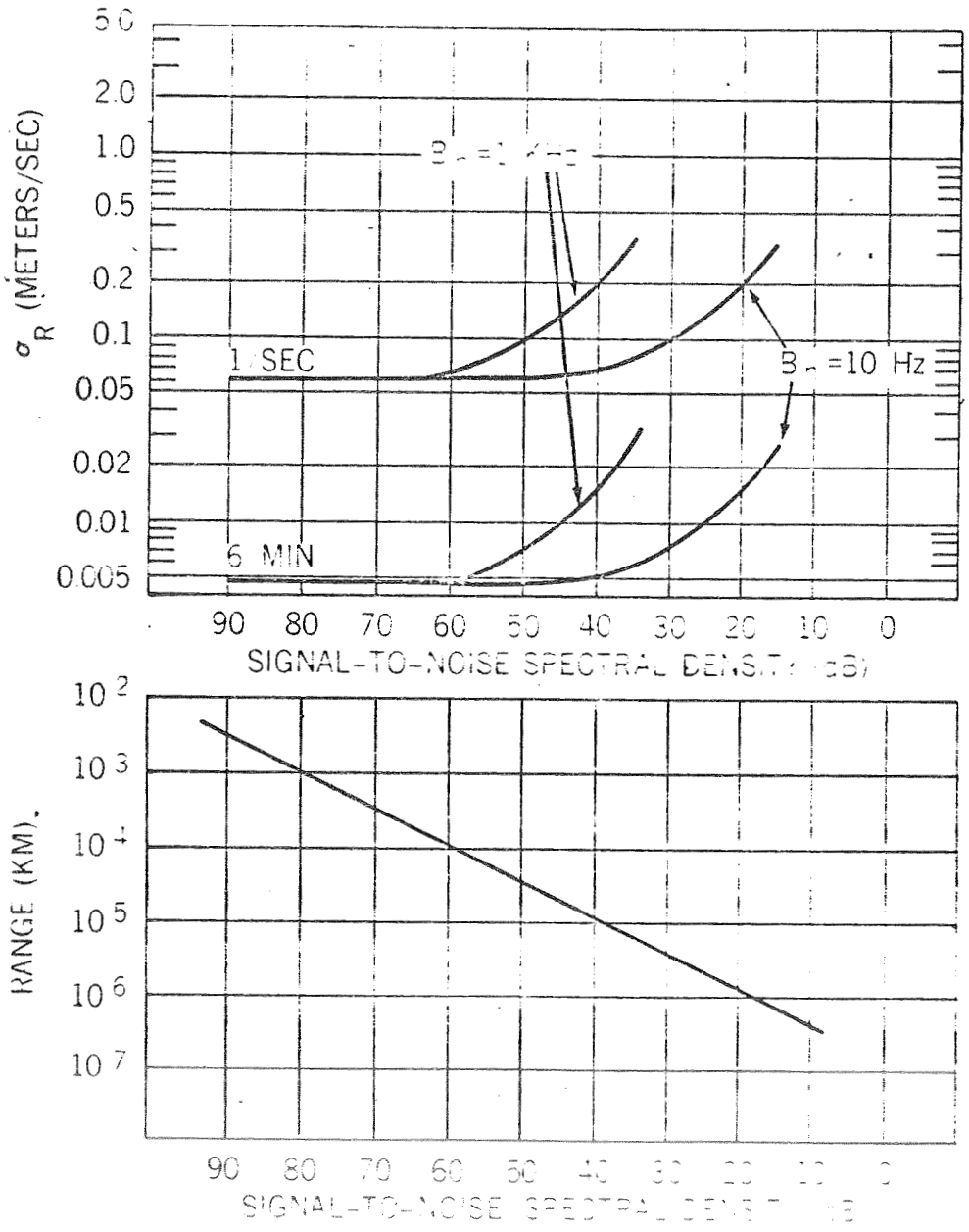

FOR
1/SEC RATE
σ_R
6 cm/sec
AT PERIGEE

Curves from Goddard Range and Range Rate System Design Evaluation Report General Dynamics Report NR.R-87-042 13 December 1967

FIGURE 5

TOP VERTICAL

EXTRACTION OF INTEGRATED ELECTRON CONTENT FROM TRACKING DATA

The following will show how the comparison of differentiated range based on sidetone ranging with range rate based on carrier Doppler leads to a value of the integrated electron content, I_V, in a vertical column above the tracking site.

RANGE IONOSPHERIC BIAS:

Figure 6 indicates the need for range corrections at VHF frequencies. Dyatime range biases easily exceed a kilometer. Range rate bias, which results from the changing phase path length as the ionosphere is scanned, can introduce meters per second of systematic error compared to system resolutions on the order of 0.5 cm/sec (refer to figure 5). Because of the extreme variability of the daytime ionosphere (e.g., factor of 3 day-to-day variations of total electron content) modeling of such biases has not been very successful. If VHF ranging is employed, real time ionospheric bias corrections are highly desirable. The magnitude of the range is bias can be estimated by:

$$\Delta R \doteq -10^{-6}\int N(s)\,ds = \frac{40.3}{f^2}\int N_e(s)\,ds = \left(\frac{40.3}{f^2 \sin E}\right) I_V \qquad (3)$$

(references 1 and 8)

where N = refractivity of ionosphere along path between ground station and spacecraft (index of refraction is given by $n = 1 + n(10^{-6})$ $n < 1.0$

f = frequency of transmission, for VHF GRARR use geometric mean i.e. $1/2\left(\frac{1}{f_u^2} + \frac{1}{f_d^2}\right)^{1/2}$ in Hz

(Reference 9)

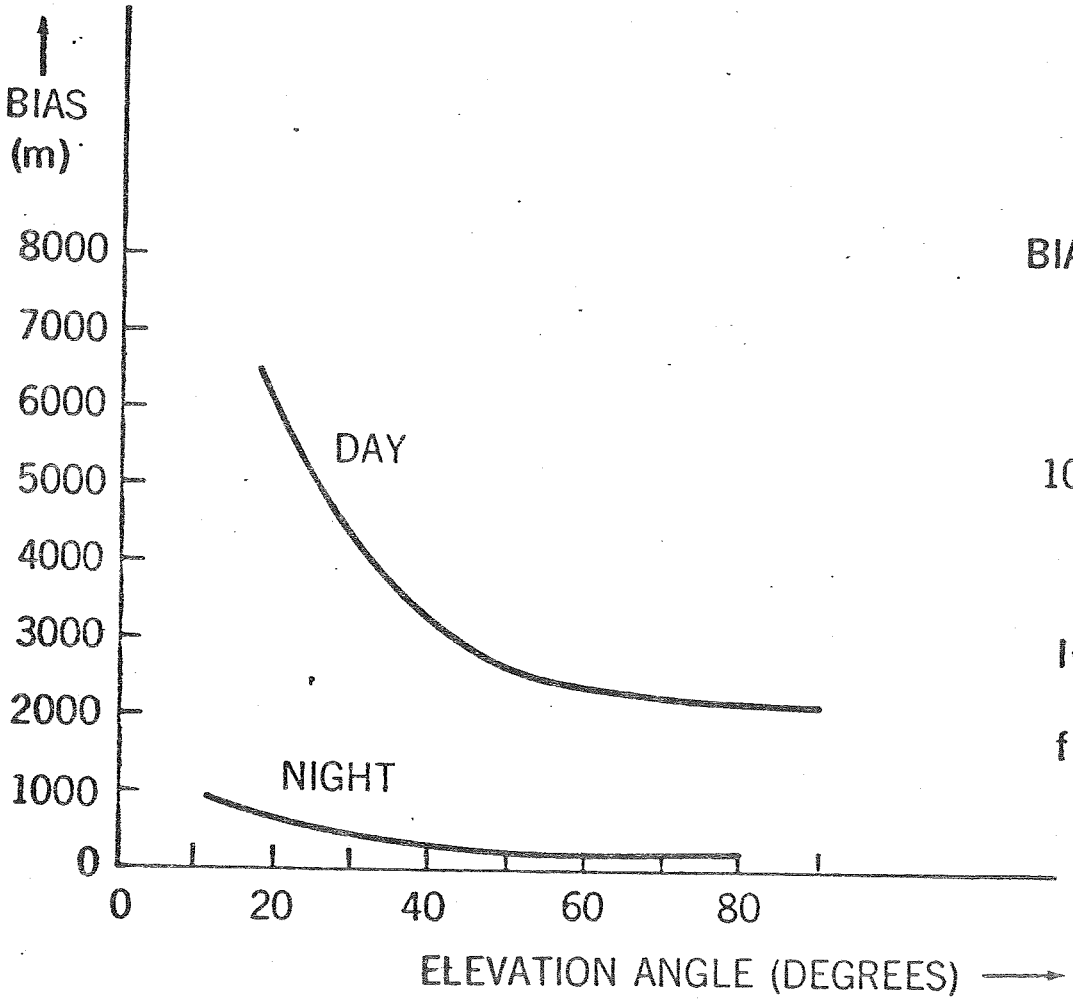

$$\text{BIAS} \doteq \frac{40.3\, I_V}{f_o^2 \sin E} \quad \text{(m)}$$

f_o = FREQUENCY (Hz)

$10^{16} < I_V < 10^{18}$ ELECTRONS/m^2

FOR THIS GRAPH

$I_V = 10^{17}$ (NIGHT) 10^{18} (DAY)

$f_o = 140$ MHz

NASA GSFC T&DS
MISSION & TRAJECTORY ANALYSIS
DIVISION BRANCH 551
DATE 10 JUNE 1970
BY P. SCHMID PLOT NO. 1281

82

FIGURE 6

N_e = electron density along ray path (electrons/m^3)

I_v = vertical integrated content above tracking station (electrons/m^2)

E = local elevation angle at the ray path at an altitude of 400 km = elevation angle at ground station

Equation (3) expresses the measured excess in range over free space range when the speed of light is used in rotating range tone group delay to true range assuming tropospheric bias is modeled out. Tropospheric component is frequency independent in the usual range of interest (20 MHz to 20,000 MHz) and has a maximum of approximately 25 meters at 5° elevation (reference 1). The troposphere range bias also has a 1/sin E dependence. At 140 MHz the ionospheric bias is seen (figure 6) to be in general much greater than that attributable to the troposphere. One can differentiate equation (3) with respect to time to obtain:

$$\dot{\Delta R} = \frac{\Delta R_1 - \Delta R_2}{\Delta T} = -\left(\frac{40.3 \cos E}{\sin^2 E}\right)\left(\frac{I_v}{f^2}\right)\dot{E} \qquad (4)$$

where:

$\dot{\Delta R}$ = ionospheric range rate bias based on range tone measurements.

$\dot{E}$ = elevation angle rate (radians/sec)

and all other parameters are as previously defined.

A more sophisticated model for the ionosphere (see equation 3) might be inserted for the integrated content along the ray path to obtain:

$$\Delta\dot{R} = -\frac{40.3}{f^2}\,\dot{E}\,\frac{\partial}{\partial t}\int N_e(s)\,ds \qquad (5)$$

However, equation (4) is what was used in the preliminary experimental verifications presented in this paper.

RANGE RATE IONOSPHERIC BIAS:

The ionospheric bias on the range rate measurement based carrier Doppler, as will be shown, is approximated by:

$$\Delta\dot{r} = \left(\frac{40.3\cos E}{\sin^2 E}\right)\left(\frac{I_v}{f^2}\right)\dot{E} \qquad (6)$$

where $\Delta\dot{r}$ is the ionospheric range rate bias based on carrier Doppler measurements

It will be noted that the only difference between equations (5) and (6) is in sign. This is the basis of the integrated electron content calculation since (5) and (6) can be combined to yield:

$$I_v = \left(\frac{1}{80.6}\right)\left(\frac{f^2}{\dot{E}}\right)\left(\frac{\sin^2 E}{\cos E}\right)\left(\dot{r} - \frac{dR}{dt}\right) \qquad (7)$$

where: $\dot{r}$ = measured range rate minus spin bias given by equation (1)

$\frac{dR}{dt}$ = differentiated range measurement

THEORETICAL BASIS FOR INTEGRATED ELECTRON CONTENT CALCULATION:

The basic principle involved in the integrated electron content extraction can be derived by considering the somewhat idealized case of unity frequency turnaround at the spacecraft. The resultant ionospheric range tone and Doppler phase bias thus determined is identical to that obtained with the actual GRARR tracking system except the frequency to be considered in the ionospheric bias calculation is a function of both up and down link frequencies (refer to equation 3) rather than a single frequency (reference 9).

Consider the following narrowband phase modulated signal:

$$E = \cos\ (\omega_o t + \beta \sin\ \omega_m t\ ) \qquad (8)$$

where:

$\omega_o = 2\pi f_o$ angular uplink carrier frequency

β = index of modulation ≤ 1.0

$\omega_m = 2\pi f_m$ angular range tone frequency

As is well known, the carrier and principal sidebands of such a signal are of the form:

$$\begin{aligned} &\cos\ \omega_o t \\ &\cos\ (\omega_o + \omega_m)\ t \\ -&\cos\ (\omega_o - \omega_m)\ t \end{aligned} \qquad (9)$$

which is the type spectrum transmitted up to spacecraft and back during GRARR tracking. The highest frequency tone, f_m, normally used with VHF GRARR is 20 kHz. Since this is a phase modulated scheme the absolute signal amplitudes during normal operation do not affect the range or Doppler measurement. Thus, the effect of two-way transit through the ionosphere on these three discrete frequencies is to be examined in terms of the Doppler and range phase demodulation at the ground site.

Doppler Phase Measurement

The effect of two-way transit through the ionosphere on Doppler phase measurement is as follows:

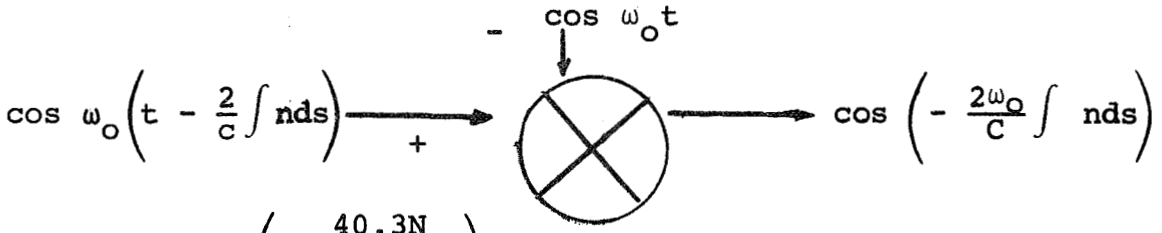

but $n = \left(1 - \frac{40.3N_e}{f^2}\right)$

(see equation 3)

Therefore the range rate phase is given by:

$$\dot{\phi}_R = \frac{-2\omega_o}{c}\left[R - \frac{40.3I_V}{f^2 \sin E}\right] \qquad (10)$$

where:

R = "true" slant range based on time delay

C = speed of light

Range Tone Phase Measurement

The effect of the same two-way transit on the range phase delay measurement is as follows:

$$\cos\left[\left(\omega_o+\omega_m\right)\left(t-\frac{2}{c}\int n_1 ds\right)\right] - \left[\left(\cos\ \omega_o-\omega_m\right)\left(t-\frac{2}{c}\int n_2 ds\right)\right]$$

CARRIER — SIDEBANDS

$\cos\ \omega_o\left(t-\frac{2}{c}\int nds\right)$ → $\frac{\pi}{2}$ → ⊗ ← $\cos W_m t$ REFERENCE TONE

$$\phi_R = \frac{2\omega_m}{c}\left(R + \frac{40.3I_v}{f^2 \sin E}\right) \qquad (11)$$

The foregoing results from the frequency dispersion introducted by the ionosphere which by way of equation 3 is linked to the respective index of refraction calculations in the following manner:

$$\frac{2}{c}\int nds = 2\left(\frac{R}{c} - \frac{40.3I_v}{f_o^{\,2}\sin E}\right)$$

$$\frac{2}{c}\int n_1 ds = 2\left\{\frac{R}{c} - \left[\frac{40.3I_v}{f_o^{\,2}\sin E}\right]\left[1 - \frac{2f_m}{f_o}\right]\right\}$$

$$\frac{2}{c}\int n_2 ds = 2\left\{\frac{R}{c} - \left[\frac{40.3I_v}{f_o^{\,2}\sin E}\right]\left[1 + \frac{2f_m}{f_o}\right]\right\}$$

Differentiation of equation 10 results in the usual expression for range rate and in the GRARR system is approximated by averaging the phase change over the time required to count a fixed number of cycles of the difference frequency plus an inserted offset bias frequency which is required to permit range rate sign determination. The difference between "time" range rate at the center of the count interval and the measured "average range rate" is a function of averaging time and the magnitudes of the odd time derivatives (i.e., 3, 5, 7...) of range (reference 10). For the IMP-4 data arcs described in the next section, the difference between "true" and "average range rate" was negligible. Equation 11 presents the measured range tone phase. Differentiation of this result and comparison with carrier Doppler range rate results in equation (7) presented previously for calculation of integrated electron content I_V. If the spacecraft is spin stabilized, then as indicated by equation (1), the carrier Doppler determined range rate must be adjusted accordingly.

EXPERIMENTAL RESULTS

In order to facilitate data analysis the plotting routine indicated in figure 7 was written. Each data stretch is examined to provide the necessary inputs required for the calculations of integrated electron content, namely, elevation angle, elevation angle rate, measured range rate and differentiated range. A typical film printout of the comparison of $\dot{r}$ and $\frac{dR}{dt}$ is given by figure 8. This film sequence which presents the calculated electron content also includes such pertinent parameters as the one-sigma limits on range noise, range rate noise and integrated electron content. Station identification, epoch, and tracked spacecraft nomenclature are also part of the standard output. Figure 8 resulted in a calculated value of I_V of 1.08 (10^{17}) electons/m^2 in a vertical column over Santiago, Chile at 10 PM local time on December 20, 1968. Subsequent values of I_V calculated at Santiago over a period of 90 minutes (figure 9) show

FILM DISPLAY OF DATA REDUCTION AND ANALYSIS

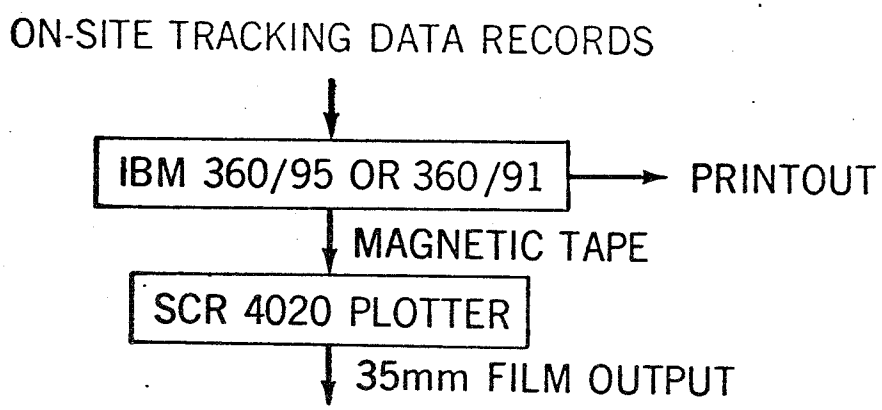

FILM OUTPUT PER DATA STRETCH INCLUDES THE FOLLOWING INFORMATION VERSUS GMT TIME

1. RANGE TONE DELAY
2. DOPPLER COUNT TIME
3. X-ANGLE MEASUREMENT
4. Y-ANGLE MEASUREMENT
5. CALCULATED ELEVATION ANGLE
6. ELEVATION ANGLE RATE
7. AVERAGE RANGE RATE & DIFFERENTIATED RANGE
   (THIS FRAME INCLUDES CALCULATED INTEGRATED ELECTRON CONTENT AT MID-POINT OF PASS)

NASA GSFC T&DS
MISSION & TRAJECTORY ANALYSIS
BRANCH 551 DATE 5 June 1970
BY P. SCHMID PLOT NO. 1282

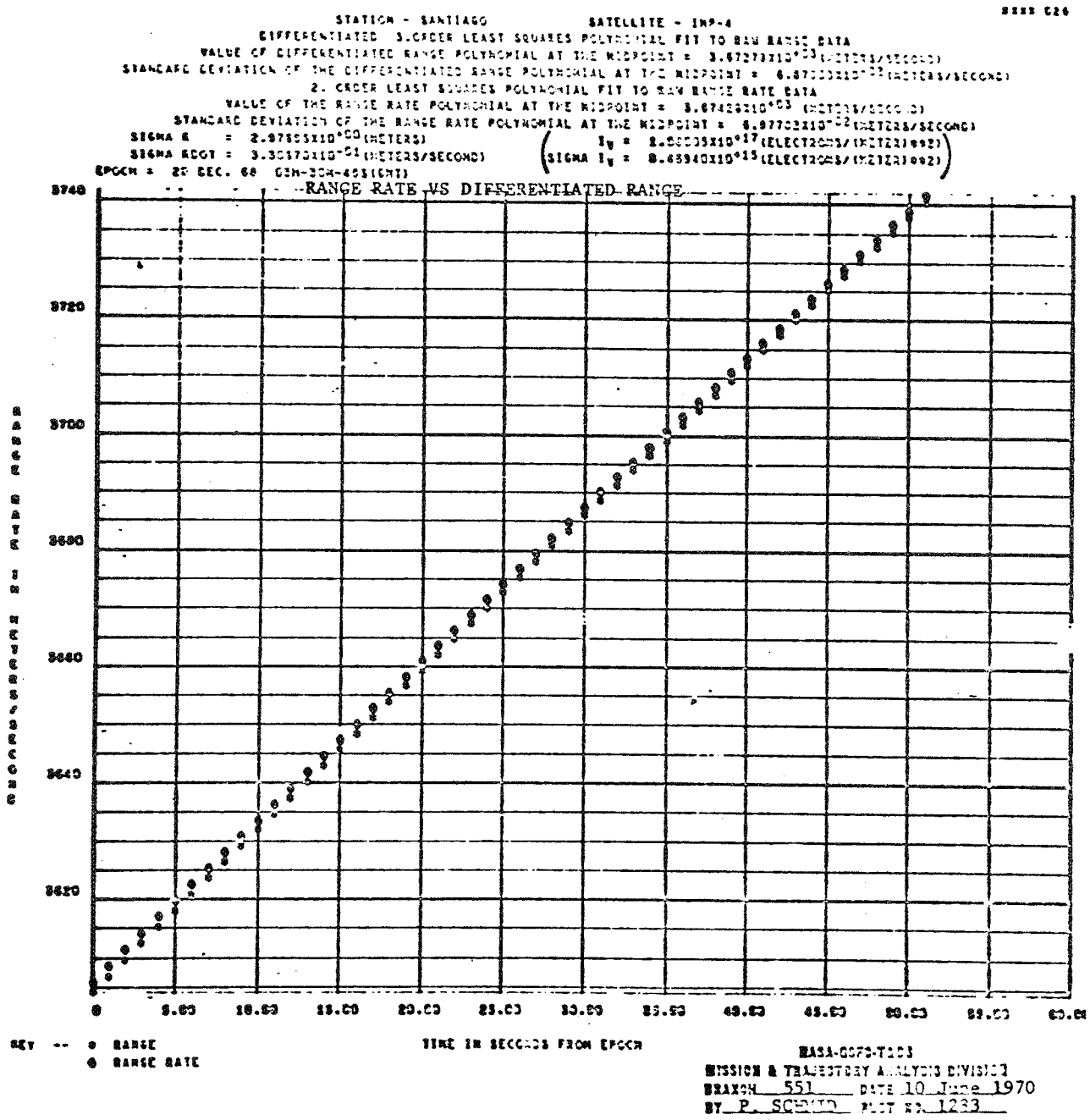
STATION - SANTIAGO SATELLITE - INP-4
DIFFERENTIATED 3.ORDER LEAST SQUARES POLYNOMIAL FIT TO RAW RANGE DATA
VALUE OF DIFFERENTIATED RANGE POLYNOMIAL AT THE MIDPOINT = 3.67279X10**03 (METERS/SECOND)
STANDARD DEVIATION OF THE DIFFERENTIATED RANGE POLYNOMIAL AT THE MIDPOINT = 6.87100X10**02 (METERS/SECOND)
2. ORDER LEAST SQUARES POLYNOMIAL FIT TO RAW RANGE RATE DATA
VALUE OF THE RANGE RATE POLYNOMIAL AT THE MIDPOINT = 3.67428X10**03 (METERS/SECOND)
STANDARD DEVIATION OF THE RANGE RATE POLYNOMIAL AT THE MIDPOINT = 6.97702X10**02 (METERS/SECOND)
SIGMA R = 2.97855X10**00 (METERS)
SIGMA RDOT = 3.30370X10**01 (METERS/SECOND)
I_V = 8.80035X10**17 (ELECTRONS/METER**2)
(SIGMA I_V = 8.48940X10**15 (ELECTRONS/METER**2))
EPOCH = 25 DEC. 68 03H-30M-46S(GMT)
--RANGE RATE VS DIFFERENTIATED RANGE--
RANGE RATE IN METERS/SECOND
3740
3720
3700
3680
3660
3640
3620
0
5.00
10.00
15.00
20.00
25.00
30.00
35.00
40.00
45.00
50.00
55.00
60.00
KEY -- * RANGE
* RANGE RATE
TIME IN SECONDS FROM EPOCH
NASA-GSFC-TIDS
MISSION & TRAJECTORY ANALYSIS DIVISION
BRANCH 551 DATE 10 June 1970
BY P. SCHMID PLOT NO. 1233

FIGURE 8

INTEGRATED ELECTRON CONTENT EXTRACTED FROM VHF RADIO AND RADIO STAR DATA

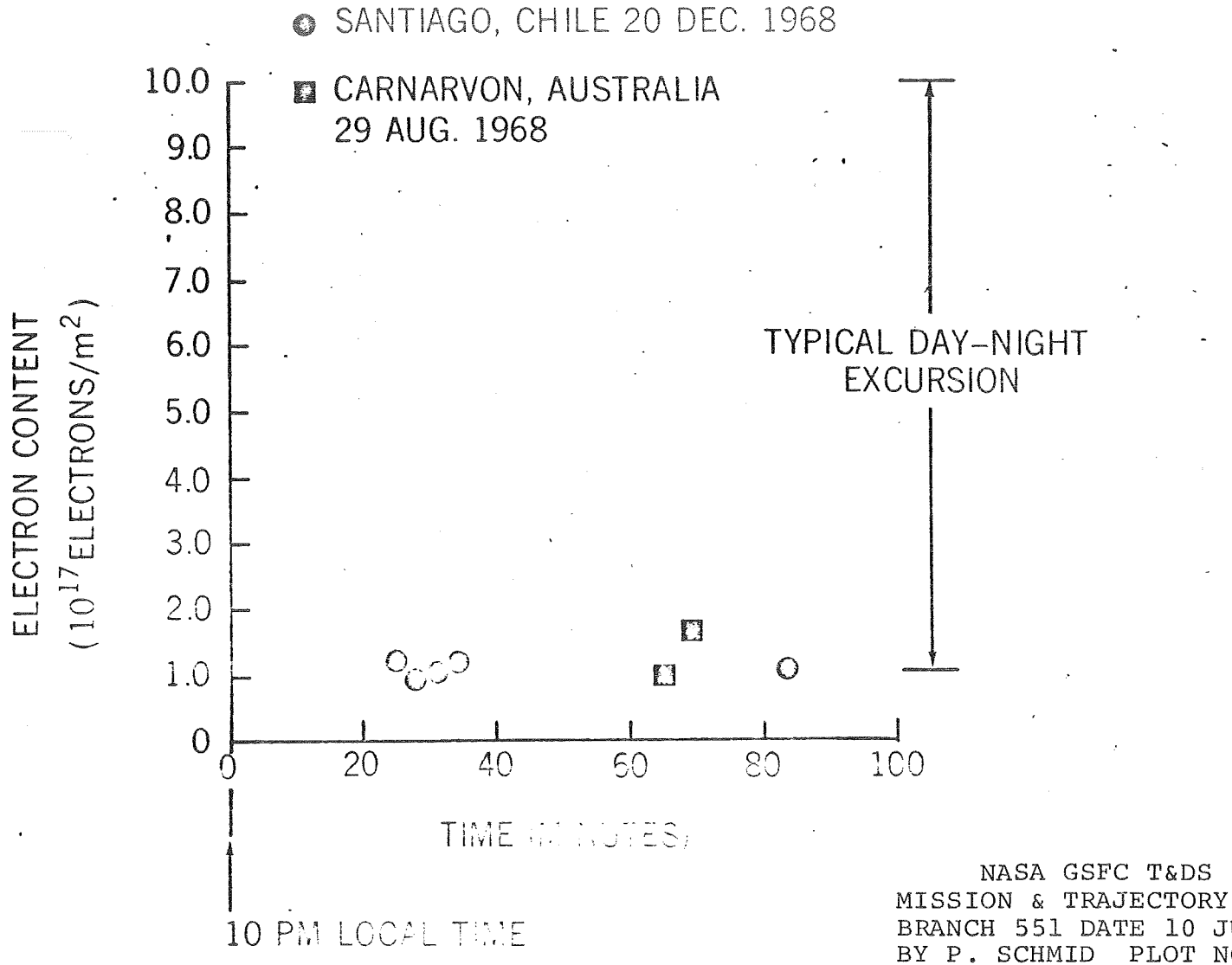

NASA GSFC T&DS
MISSION & TRAJECTORY ANALYSIS
BRANCH 551 DATE 10 JUNE 1970
BY P. SCHMID PLOT NO. 1284

FIGURE 9

After J. A. Klobuchar
September 1969

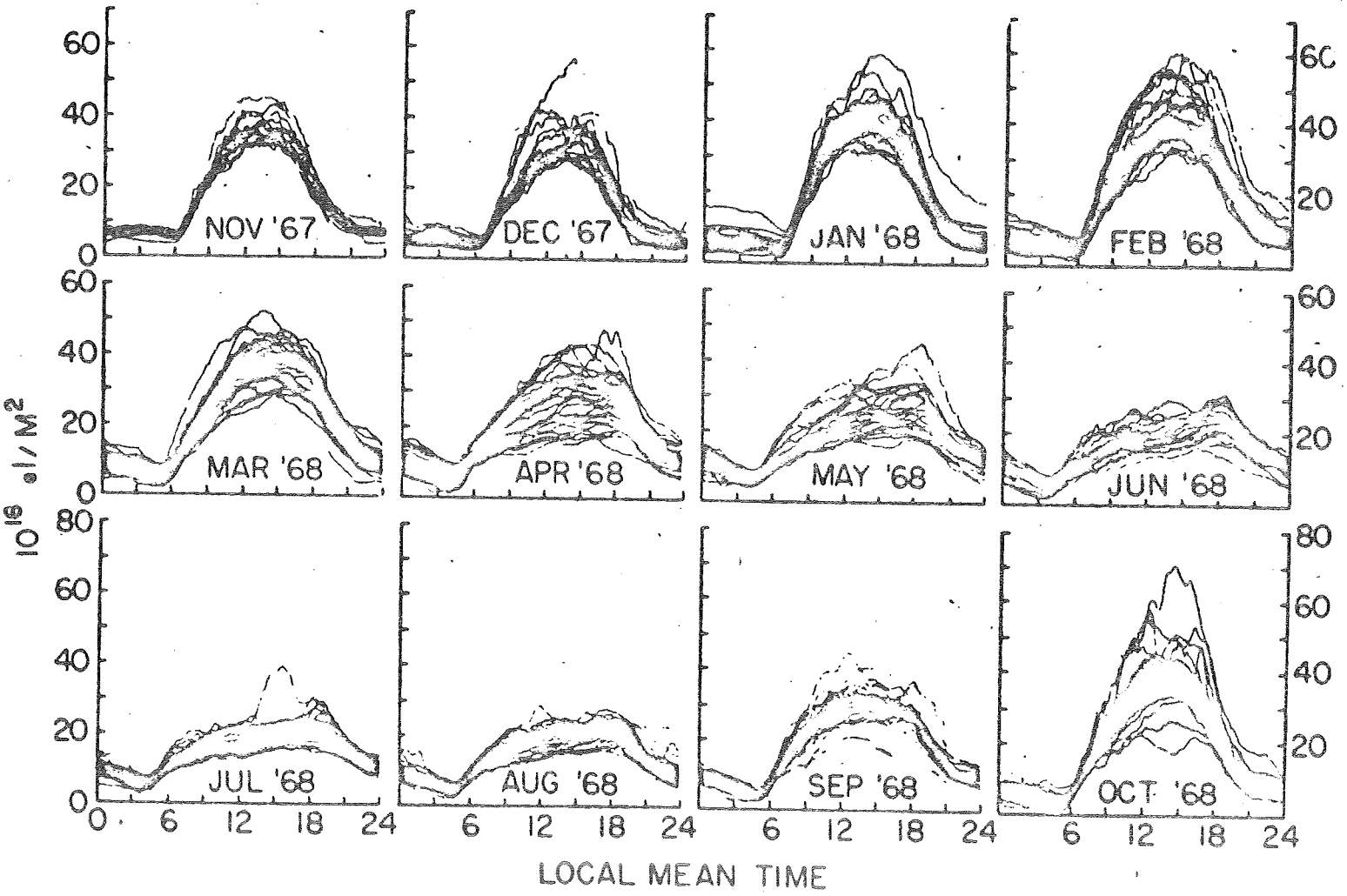

TOTAL EQUIVALENT VERTICAL ELECTRON CONTENT FROM HAMILTON, MASS. (Looking towards ATS-3).

FIGURE 10

DIURNAL VARIATION OF ELECTRON CONTENT AT THE UNIVERSITY OF HAWAII FOR OCTOBER 9–14, 1964, INCLUSIVE.

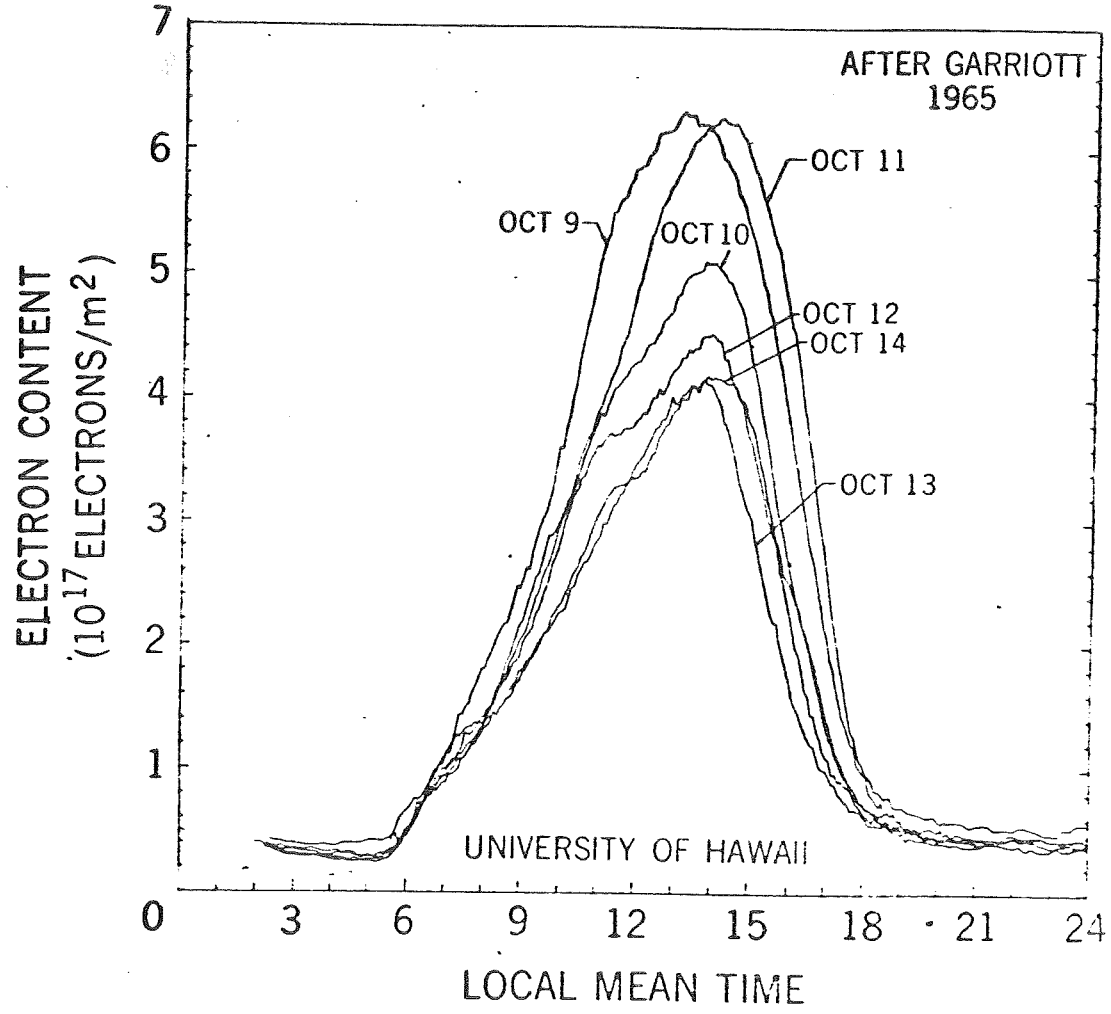

FIGURE 11

good agreement with an observed RMS deviation from the mean of 10%. This is also the calculated uncertainty based on angle range and range rate measurement noise. Figure 9 also includes two calculations from Carnarvon, Australia on August 29, 1968 at approximately 11 PM local time. The possibilities for further reducing measurement noise are discussed in the conclusions presented as the final section of this paper.

Figure 10, which is based on independent Faraday rotation data (reference 11) is presented as tentative verification of the electron content values extracted at, for example, Carnarvon on August 29, 1968, and Santiago on December 20, 1968. Since the total content varies between 10^{16} to 10^{18} electrons/m^2 depending on time of day, season, and state of solar activity, the calculated night time values of 10^{17} electron/m^2 appear quite reasonable for 1968, which was near the peak of the 11 year sunspot cycle. Figure 11 shows the night time (10 PM local) integrated content over Hawaii to be on the order 0.4 (10^{17}) electron/m^2 which reflects the lower sunspot activity of 1964. The last solar sunspot minimum occurred in 1964 and the maximum in 1968.

CONCLUSIONS

At VHF range measurements uncorrected for the ionosphere can be in error by kilometers. Uncorrected range rate can be biased by the ionosphere on the order of meters per second. Since the VHF GRARR tracking system resolution is on the order of a few meters in range and with a 10 second integration less than one cm/sec in range rate these biases must be modeled out. Since the range and range rate ionsopheric induced bias is directly proportional to I_v the integrated electron content, it is advantageous to measure I_v in real time.

The often used integrated electron content values based on average monthly predictions can easily be in error by 50%,

especially during the daylight hours. This paper has presented the theory and preliminary experimental verification whereby the desired quantity, I_v, is extracted directly from tracking measurements of angle, range and range rate at a nominal 140 MHz.

The accuracy of this electron content determination scheme can be improved and the concept perhaps extended to reliable lunar distance real time corrections. Such improvements are anticipated as a result of considerations to:

1. Include earth curvature
2. Model out harmonic terms in data due to spacecraft spin and multipath
3. Use longer doppler averaging time (6 per minute setting)
4. Use higher frequency range tone (100 kHz setting)
5. Use elevation angle rates based on orbit computation
6. Record VHF tracking data during more daytime passes (IMP-6)
7. Intercompare with best estimate ray traces based on top and bottom side sounding
8. Determine optimum data pass length
9. Investigate the calculation of electron content at points other than the midpoint of the data arc.

This work is part of a continuing effort within the Mission and Trajectory Analysis Division (GSFC) to improve the efficiency and accuracy of NASA tracking data utilization in orbit and trajectory computation.

ACKNOWLEDGEMENT:

The authors wish to acknowledge the excellent computer programming support provided by John F. Cook (code 551 MTAD-GSFC) who developed the entire SCR 4020 computer plot package based on the mathematics outlined in these pages.

REFERENCES

1. Schmid, P.E., "Atmospheric Tracking Errors at S- and C-Band Frequencies," NASA TN D-3470, August 1966.

2. Schmid, P.E., "The Feasibility of a Direct Relay of Apollo Spacecraft Data Via A Communication Satellite," NASA TN D-4048, August 1967.

3. Marini, J.W., and Murray, C.W., "Effect of Satellite Spin on Explorer 33 and 35 Doppler Tracking Data," GSFC X-551-69-52, February 1969.

4. Marini, J.W., "The Effect of Satellite Spin on Two-Way Doppler Range Rate Measurement," GSFC X-551-69-104, March 1969.

5. Murray, C.W., "Detection of Range Rate Bias in the Two-Way Doppler Measurements of Explorer 34," April 1970.

6. Goddard Range and Range Rate System Design Evaluation Report, General Dynamics Report Nr. R-67-042, December 13, 1967.

7. Kronmiller, G.C., Jr., Zillig, D.J., "The Goddard Range and Range Rate System Performance While Tracking IMP-F," GSFC X-571-67-532, November 1967.

8. DaRosa, A. V., "Propagation Errors in VHF Satellite-to-Aircraft Ranging," IEEE Transactions on Antenna And Propagation, Vol. AP-17, No. 5, Sept. 1969.

9. Parker, H. C., RCA-GSFC Support Group, "GRARR Ionospheric Errors," Memorandum to J. H. Berbert, Code 514 GSFC, November 28, 1969.

10. Schmid, P.E., "The Conversion of Fundamental Tracking Data to Metric Form," GSFC X-551-69-3, January 1969 .

11. Klobuchar, J. A., "Total Electron Content Predictions for the Systems Engineer," Proceedings of Symposium on the Application of Atmospheric Studies to Satellite Transmissions, Ionospheric Physics Laboratory, AFCRL, September 3-5, 1969

A TWO-LASER COLLOCATION EXPERIMENT

M. R. Pearlman, C. G. Lehr, G. M. Mendes, and M. R. Wolf

To be presented at Geos 2 Review Meeting
Goddard Space Flight Center, Greenbelt, Maryland

June 1970

Smithsonian Institution
Astrophysical Observatory
Cambridge, Massachusetts 02138

006-92

A TWO-LASER COLLOCATION EXPERIMENT

M. R. Pearlman, C. G. Lehr, G. M. Mendes, and M. R. Wolf

INTRODUCTION

A two-laser collocation experiment has been performed on the Geos 2 satellite with the Smithsonian Astrophysical Observatory (SAO) prototype ranging system and the NASA mobile laser unit. The object was to determine the relative accuracy of these two laser systems, both of which are being used in the routine collection of satellite geodetic data. The effort was conducted at the SAO Observatory at Mt. Hopkins, Arizona, during the period October 1969 to January 1970. The two laser systems demonstrated a relative accuracy of 1 to 2 m, determined from short-arc single-pass calculations. From a point-by-point analysis of near-simultaneous satellite returns, we were able to extract the displacement of the collocated lasers to an accuracy of a few meters over a baseline of ~130 m.

The laser data have also been included in 2-week long-arc calculations to which Baker-Nunn camera data were added. Laser range residuals of 10 m or better and angular-data residuals of 3 to 6 arcsec were achieved. From this long-arc analysis, relative station positions were determined to better than 10 m.

THE LASER SYSTEMS

The SAO ranging system is the prototype of the units being deployed at the Observatory's network of stations. It uses a ruby laser with an oscillator-amplifier configuration. The laser has an output of 7.5 J and a nominal pulse

This work was supported in part by grant NGR 09-015-002 from the National Aeronautics and Space Administration.

width of 15 nsec. The system has a static pointing mount that permits the laser to be pointed to predicted positions and fired by the clock at the appropriate epoch. This mode of operation enables us to range to satellites when they are in the earth's shadow and during daylight hours. Range measurements are made with a time-interval counter with a 1-nsec resolution. During the experiment, the laser was operated at a firing rate of 1 to 2 per min. Further details on the system are given by Lehr (1969) and Lehr and Pearlman (1969).

The NASA mobile unit (MOBLAS) used a ruby laser with an output of 1 J and a pulse width of 30 nsec. The laser has a firing-rate capability of 1 per sec. For the experiment the system had an on-site computer facility for tracking and searching purposes and used a 10-nsec time-interval counter for range measurements. The mobile laser is discussed in detail by Johnson, Plotkin, and Spadin (1967).

The NASA station was located approximately 100 m north of the SAO laser (see Figure 1). The experiment was divided into two phases, corresponding to two NASA locations (HOMLAS and HOMLA2) approximately 10 m apart on an east-west baseline. Phase I lasted through November 15, while Phase II comprised the remainder of the experiment. For the experiment, the SAO Mt. Hopkins laser was referred to as HOPLAS. Our intention was to retrieve the 100-m interstation separation and then to recover the 10-m shift in the MOBLAS station location.

SHORT-ARC ANALYSIS

We used short-arc single-pass analyses to make a simple and direct intercomparison between the two laser systems (see Tables 1a and b). Owing to the relatively large data rate of the NASA laser, we used their data to compute a short reference arc with which to compare the SAO satellite returns. The relative bias between the two systems was taken as the difference between the system biases to the reference arc. The standard deviation was taken as the square root of the sample variance.

During both phases of the experiment, the two systems demonstrated a relative ranging accuracy of 1 to 2 m. The relatively small number of SAO points listed per pass is attributed mainly to the relative data rates, but it also reflects the method of analysis. Only the SAO satellite returns that were encompassed by the NASA data or that fell very close to the extremities of the NASA data have been included.

The sign of the bias between the systems changed several times during the 4-month experiment, but it was predominently negative during Phase I and positive during Phase II. This bias component was probably introduced into one or both of the systems during the calibration procedure, which involved a determination of the system delay by ranging on a target at a known distance from each laser.

Measurements of this nature are extremely sensitive to changes in return-pulse height caused through variations in output-power level, receiver gain (including photomultiplier settings), counter trigger threshold, or attenuation in the optical train that may have occurred during the calibration procedure. Even a change of a factor of 2 in the ratio of pulse peak amplitude to trigger level can introduce a change in the system calibration equal to 25% or more of the pulse halfwidth. In our experiment, this error could be 0.5 m for the SAO system and 1.0 m for MOBLAS. These errors would be considerably larger for larger changes in the ratio of peak-signal strength to trigger threshold.

The standard deviations in the data for each system indicate that in the present configuration, each has a noise level of the order of 1 m. Considering the size of the output-pulse widths and the pulse-height statistics, this value appears to be quite reasonable. These systems would be capable of an improved signal-to-noise value if shorter pulses were used or if calibration and satellite range measurements took some account of pulse size and shape (Lehr, Pearlman, and Scott, 1970).

Several system errors were detected by the early collocation results. These included errors arising from system misalignment, calibration taken infrequently or not taken immediately following an instrumentation modification, and even overshooting the target during calibration. Each of these involved an error amounting to no more than a few meters and it is indeed gratifying that the lasers were capable of detecting these offsets while ranging to satellites.

DETERMINATION OF RELATIVE STATION POSITIONS

We calculated relative station coordinates by examining the pertinent geometry for pairs of nearly simultaneous data points taken by the two laser systems (see Table 2). Both the interstation baseline and the 10-m NASA station shift are clearly discernible in the data. The values for station separation are solutions of a least-squares fit of the appropriate data, and the residuals are the standard deviations. The SAO firing epoch was adjusted to be as close as possible to that of the NASA laser. Epoch differences were compensated for by linear interpolation between successive NASA data points. With this interpolation procedure, separations in firing time of up to 10 msec appear to be consistent with a 1-m accuracy. The 10-msec criterion was used in selecting data. Although the interpolations involved approximations and there were few data points, the results bear out the 1- to 2-m accuracy capability of the present laser systems.

LONG-ARC ANALYSIS

Long-arc calculations permit us to add significant amounts of Baker-Nunn data to the analysis and thereby test the relative accuracies of two independent techniques. In addition, long-term orbits are essential for the dynamical geodesy that we hope to do with the satellite data. Accordingly, it is of interest to see how well we can fit long arcs to the data.

We used the 1969 Smithsonian Standard Earth (II) to calculate two-week orbits from laser and photoreduced Baker-Nunn data (see Table 3). To maintain

a reasonable balance in the data, we selected every tenth NASA return instead of using the total data. In the orbital solutions, the laser and camera observations have been given weights of 5 m and 4 arcsec, respectively. For these solutions, the standard errors of unit weight are in the vicinity of 1.0, indicating that the choice of weights is reasonable. It must be pointed out that we have a preponderance of laser data that are not well distributed; consequently, our orbits probably do not represent the best that could be obtained.

The value chosen for the Baker-Nunn camera data is an estimate of its accuracy. The residuals obtained in the solution were in the neighborhood of 3 to 6 arcsec.

The accuracy of the laser data appears from the short-arc analysis to be well below the 5-m weight ascribed to it. However, the uncertainties in the gravity-field model, which are larger than the errors in satellite range measurements, dominate the solutions for the laser data.

When the standard error of unit weight is very nearly equal to 1.0, the laser residuals are close to the 5-m weighting factor. For values below 1.0, the residuals are small, indicating that the lasers may be weighted too heavily for this particular solution. Alternatively, for data in which the standard error of unit weight is above 1.0, the lasers are probably not being weighted enough, and indeed the accompanying range residuals are quite large.

Relative station locations have been extracted from the long-arc solutions (see Table 4). Averaging over the limited amount of data does not permit us to overcome the existing modeling errors. We are able to separate the NASA and SAO station locations but do not have enough accuracy to measure the MOBLAS station shift with any reasonable certainty.

CONCLUSIONS

We conclude that lasers are capable of ranging to an accuracy of 1 to 2 m with respect to one another. We also find that the laser data, when compared to the Baker-Nunn camera data, appear to be at least as good as the gravity model used in the calculation.

Considerably more data would be required to obtain better results with long-arc analyses. This conclusion comes as no surprise, as we know the enormous amounts of data that will be required to pursue any reasonable program in dynamical geodesy.

REFERENCES

JOHNSON, T. S., PLOTKIN, H. H., and SPADIN, P. L.

1967. A laser satellite ranging system. IEEE Journ., vol. QE-3, No. 11.

LEHR, C. G.

1969. Geodetic and geophysical applications of laser satellite ranging. Paper presented at IEEE Geoscience Electronics Symposium, Washington, D.C., April.

LEHR, C. G., and PEARLMAN, M. R.

1969. Laser ranging to satellites. Paper presented at COSPAR International Space Science Symposium, Prague, Czechoslovakia, May.

LEHR, C. G., PEARLMAN, M. R., and SCOTT, J. L.

1970. A photographic technique for improved laser ranging accuracy. This conference.

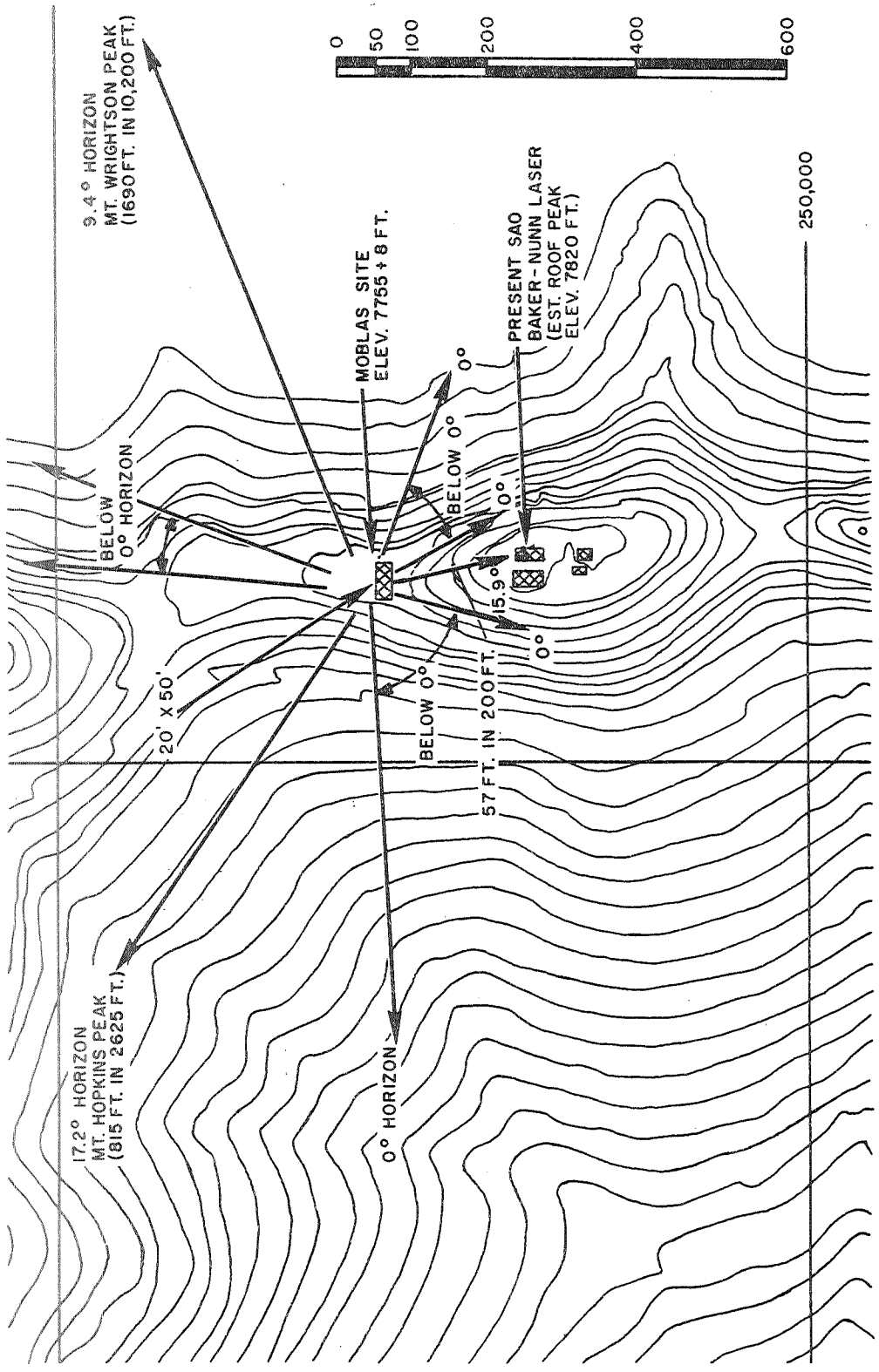

Figure 1. Collocated stations.

Table 1a.

LASER COLLOCATION EVALUATION
(short arc)
PHASE I

Pass	Range Bias	Hoplas		Homlas	
Date Time	Hoplas-Homlas (meters)	No. Returns/St.	Dev.(m)	No. Returns/St.	Dev(m)
10/06 09h	.7	6	1.0	423	1.0
10/09 19h	.5	5	1.3	222	1.2
10/12 09h	1.5	3	3.3	186	1.2
10/16 09h	- .3	5	1.8	221	1.2
10/18 09h	- .6	5	.8	314	.9
10/19 10h	1.3	3	.5	153	.9
10/23 09h	-1.3	6	.6	299	1.1
10/23 20h	-1.0	5	.6	284	.9
10/25 10h	-1.9	4	1.3	152	.9
10/29 20h	-2.2	4	.6	290	.9
10/30 20h	-2.2	3	1.1	373	1.0
10/31 20h	-1.6	3	1.4	463	1.2
11/06 10h	-1.1	4	1.6	237	1.1

Table 1b.

LASER COLLOCATION EVALUATION
(short arc)
PHASE II

Pass	Range Bias	Hoplas		Homla2	
Date Time	Hoplas-Homla2 (meters)	No. Returns/St. Dev.(m)		No. Returns/St. Dev.(m)	
12/13 11h	2.0	6	1.1	372	1.3
12/14 11h	1.2	4	1.6	206	1.0
12/19 11h	1.2	8	1.2	197	1.0
12/19 21h	.8	4	.6	374	.9
12/20 11h	- .9	2	.9	244	1.0
12/20 22h	.6	4	.7	306	1.1
12/21 11h	4.4	5	1.4	83	.8
12/21 22h	2.0	3	.8	140	1.1
12/23 21h	2.4	4	1.2	82	1.0
1/14 22h	-1.4	2	1.8	245	1.1
1/16 12h	.3	2	1.1	150	1.0
1/27 12h	1.1	12	.9	359	1.2
1/29 11h	1.8	6	1.6	66	1.2
1/30 11h	-2.1	11	1.2	223	1.1
1/31 22h	.7	6	1.3	163	1.2

Table 2.

INTERSTATION SEPARATION

(NASA-SAO)

Coordinate	No. Data Pairs	Calculated(m)	St. Dev.(m)	Surveyed(m)	
N	17	132.0	.7	132.9	
E	17	- 1.4	1.1	0.3	PHASE I
Z	17	- 20.1	.4	- 18.3	
N	25	130.3	1.0	130.1	
E	25	- 14.2	1.2	- 10.3	PHASE II
Z	25	- 17.1	.6	- 18.4	

Table 3.

LONG-ARC RESIDUALS

LASER STATION	Oct 1-15	Oct 16-31	Nov 1-15	Nov 16-30	Dec 1-15	Dec 16-31
Arizona - SAO Laser Residuals (m)	6.0	9.9	5.8	7.6	5.8	2.0
No. Passes	9	12	4	6	5	6
Arizona - NASA Laser Residuals (m)	4.1	9.2	5.5	2.5	5.0	3.1
No. Passes	7	15	6	2	7	5
No. Baker-Nunn Obs.	58	80	70	69	82	51
Standard Error of Unit Weight for Total Orbital Solutions (Laser weighted at 5 m, B/N at 4 arcsec)	.97	1.69	1.20	.91	.99	.60

Table 4.

INTERSTATION SEPARATION

LONG ARC

(NASA - SAO)

Coordinate	Calculated Difference from Survey (m)	St. Dev. (m)	Surveyed (m)	
X	- 5.6	2.0	30.6	
Y	- 7.0	1.1	79.4	PHASE I
Z	+ 3.7	1.6	103.1	
X	+ 0.5	3.8	20.3	
Y	- 8.2	2.8	81.9	PHASE II
Z	- 9.6	3.4	100.7	

MINITRACK SELF CALIBRATION

Prepared for the GEOS-2

REVIEW CONFERENCE

June 22 - 24, 1970

by

J. Oosterhout
D. Harris

MINITRACK SELF CALIBRATION

Goddard's Minitrack interferometers provide the bulk of satellite tracking for Goddard's Space Tracking and Data Acquisition Network (STADAN). They are still calibrated by comparing Minitrack and optical observations of a number of aircraft passes. There are several possible sources of error in the Minitrack system but the principle one is a phase bias added by the interferometer to the phase difference that is being measured. Fortunately this phase bias, or zero set error, is fairly stable and may remain constant for many years. However, when it changes it can be a sudden change and all observations taken with that particular interferometer baseline will carry that bias until the next aircraft calibration -- a time period that may be as long as a year.

It would clearly be desirable to devise a calibration scheme for Minitrack that would update calibration values more often than can be done with the aircraft. Several schemes have been tested but the one that offers the best hope is a bootstrap method that regresses on zero set values simultaneously with the determination of long arc orbits. Minitrack interferometers are located at eight STADAN sites. There are four primary baselines at each site, each having its own zero set value. A satellite in an orbit of sufficiently high inclination can, in time, be observed by all 32 baselines. Consequently in addition to the orbital elements there are 32 bias parameters to solve for. These additional unknowns require that the observational period be of sufficient length to allow for adequate statistical control. An accuracy in determining the orbit of about eight seconds of arc is sufficient for the determination of Minitrack zero set. Even less accuracy is tolerable if the errors in the computation have a low correlation between one pass at a given station and the next.

The NONAME orbit generator that has been used extensively at Goddard for geodetic studies, taken with recent earth model refinements based on GEOS II observations, appeared to be a suitable instrument for testing the feasibility of the self calibration concept. NONAME has demonstrated an accuracy in fitting optical observations for periods up to a week that is more than sufficient for the purpose of Minitrack calibration. Furthermore, one version of NONAME had the convenient capability of regressing on Minitrack zero sets simultaneously with the determination of orbital parameters.

Sufficient data to perform this test was available from the GEOS II data bank. Minitrack and MOTS camera observations were chosen covering the period in 1968 from February 21 to March 27.

The basic strategy of the experiment was to take a week's worth of Minitrack observations of GEOS II and, using the NONAME program, solve for Minitrack zero set. These zero sets were then to be applied to the preprocessing of the Minitrack observations of GEOS II made the following

week. Using NONAME again, an orbit would be fitted to the second week's batch of observations, this time solving for orbital parameters alone. This latter orbit would be compared with the MOTS camera observations taken during that time. Then another orbit would be computed for the second week, only in this case the Minitrack observations would have been pre-processed with zero sets taken from aircraft calibrations of the interferometers. It, too, would be compared with the MOTS observations. (The MOTS observations on GEOS II, accurate to two seconds of arc, or better, are an excellent standard of comparison.) The orbit that best agreed with the MOTS sightings would tell which calibration method is best. (In actual practice this confidence would be enhanced by solving for zero sets using the observations of a number of different satellites in different orbits. This would nullify any interaction between the determination of zero sets and the gravity model errors that might be peculiar to a given orbit (resonant terms) and it would ensure good coverage for each set of baselines in the tracking network.)

Actually, not just two but five successive weeks of data were studied. Not only was the basic experiment carried out but a number of variations and side paths were explored.

In the determination of Minitrack zero set from orbital data no a priori information, i.e., previously determined aircraft calibration values, was employed. Initial estimates of phase bias were arbitrarily set at zero when, in fact, they might be up to $\pm 180^{\circ}$ for a given baseline. This device of starting in a degenerate condition was employed to allay any doubt that a self calibration system might slowly diverge from a previously established, satisfactory set of calibration values. If one could converge to a proper set of estimates from a starting point of total ignorance, then the doubt would be unwarranted.

To date, the results of this experiment have been negative, i.e., other than expected. The solutions for Minitrack zero sets converged to a set of incorrect values, and the simultaneously determined orbital parameters exhibited corresponding errors. These errors were large and systematic. The errors in zero set determination ranged as high as 4 to 5 times the errors that typically exist when the aircraft calibration values are used. The error in determining the orbit was principally along track. The error was primarily manifested as a declination error when the computed orbit was compared to MOTS camera observations. The bias in these declination residuals ranged up to a minute of arc.

Table 1 shows the MOTS camera residuals when these observations are compared to GEOS II orbits whose parameters have been determined simultaneously with the determination of Minitrack zero set. The optical data was given a weight of zero in this computation. Chiefly to be noted is the consistent negative sign and the relatively large value of the average

errors in declination. The values in the table are an average of all the points from all the passes taken by the given camera during the week's period for which the orbit was computed. Each of the five trajectories was based on a different set of Minitrack observations and there was no overlap in either the Minitrack data or in the optical data from one week to the next. The bias in the declination residuals for weeks three and four are less than those for the other weeks but the bias is in the same direction. It should be pointed out that the relative positions of sun, earth, and satellite orbit precluded any photographing of GEOS II by MOTS during this period when the satellite was moving north to south.

Table 2 shows the difference between the Minitrack calibration values computed by the simultaneous regression on orbital elements and zero sets and those determined by aircraft calibration. The numbers given are averages of the values calculated separately for each of the five weeks. The two methods of calibration are in much better agreement for the east-west baselines than they are for the north-south baselines. This is contrary to what had been expected. The expectation was that, for a satellite in polar orbit like GEOS II, any adverse interaction between the computation of along track satellite position and baseline zero set would be self correcting. The north-south baseline intercepts north going passes on one side of the orbit and, twelve hours later, south going passes on the other. A balance of passes in the two directions was presumed to negate the possibility of compensating biases developing in the regression on zero set and orbital parameters. Apparently the interaction between these factors is more complex than the intuitive model allowed for.

Figure 1 shows three curves that represent the along track, cross track and radial components of the differences between the reference orbit determined by MOTS camera observations and the orbit resulting from simultaneous regression on zero set values and orbital elements with Minitrack observations as sole input. The graph shows only about one orbital cycle but this same pattern is repeated throughout the seven day period covered by the orbital fit.

The results of this experiment are still under investigation. Many computer runs have been made to check various hypotheses about the basic results. The orbits were recomputed with various combinations of Minitrack stations totally omitted from the computation. This produced no major change in the results. Numerous checks, some involving simulated data, have been made to ensure that no sources of large errors exist in the data processing or orbit computation systems. No gross errors have been found but the possibility of some form of mishandling of the Minitrack observations has not been dismissed. Just beginning is a study of the more subtle statistical elements in the distribution and character of the Minitrack observations.

Whether Minitrack self calibration is feasible is still a question. Certainly the attempt described here produced an unsatisfactory result. Why this was so is not understood. Gaining this understanding is the next step. Such an understanding should help in determining the proper technique for Minitrack self calibration if, indeed, this is a practical possibility.

DIFFERENCES BETWEEN MINITRACK SELF-CALIBRATION AND OPTICAL ORBITS : ALONG TRACK, ACROSS TRACK AND RADIAL. FEBRUARY 21, 1968.

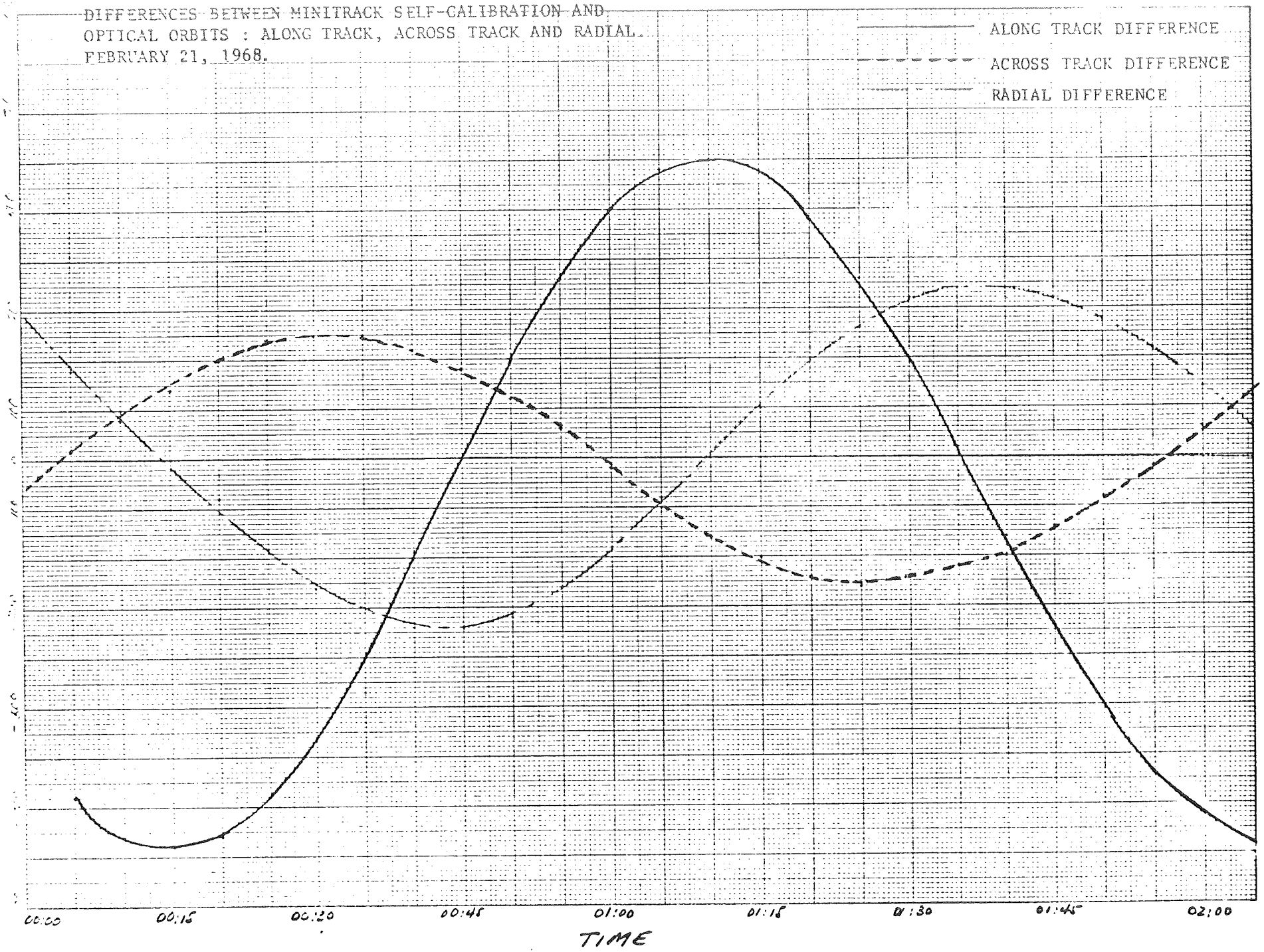

Table 1

OPTICAL RESIDUALS (ARC SEC) FOR
MINITRACK ORBIT & BIASES SOLUTIONS

STATION		Week #1	Week #2	Week #3	Week #4	Week #5
FTMYRS	Rt. Asc.	-10.3	25.5		1.4	0.0
	Declin	-56.9	-46.5		7.8	-49.1
SNTAGO	Rt. Asc.	11.9			-7.4	8.3
	Declin	-74.8			-6.3	-33.3
MOJAVE	Rt. Asc.	-1.6	21.2	14.0	2.4	5.3
	Declin	-45.8	-35.1	-18.1	3.2	-57.6
JOBURG	Rt. Asc.	15.8			-1.8	18.9
	Declin	-66.3				-56.7
WNKFLD	Rt. Asc.	-9.8			11.5	-1.5
	Declin	-61.1			-23.6	-58.9
ORORAL	Rt. Asc.	7.7	16.6	12.3	8.9	11.4
	Declin	-78.5	-47.2	-60.1	-23.6	-58.9
UNDAK	Rt. Asc.	-9.8	21.2	0.2	5.0	-3.3
	Declin	-47.7	-23.9	-20.0	-18.2	-40.5
EDINB	Rt. Asc.	-3.6	12.0	-2.0	11.8	3.7
	Declin	-53.4	-25.6	-7.7	9.5	-40.3
COLBA	Rt. Asc.	-8.1	14.9	9.3	-2.4	-3.4
	Declin	-53.3	-37.6	-5.2	3.0	-41.8
BERMD	Rt. Asc.	-13.9	17.5	8.4		1.7
	Declin	-46.3	-39.5	-25.1		-47.4
PURIO	Rt. Asc.	-3.4		4.0		5.3
	Declin	-63.5		-18.5		-42.5
DENVR	Rt. Asc.	1.8	13.5		5.5	4.5
	Declin	-41.8	-31.4		-8.0	-28.1
SUDBR	Rt. Asc.	-6.6	14.0	16.1	2.7	1.9
	Declin	-48.5	-28.5	-26.4	-11.1	-36.9

Table 1 (Continued)

STATION		Week #1	Week #2	Week #3	Week #4	Week #5
JAMAC	Rt. Asc.	-7.3	12.5		-4.6	-1.3
	Declin	-26.9	-20.8		4.8	-38.7
GSFCN	Rt. Asc.	-5.0	17.2			
	Declin	-55.1	-32.2			
ROSMA	Rt. Asc.	-8.6	22.3	6.0	-7.3	0.3
	Declin	-48.0	-36.0	-22.5	2.0	-40.2
ULASKA	Rt. Asc.		-1.4	-12.9	-5.2	-0.1
	Declin		-15.9	-5.2	-5.4	-35.8
TANANA	Rt. Asc.			23.2		
	Declin			-80.2		

Table 2

FIVE WEEK AVERAGE OF DIFFERENCE BETWEEN
MINITRACK SELF CALIBRATION DETERMINED ZERO SET
AND BEST ESTIMATE ZERO SET FROM AIRCRAFT
CALIBRATION AND QUALITY ASSURANCE

Station	Antenna System	Baseline	Difference Wavelengths x 10^{-3}
FTMYRS	Polar	EW	2.0
		NS	-19.6
	Equatorial	EW	4.0
		NS	-12.1
QUITOE	Polar	EW	5.9
		NS	-4.7
	Equatorial	EW	9.5
		NS	4.0
LIMAPU	Polar	EW	11.2
		NS	-13.5
	Equatorial	EW	8.3
		NS	-3.0
SNTAGO	Polar	EW	2.4
		NS	-0.3
	Equatorial	EW	-3.0
		NS	-4.4
NEWFLD	Polar	EW	-0.4
		NS	-20.5
	Equatorial	EW	-6.5
		NS	-13.6
WNKFLD	Polar	EW	-0.6
		NS	-8.2
	Equatorial	EW	-2.6
		NS	-4.8
JOBURG	Polar	EW	-1.8
		NS	-8.7
	Equatorial	EW	0.9
		NS	-5.9
ULASKA	Polar	EW	-2.0
		NS	-6.9
	Equatorial	EW	-1.6
		NS	-7.2
MADGAR	Polar	EW	-3.4
		NS	-5.0
	Equatorial	EW	-7.3
		NS	-5.5
ORORAL	Polar	EW	-3.0
		NS	-15.3
	Equatorial	EW	-1.0
		NS	-3.6

X-552-69-539
PREPRINT

AN INTERCOMPARISON OF NAVY TRANET DOPPLER DATA AND OPTICAL DATA FROM THE GEOS-I SATELLITE

Russell W. Agreen
James G. Marsh
Mission Trajectory Determination Branch
Mission and Trajectory Analysis Division

December 1969

GODDARD SPACE FLIGHT CENTER
Greenbelt, Maryland

AN INTERCOMPARISON OF NAVY TRANET DOPPLER DATA AND OPTICAL DATA FROM THE GEOS-I SATELLITE

Russell W. Agreen
James G. Marsh

ABSTRACT

Orbital solutions for the GEOS-I satellite obtained from U. S. Navy TRANET Doppler data and those from optical flash data recorded by the NASA Space Tracking and Data Acquisition Network and Smithsonian Astrophysical Observatory systems were intercompared. The orbital arcs used for this study were two days in length and were in the period July 9 through August 7, 1966. RMS of fits for the orbital solutions were on the order of 1.9 seconds of arc for the optical solutions and 2.7 cm/sec for the Doppler solutions. Comparisons of the corresponding optical and Doppler orbital ephemerides showed total RMS position differences ranging from 20 to 40 meters. Biases in the base frequency value of the Doppler data were solved for; consistent biases in the base frequency around 9 cm/sec ±3 cm/sec were found.

CONTENTS

AN INTERCOMPARISON OF NAVY TRANET DOPPLER DATA AND OPTICAL DATA FROM THE GEOS-I SATELLITE

by
Russell W. Agreen and James G. Marsh
Goddard Space Flight Center

I. INTRODUCTION

This report presents the results of an intercomparison between orbits determined from Navy TRANET Doppler data and those determined from optical flash data from the GEOS-I satellite. This investigation was conducted for the purpose of establishing our capability to handle the Doppler data for geodetic purposes. In the past, our geodetic studies have used optical data as a standard.

The NONAME Orbit and Geodetic Parameter Estimation System (Reference 1) was used to determine all orbital solutions and to generate the intercomparisons. All of the data were obtained from the National Space Sciences Data Center at Goddard Space Flight Center. It was taken during the periods July 9—July 26 and July 31—August 7 of 1966.

In addition to evaluating orbits generated from Doppler data, the data were examined for biases in the base frequency value and in the time tags associated with each measured frequency (or observation).

II. OBSERVATIONAL DATA AVAILABLE

Table 1 presents the orbital characteristics of the GEOS-I satellite; all data used in this study were from this satellite.

GEOS-I was launched by the National Aeronautics and Space Administration under their National Geodetic Satellite Program. The orbit was chosen to minimize the perturbative effects of air drag and solar radiation pressure. On board the satellite were flashing lamps, Doppler transponders, laser corner reflectors and

Table 1

Orbital Characteristics of the GEOS-I Satellite.

Apogee Height	2273.0 Kilometers
Perigee Height	1116.0 Kilometers
Eccentricity	.07
Inclination	59.4 Degrees
Anomalistic Period	120.3 Minutes

other electronic tracking instruments which enabled the numerous participating agencies to record large amounts of valuable tracking data.

Optical Data

The GEOS-I optical flash data used in this analysis were obtained from the Geodetic Satellite Data Services of the National Space Science Data Center located at Goddard Space Flight Center. It is composed of observations from the NASA STADAN Minitrack Optical Tracking System (MOTS), the Goddard Special Optical Tracking System (SPEOPT), and the Smithsonian Astrophysical Observatory (SAO) Baker-Nunn camera stations. All optical station positions are referenced to the SAO C-7 system (a_e = 6378142 meters, Reference 2).

The orbits generated from this optical data are used as the standard to which the TRANET Doppler orbits are compared because it is generally felt that the optical flash (or active) data from GEOS-I forms a very high-precision data set. The accuracy of the optical data is on the order of 2 seconds of arc which amounts to a positional error of approximately 15 meters for GEOS-I. Among the reasons for this confidence are the use of a stable on-board clock to set off the optical beacon flash intervals, exacting the time of observation to millisecond accuracy, and the short duration (about 1.3 ms.) of the flashes, enabling the cameras to record the observations as point images against a background of reference stars rather than less exacting streak images (Reference 3).

Substantial evidence of this quality is seen in the orbital RMS's of fit; for each of the thirteen 2-day arcs generated from optical data, the RMS of fit is on the order of 2 seconds of arc. This is a very good fit considering that the NASA (MOTS and SPEOPT) and SAO (Baker-Nunn) data were processed through independent systems, yet weighted equally in the orbital solutions. The MOTS and SPEOPT data were obtained by MOTS 40 and PTH-100 cameras and all plates were reduced at the New Mexico State University to yield right ascension and declination pairs and U.T.C. time tags. The SAO data were taken by Baker-Nunn cameras on film and reduced by SAO to yield right ascension and declination pairs and time tags in A.S. atomic time (Reference 4).

Some preprocessing of the data received from the Space Science Data Center is done using the NONAME orbit determination system. MOTS and SPEOPT data time tags are corrected for flash buildup time; no other preprocessing is necessary. SAO data has atomic time (A.S.) tags and NONAME is used to apply the conversion to Universal Time Coordinated (U.T.C.). Also, a transit time correction is applied to the SAO data to refer the observation from station time to satellite time. Finally, SAO observations are referred to the mean equator and equinox of 1950.0, and it is necessary to apply precession and nutation from that epoch to the true equator and equinox of epoch of the observations (Reference 1).

Station network, name, number, location, and camera type are presented in Table 2 for all of the optical stations used in this study.

Table 2

Optical and Doppler Stations Used in the Analysis.

Network	Station	Number	Camera Type (optical)	Location
STADAN	1BPOIN	1021	MOTS 40"	Blossom Point, Md.
	1FTMYR	1022	MOTS 40"	Fort Myers, Fla.
	1OOMER	1024	MOTS 40"	Woomera, Australia
	1MOJAV	1030	MOTS 40"	Mojave, Calif.
	1JOBUR	1031	MOTS 40"	Johannesburg, Union of S. Africa
	1GFORK	1034	MOTS 40"	East Grand Forks, Minn.
	1ROSMA	1042	MOTS 40"	Rosman, N. C.
	1TANAN	1043	MOTS 40"	Tananarive, Madagascar
SPEOPT	1EDINB	7036	MOTS 40"	Edinburg, Texas
	1COLBA	7037	MOTS 40"	Columbia, Mo.
	1BERMD	7039	MOTS 40"	Bermuda
	1PURIO	7040	MOTS 40"	San Juan, Puerto Rico
	1GSFCP	7043	PTH-100	GSFC, Greenbelt, Md.
	1DENVR	7045	MOTS 40"	Denver, Calif.
	1SUDBR	7075	MOTS 40"	Sudbury, Ontario
	1JAMAC	7076	MOTS 40"	Jamaica, B.W. I.
SAO	1ORGAN	9001	Baker-Nunn	Organ Pass, N. M.
	1OLFAN	9002	Baker-Nunn	Olifantsfontein, Union of S. Africa
	1SPAIN	9004	Baker-Nunn	San Fernando, Spain
	1NATOL	9006	Baker-Nunn	Naini Tal, India
	1QUIPA	9007	Baker-Nunn	Arequipa, Peru
	1SHRAZ	9008	Baker-Nunn	Shiraz, Iran
	1CURAC	9009	Baker-Nunn	Curacas, Lesser Antilles
	1JUPTR	9010	Baker-Nunn	Jupiter, Fla.
	1VILDO	9011	Baker-Nunn	Villa Dolores, Argentina
	1MAUIO	9012	Baker-Nunn	Maui, Hawaii
	AUSBAK	9023	Baker-Nunn	Woomera, Australia
NAVY TRANET DOPPLER	ANCHOR	2014		Anchorage, Alaska
	WAHIWA	2100		South Point, Hawaii
	LACRES	2103		Las Cruces, N. M.
	LASHM2	2106		Lasham, England
	APLMND	2111		APL Howard County, Md.

Doppler Data

The GEOS-I TRANET Doppler data used in this study were also obtained from the National Space Science Data Center. Data from only the 5 stations listed in Table 2 are used for the period under consideration. Data are available from the Doppler station in American Samoa (TAFUNA, #2017) but it is not used because of uncertainties in the station position. The data available from McMurdo Sound, Antarctica (MCMRDO, #2019) are not used because of the very low maximum elevation angles on all of the passes. The 5 Doppler stations used are referenced to the SAO-C7 system.

All of the Doppler data used in this study are converted from frequency measurements to range rate using the following equation for one-way Doppler data:

$$\dot{R} = \frac{c(F_B - F_M)}{F_M}$$

where

F_B = base frequency

F_M = measured frequency

c = speed of light $(2.997925 \times 10^8$ m/sec)

Among the preprocessing done on the data before it was submitted to the Data Center was a first-order ionospheric refraction correction applied at the tracking stations (Reference 5). The NONAME system is used to further correct on the range rate values for tropospheric refraction as follows (Reference 1):

$$\Delta\dot{R} = \left[\frac{2.77 N_s \cos E}{328.5(.026 + \sin E)^2} \dot{E}\right] \text{ meters/second}$$

where

N_s = (surface index of refraction - 1.) $\times 10^6$, = 328.5 in the absence of a better value for the surface index of refraction

E = elevation angle computed from the initial estimate of the trajectory

$\dot{E}$ = computed rate of change of elevation

A transit time correction is also applied to the observations to put the time tags at the satellite.

In addition, it is felt necessary to include in the NONAME preprocessing an adjustment to the base frequency (of the spacecraft oscillator) for each pass over a station. Even though a nominal value of the satellite oscillator frequency exists for GEOS-I, it was modified by NWL for each pass of data (Reference 6). NWL computed a reference orbit with their ASTRO Computer Program and

derived an expected satellite frequency for each observation time. Then (o-c) values were calculated and used to produce a corrected nominal satellite oscillator frequency for each pass of data. This "base frequency" was included in the Doppler data submitted to the Data Center. Due to the differences (gravity model, station positions, and other constants) between the ASTRO and NONAME Orbital Computation Systems, better orbits are obtained in NONAME when the base frequency for each pass of Doppler data is adjusted along with the six orbital elements ($\bar{R}$ & $\bar{V}$). This is done in NONAME by adjusting on the range rate measurement bias for each pass of data since a linear relationship exists between $\dot{R}$ and F_B in the formula for converting Doppler data to range rate. It is recognized that residual refraction effects, unmodelled orbital errors, and other small unknown biases may be absorbed into this base frequency adjustment.

III. INTERCOMPARISON OF DOPPLER AND OPTICAL ORBITS

NONAME and Perturbations Applied

Designed to provide accuracy in geodetic studies, the NONAME system at Goddard consists of a definitive orbit and geodetic parameter estimation program with a number of auxiliary programs. The main program of the system, the NONAME ODP, can operate in either the data reduction or orbit generation modes (Reference 2).

In the data reduction mode, the NONAME ODP can estimate the following parameters from satellite tracking data:

1. the six orbital parameters $x, y, z, \dot{x}, \dot{y}, \dot{z}$ for some specified epoch
2. certain physical constants relating to atmospheric drag or solar radiation pressure
3. tracking station co-ordinates relative to the center of mass of the earth
4. tracking instrument errors—zero set bias or timing bias
5. geopotential coefficients

All observation time tags are transformed to U.T.C. time at the satellite and numerous preprocessing options exist for various data types (i.e. right ascension, declination, range, range rate, direction cosines, X and Y angles, azimuth, elevation).

The orbit is numerically integrated (Cowell's method) in fixed steps and interpolated to get computed observations for residuals, (o-c) values. A Bayesian least squares estimation scheme and a Newton-Raphson iteration formula are used in correcting on the six orbital elements and any other specified parameters. There are convergence criteria for the iterations, rejection criteria for observations, and observational data weighting schemes optional to the user.

In the orbit generation mode, an initial epoch and position and velocity vectors are input and the equations of motion are numerically integrated (Cowell) to give an ephemeris of position, velocity, and time.

The potential of the earth is represented by a normal potential of an ellipsoid of revolution (SAO C-5, C-6, C-7, etc.) and small variations, expressed by a set of spherical harmonics (SAO M-1, APL 3.5, etc.). In addition, the following perturbations may be represented as disturbing functions as optioned by the user:

1. solar gravitation
2. lunar gravitation

3. solar radiation pressure
4. atmospheric drag force (NONAME uses the Jacchia-Nicolet model for the atmosphere)

In this study, the earth ellipsoid used is that of the SAO C-7 system and the gravity model used is the SAO-M1 modified by the 12th order terms of Gaposchkin and Veis (References 2 and 7). The perturbations applied in NONAME are solar gravitation (M_s/M_e = 332951.25), lunar gravitation (M_m/M_e = .0123), and solar radiation pressure (4.5×10^{-6} Newtons/m^2).

Discussion of Comparison

The period of data that was intercompared covers from July 9th through July 26th and from July 31st through August 7th of 1966. The data were separated into thirteen 2-day arcs since any longer arcs are more affected by errors due to uncertainties in the earth's gravity model, solar radiation pressure or other parameters.

Both the optical and Doppler data were run separately on the NONAME ODP in the data reduction mode. All optical observations were assigned a weight of 2 seconds of arc, and the right ascension measurements were further down-weighted by the cosines of the corresponding declination measurements due to the geometry of the pair (i.e. the higher the declination, the larger the uncertainties introduced into the right ascension). The Doppler data, converted to range rate, were assigned a weight of 10 cm/sec. Based on an editing criteria of 3σ there was approximately a 1% rejection rate on both data types.

The converged solution state vectors for both the optical and Doppler coincident arcs were then input into the NONAME ODP in the orbit generation mode. The orbits generated were compared to obtain the position differences every ten minutes. Table 3 presents the RMS of solution values for the data reduction runs and the summary data of the orbit intercomparisons. Appendix B shows position difference plots of five of these 2-day arc intercomparisons.

See Appendix A for a complete breakdown of the optical and Doppler data used in these 2-day arc studies.

As seen from Table 3, the RMS of total position differences over the 2-day arcs is on the order of 20 to 40 meters with maximum position differences on the order of 30 to 70 meters. It is important to note that only 5 stations in the Northern global hemisphere were used to obtain the Doppler orbits and all low elevation data was included, indicating good-quality refraction corrections. The large amplitude of some of the cross track position differences might seem odd at first glance since the along track errors usually dominate; however, this could possibly be attributed to difficulty in determining the inclination of the orbit in the Doppler solution since, again, the five Doppler stations are poorly distributed around the globe. These consistent results show that the capability to handle Doppler data and determine orbits of the quality demanded in geodetic studies from such data exists in the NONAME System at Goddard.

Table 3

Position Differences Between Orbits Generated From TRANET Doppler Data and Orbits Generated From Optical Data (2 day arcs).

Arc of Compare (1966)	*RMS of Fit		RMS of Position Differences (meters)				Maximum Difference (meters)
	Doppler (cm/sec)	Optical (secs. arc)	Radial	Cross Track	Along Track	Total	
July 9-10	2.7	1.8	12	7	38	41	70
July 11-12	2.8	1.9	7	16	19	26	36
July 13-14	2.8	1.8	13	9	26	30	44
July 15-16	2.8	1.8	10	23	23	33	51
July 17-18	2.7	1.9	7	10	20	23	35
July 19-20	2.6	1.9	12	10	36	39	67
July 21-22	2.7	2.1	12	10	38	41	77
July 23-24	2.7	1.8	3	14	11	19	27
July 25-26	2.7	1.7	7	9	16	20	38
July 31—August 1	2.8	1.9	6	5	18	20	39
August 2-3	3.0	2.1	5	9	18	21	47
August 4-5	2.7	2.0	6	25	32	41	66
August 6-7	2.7	1.9	11	21	32	40	60

*Approximate number of observations per arc: Doppler – 1880, Optical – 870.

IV. EFFECT OF STATION POSITIONS ON THE DOPPLER ORBITAL SOLUTIONS

As previously mentioned, the 5 Doppler tracking stations are in the Northern hemisphere of the globe; Figure 1 shows the locations of all the optical and Doppler tracking stations from which data were used for this study. It is interesting that all optical stations tracked the satellite only as it passed from south to north over the station. Thus the South American optical stations were often tracking just minutes before the Doppler stations in Maryland and England started tracking. The reason for this consistent south to north tracking by the optical stations lies in the facts that for the GEOS-I satellite, the right ascension of the ascending node traverses the celestial sphere at a rate of approximately 2-1/4 degrees per day, and only night tracking of the flash sequences is possible. Thus, for this month long period, the right ascension of the node was in the earth's shadow, causing the consistent south to north tracking. The Doppler stations have no such restriction and were able to track whenever the satellite passed over their vicinity.

It was thought that perhaps the poor global distribution of the available Doppler stations caused the Doppler orbit to be weakened in the southern hemisphere where no stations existed and thus where no (o-c) values could be determined to correct on the state vector. Thus it was decided to take 4 of the 2-day Doppler and optical arcs and examine how accurately the Doppler determined orbits fit the optical data from each optical station around the entire globe.

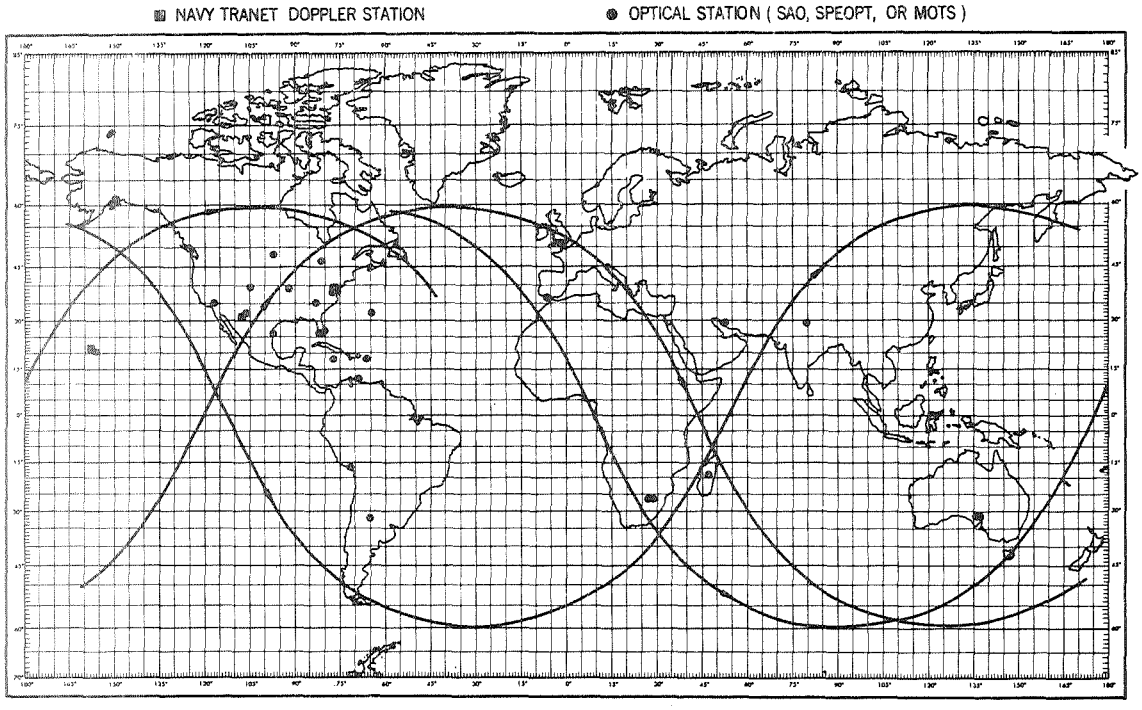

Figure 1—Locations of all TRANET Doppler and optical stations used in intercomparisons and typical GEOS-I orbital paths July-August, 1966.

The approach is to take the converged vector solution, for each of the arcs, as determined by the Doppler arc and input it as the state vector for the corresponding optical arc. The Doppler solution is passed through the optical data to note the optical station data fits to the Doppler determined orbit. The observation residual summary by optical station is examined to see which groups of stations representing areas of the globe have the largest increases in the RMS of solution when compared to the final iteration of the original optical solution for that arc. For each station appearing in two or more of the four arcs, the RMS's of fits were combined to yield one summary value for that station. As an example, if a station appeared in two of the arcs and had respective RMS values of RMS_1 and RMS_2, where:

$$RMS_1 = \sqrt{\frac{\sum_{i=1}^{m} (o - c)_i^2}{m - 1}} \quad ; \quad RMS_2 = \sqrt{\frac{\sum_{i=1}^{k} (o - c)_i^2}{k - 1}}$$

then the combined RMS would equal:

$$\sqrt{\frac{(m - 1)(RMS_1)^2 + (k - 1)(RMS_2)^2}{m + k - 1}}$$

Table 4 shows all of the optical stations used, the number of observations each has over the four 2-day arcs of this station position study, what arcs the data appear in, the combined RMS values

Table 4

Summary, by Station, of Optical Data Fits to the Optical and Doppler Orbital Solutions (July 9-16, 1966).

Optical Station	Latitude (degrees)	Observations		RMS of Fit (secs. arc)	
		Total Number	*From Arcs	To Optical Orbit	To Doppler Orbit
1GFORK	48	73†	I, II	1.9	2.0
		73‡		1.5	1.7
1SUDBR	46	60	II, IV	1.9	2.3
		60		1.5	1.9
1DENVR	40	20	I	2.4	2.7
		20		1.3	1.2
1COLBA	39	93	I, II	1.3	1.6
		94		1.2	1.7
1BPOIN	38	45	I, II	1.3	1.5
		44		2.1	2.1
1SPAIN	36	73	I, II, III, IV	2.7	3.3
		77		1.7	2.1
1MOJAV	35	35	II	1.8	2.4
		35		1.5	1.9
1ROSMA	35	33	I, II	1.3	1.3
		32		2.3	2.2
1ORGAN	32	224	I, II, III, IV	1.6	1.6
		224		1.6	1.8
1BERMD	32	49	II, IV	2.6	2.6
		48		3.2	2.5
1SHRAZ	30	28	II, III	1.8	2.1
		25		2.8	2.4
1NATOL	29	25	III	1.4	1.4
		25		1.7	2.3
1JUPTR	27	305	I, II, III, IV	1.7	1.8
		304		1.8	2.3
1EDINB	26	69	I, II	0.7	1.2
		70		1.1	1.6
1MAUIO	21	56	I, IV	2.2	2.5
		56		1.4	1.4
1JAMAC	18	35	II	1.3	1.4
		34		1.9	2.6
1CURAC	12	27	I	1.7	1.6
		27		2.3	2.6
1QUIPA	-16	69	I, II, III, IV	2.0	2.0
		69		2.7	3.6
1TANAN	-19	14	II	1.8	1.6
		14		0.9	1.2

*I - July 9-10, II - July 11-12, III - July 13-14, and IV - July 15-16.
†declination
‡right ascension

Table 4 (Continued)

Optical Station	Latitude (degrees)	Observations		RMS of Fit (secs arc)	
		Total Number	*From Arcs	To Optical Orbit	To Doppler Orbit
1JOBUR	-26	61†	I, II, III, IV	1.7	3.4
		52‡		2.0	2.9
1OLFAN	-26	132	I, II, III, IV	1.7	3.4
		130		2.1	3.0
1OOMER	-31	42	I, II	1.8	3.0
		41		2.1	3.6
AUSBAK	-31	69	I, II, III, IV	1.6	2.5
		69		2.2	2.8
1VILDO	-32	31	II, IV	3.0	3.5
		33		3.3	3.9

*I - July 9-10, II - July 11-12, III - July 13-14, and IV - July 15-16.
†declination
‡right ascension

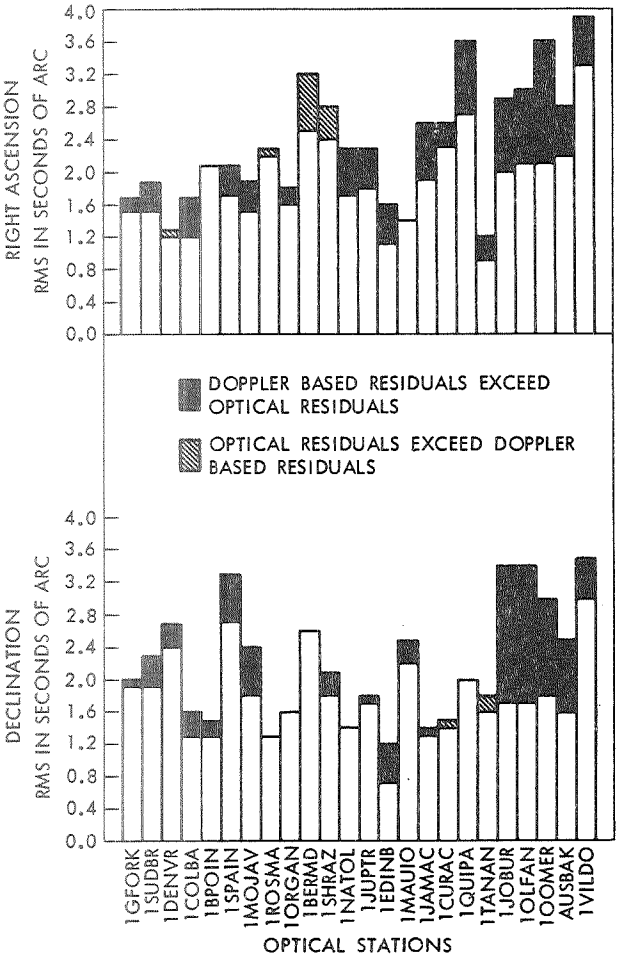

Figure 2—Summary of optical residuals based upon TRANET Doppler orbits for the period July 9-16, 1966.

from the original optical solutions, and the combined RMS values when the Doppler state vector was passed through the optical data. The stations are grouped according to hemispheric location. By comparing the optical based RMS values against the Doppler based RMS values for a given station, some feeling for the relative strengths of the two solutions can be obtained.

Figure 2 presents the RMS differences in graphical form. For a few stations, the Doppler orbit fits the optical data slightly better than the optical orbit. This could be due to errors in the station position, instrument errors, or other factors. However, the general trend for northern hemisphere optical stations is for the optical orbit to fit the optical data a little better than the Doppler orbit. In the southern hemisphere, the Doppler orbit has obvious difficulty fitting the optical data. Thus, it seems that the good orbital comparisons that were achieved would have been even better if data were available from Doppler stations in the southern hemisphere to tie down that half of the GEOS-I orbit.

Figure 2 should be interpreted with the information presented in Table 4 in mind. As an example, the histogram for the station in

Madagascar (1TANAN) seems to disagree with those of the two nearby South African stations in Olifantsfontein and Johannesburg. However, data from Tananarive consists of 28 observations in only one arc while there are 113 observations from Johannesburg and 262 from Olifantsfontein and these data are distributed through all 4 arcs. Thus, this indicates that the Tananarive results should be discounted.

V. FURTHER STUDY OF THE INTERCOMPARISONS

Evaluation of Atmospheric Refraction Corrections on Low Elevation Doppler Observations

It was thought that the optical and Doppler solutions might be brought into even better agreement by dropping the low elevation measurements from the Doppler data. The logic behind this is that perhaps the refraction effects, which are greatest at low elevations, are not sufficiently modelled. Additional NONAME solutions were generated with all Doppler observations of elevation less than 20° dropped from the data; two 2-day arcs were tested. Table 5 indicates a very slight drop in the RMS of solution and shows the results of the position comparisons against the corresponding optical arcs. These "elevation cut-off" Doppler versus optical comparisons show an

Table 5

Effects of Removing Low Elevation Observations From Doppler Data on the Doppler Solutions and on the Doppler Versus Optical Orbital Comparisons.†

Navy TRANET Doppler Solutions					
2-Day Arc 1966	Station	Total Number of Observations Used	Total Number of Observations > 20° Elevation Used	Original RMS of Fit (cm/sec)	RMS of Fit (>20°) (cm/sec)
July 17-18	ANCHOR	429	272	3.1	3.0
	WAHIWA	227	111	2.5	2.6
	LACRES	387	187	2.9	2.8
	LASHM2	447	298	2.5	2.2
	APLMND	423	266	2.4	2.3
	ALL	1913	1134	2.7	2.6
July 19-20	ANCHOR	522	303	2.8	2.6
	WAHIWA	234	149	2.7	2.5
	LACRES	307	190	2.7	2.3
	LASHM2	410	277	2.1	2.0
	APLMND	483	271	2.6	2.5
	ALL	1956	1190	2.6	2.4

Table 5 (Continued)

Doppler Versus Optical Orbital Comparisons							
2-Day Arc of Compare (1966)	RMS of Fit		RMS of Position Differences (meters)				Maximum Difference (meters)
	Doppler (cm/sec)	Optical (secs. arc)	Radial	Cross Track	Along Track	Total	
July 17-18	2.6*		7	11	21	24	38
		1.9					
	2.7		7	10	20	23	35
July 19-20	2.4*		13	10	37	41	68
		1.9					
	2.6		12	10	36	40	67

*Observations with $> 20^{\circ}$ elevation only.
†Note: the inclusion of low elevation Doppler data does not degrade the solution.

increase in the total RMS of position differences of about 1 meter over the original Doppler versus optical comparisons presented in Table 3. Thus it is felt that the inclusion of low elevation Doppler data does not degrade the solution. In fact, the low elevation points add to the geometry of the Doppler solutions since they increase the tracking range in the GEOS-I satellite by approximately 60 miles/degree of elevation on both ends of any specific pass.

Effect of Arc Length on Solution

Two day arc lengths may be less accurate than shorter arc lengths due to the effects of data distribution, gravity model errors, perturbation model errors, and unmodelled parameters. However, two day arc lengths were chosen for this study because it was thought that none of these errors would have an adverse effect over a 2-day period. This section presents the results of a check made to determine the quality of 2-day versus shorter length orbital solutions.

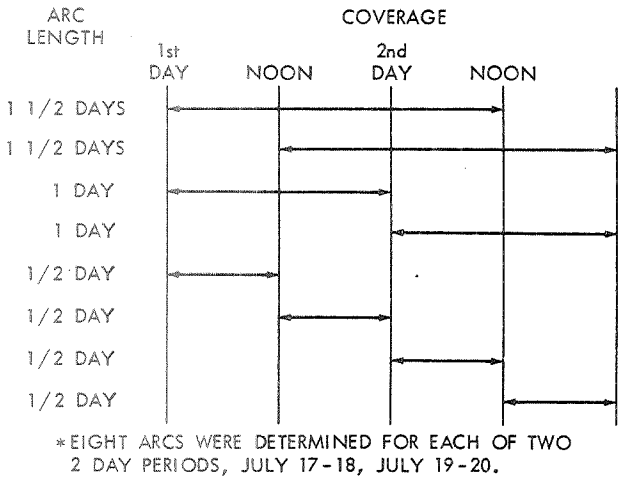

Figure 3—Reduction of two day arcs into shorter arc lengths.*

In order to assess the accuracy of orbital arc solutions of less than 2-day length, two arcs (July 17-18, July 19-20) are broken into smaller arcs of length 1-1/2, 1, and 1/2 day length as shown in Figure 3. Doppler and optical orbits are determined for these 16 shorter arcs and then intercompared as in the initial 2-day orbital solutions.

The results of 9 of these 16 intercomparisons along with the results of the two 2-day intercomparisons are presented in Table 6. Seven results are not presented since very poor data distribution over the arc length prevented the determination of sufficiently accurate orbits. The results indicate that the fit of the data to the orbit does not appreciably improve as the arc length of solution decreases; thus, the orbital solutions of length less than 2-days are not of better quality than the 2-day solutions.

Table 6

Position Differences Between TRANET Doppler Orbits and Optical Orbits for Arc Lengths Less Than 2 Days.

Arc of Compare			RMS of Fit		RMS of Position Differences (meters)				Maximum Difference
Epoch (1966)		Length in Days	Doppler (cm/sec)	Optical (secs. arc)	Radial	Cross Track	Along Track	Total	
Day	Hour								
July 17	0	2	2.7	1.9	7	10	20	23	35
July 17	0	1-1/2	2.7	1.9	5	9	18	21	34
July 17	12	1-1/2	2.7	1.9	8	2	27	29	54
July 17	0	1	2.5	1.8	8	11	23	27	53
July 18	0	1	2.8	1.9	8	8	22	25	49
July 17	0	1/2	2.5	1.8	1	16	7	17	26
July 18	0	1/2	2.6	1.9	4	2	13	13	26
July 19	0	2	2.6	1.9	12	10	36	39	67
July 19	0	1-1/2	2.7	1.8	10	11	29	32	53
July 19	0	1/2	2.5	1.6	11	6	38	40	65
July 20	0	1/2	2.2	1.7	12	11	33	37	62

The position comparisons of the Doppler and optical orbits are generally in the same range. The two comparisons having very low RMS of position differences over the half day solutions on July 17th and July 18th are the results of very dense data in the period. Each of the thirteen 2-day arcs composed of optical data have an average of 870 observations in it, but both of the above mentioned half day arcs have over 400 optical observations in them. They also have over 400 Doppler observations. These comparisons are further evidence of the quality of the Doppler orbits.

The plots of position differences for these 9 shorter arcs appear in Appendix C.

VI. BIAS STUDY OF DOPPLER DATA

Timing Errors

One of the ancillary programs in the NONAME system processes the residuals calculated in the last iteration of a NONAME ODP data reduction run to determine zero-set and timing errors (Reference 1).

Table 7

Summary of Timing Biases (Δt)* Found in the TRANET Doppler Data

2-Day Arc (1966)	Station	Number of Passes	Timing Error (Δt) ± 1 Standard Deviation (msecs.)
July 17-18	APLMND	10	0.6 ± 4.2
	LASHM2	10	0.0 ± 3.2
	ANCHOR	10	-0.8 ± 3.2
	LACRES	9	-0.4 ± 5.5
	WAHIWA	5	2.7 ± 5.5
July 19-20	APLMND	11	0.4 ± 5.8
	LASHM2	9	-2.1 ± 3.0
	ANCHOR	12	-1.7 ± 2.7
	LACRES	7	2.9 ± 1.5
	WAHIWA	5	3.5 ± 6.3

*$\Delta R = \Delta B + \Delta t\,\dot{O}$ where ΔR = Residual (o-c), ΔB = Zero Set Bias, Δt = Timing Error, and $\dot{O}$ = Rate of Change of Observation.

The residuals are investigated with the following regression model:

$$\Delta R = \Delta B + \Delta t\,\dot{O}$$

where

ΔR = the residual for a specific observation.

ΔB = the zero-set error in the observing instrument.

Δt = the timing error in the observing instrument.

$\dot{O}$ = the rate of change of the observation.

This program, GEORGE, was used to determine the timing errors for the July 17-18 and July 19-20 Doppler arcs. Table 7 summarizes the results which appear in full in Appendix D. Although zero-set errors were computed by GEORGE, they are neglected because such errors were absorbed into the adjustment of the range rate measurement bias (the base frequency adjustment).

It is obvious from the table that no significant timing errors were found.

Results of the Range-Rate Bias Adjustment on TRANET Doppler Data

As mentioned previously, the NONAME Orbit and Geodetic Parameter Estimation System is used to adjust on a range-rate or base frequency bias for each pass of data in all Doppler orbital solutions (refer to Section II).

Table 8

Summary of Biases Found in the TRANET Doppler Data Over the Period July 9-26 July 31-August 7, 1966.

Station	Number of Passes	Range Rate Bias ± 1 Standard Deviation (cm/sec)
APLMND	140	10.2 ± 3.4
LASHM2	138	8.2 ± 2.6
ANCHOR	138	8.3 ± 3.1
LACRES	94	8.2 ± 3.2
WAHIWA	60	9.3 ± 2.4
ALL	570	8.8 ± 3.1

The bias values that are determined in the NONAME System are consistent throughout all of the Doppler orbital solutions. Table 8 presents a summary of all range-rate biases determined over the entire period of the study. Appendix D presents the determined biases in more detail. The biases for each station generally range from 8 to 10 cm/sec with standard deviations of 2 to 3 cm/sec.

Analysis of simultaneous GEOS-II Doppler and laser data at Wallops Island by Berbert and Parker (Reference 8) also indicated the presence of a positive bias in the Doppler data. Using 10 passes of laser data to determine

reference orbits, Berbert and Parker noted TRANET range rate biases averaging +16 cm/sec. Discussions between the investigators and NWL personnel uncovered a procedure in the preprocessing program at NWL which was responsible for the large positive biases. After NWL provided corrections to the base frequency, the average bias dropped to +4 cm/sec.

Effect of Arc Length on the Range-Rate Bias Adjustment

The question of independence of the range-rate bias adjustment on arc length is investigated Two of the 2-day arcs, July 17-18 and July 19-20 are broken into smaller arcs of 1-1/2, 1, and 1/2 day lengths (see Figure 3); 8 arcs are thus formed in each 2-day period. If a particular pass lasts from morning into the afternoon (G.M.T.), then only two of these shorter arcs can be used to get a range-rate bias for that pass, the reason being that the pass must fall completely within an arc in order to get a bias adjustment for the entire pass. For passes within the first and last quarters of the 2-day period, 3 of these shorter arcs can be used to determine a range-rate bias, and for passes within the center quarters of the 2-day period, 4 shorter arc solutions for range-rage bias are possible.

Table 9

Dependency of the TRANET Doppler Range Rate Bias Adjustment on Arc Length.

Pass for Which Bias is Computed		Arcs Used			Adjusted $\dot{R}$ Bias (cm/sec)	Mean Bias ± 1 Standard Deviation (cm/sec)
Station Day		Epoch (1966)		Length in Days		
Start	End	Day	Hour			
APLMND July 17		July 17	0	2	5.6	
		July 17	0	1-1/2	5.6	
9:48	10:17	July 17	0	1	5.9	6.0 ± 0.5
		July 17	0	1/2	6.7	
ANCHOR July 17		July 17	0	2	7.5	
		July 17	0	1-1/2	7.7	
15:49	16:18	July 17	12	1-1/2	6.5	7.1 ± 0.5
		July 17	0	1	6.8	
		July 17	12	1/2	6.9	
LASHM2 July 18		July 17	0	2	8.3	
		July 17	0	1-1/2	7.8	
3:48	4:17	July 17	12	1-1/2	8.0	7.8 ± 0.4
		July 18	0	1	7.7	
		July 18	0	1/2	7.3	
WAHIWA July 19		July 19	0	2	12.4	
		July 19	0	1-1/2	12.7	
16:06	16:35	July 19	12	1-1/2	11.9	11.8 ± 0.8
		July 19	0	1	11.3	
		July 19	12	1/2	10.7	
LACRES July 20		July 19	0	2	11.9	
		July 19	12	1-1/2	12.5	
12:04	12:33	July 20	0	1	12.7	11.9 ± 0.9
		July 20	12	1/2	10.6	

Table 9 presents the results for 5 representative passes to show the general consistency of the range-rate or base frequency adjustment. Appendix E presents the results for all 88 passes covering the 4 days of July 17-20, 1966. Most of the passes show a mean bias value with a standard deviation of about 2-10% of the mean. This result indicates a strong level of independence between arc length and the bias adjustment on range-rate, and it provides further evidence that the TRANET Doppler data are being processed properly in the NONAME System.

VII. CONCLUSIONS

The thirteen 2-day optical orbits and the thirteen 2-day Doppler orbits have RMS of fits in the ranges of 1.9 seconds of arc and 2.7 cm/sec respectively, indicating for both data types that the fits of the data to the orbits are almost down to the noise level of the data. The RMS of position differences between corresponding optical and Doppler orbits range from 20-40 meters, and maximum position differences are from 27-77 meters for the thirteen 2-day arcs. Since the noise level on both data types is from 10-15 meters, it is felt that these results are very consistent and that they demonstrate the ability to generate Doppler orbits of quality comparable to the optical orbits that are being used in geodetic studies at Goddard.

Furthermore, the study of the effects of station positions on the Doppler orbital solutions indicates that even better agreement between the Doppler and optical orbits would have been attained if there had been data available from Doppler stations located in the southern hemisphere to tie down those halves of the Doppler orbits.

It is felt that the NONAME ODP models tropospheric refraction well enough to enable the use of Doppler observations far below 20° in elevation. The use of observations in the range of 10°-20° elevation increases the geometry of any pass of the GEOS-I satellite by approximately 60 miles per degree of elevation on either end of the pass; thus, this ability is quite valuable in determining orbits of geodetic quality.

Biases in the base frequency values sent along with each pass of Doppler data were consistently on the order of 8-10 cm/sec ±2-3 cm/sec for each of the 5 stations used in this study. Also, the range-rate biases adjustment in the NONAME System was found to be highly independent of arc length of solution. No significant timing biases were found in the Doppler data.

Finally, this report indicates that Navy TRANET Doppler data can currently be used to supplement optical data in geodetic studies using the NONAME Orbit and Geodetic Parameter Estimation System at Goddard or in a system having similar capacity to handle Doppler data.

Work is currently in progress performing additional studies of this nature using data from other satellites (GEOS-II, BEB, BEC).

VIII. ACKNOWLEDGMENT

The authors wish to thank Mr. Thomas David Meadows for performing the NONAME computer runs used in this report.

IX. REFERENCES

1. O'Neill, Brian, "NONAME, An Orbit and Geodetic Parameter Estimation System, Volume I, Systems Description," Wolf Research and Development Corp., College Park, Md., August 1968.

2. "Geodetic Satellite Results During 1967," edited by C. A. Lundquist, SAO Special Report No. 264, December, 1967. pp. 73-100, p. 65.

3. Goddard Space Flight Center, NASA-GSFC OPERATIONS PLAN 11-65, GEODETIC SATELLITE (GEOS-A), Document No. X-535-65-345, August, 1965.

4. Hotter, Frank D., "PREPROCESSING OPTICAL SATELLITE OBSERVATIONS," The Ohio State University Research Foundation, Columbus, Ohio, April, 1967, revised May, 1968.

5. Dunnel, C. A., "U. S. Navy Doppler Tracking System TRANET," TG-874, The John Hopkins University, Applied Physics Laboratory, December, 1966.

6. Gross, Joseph E., III, "Proprocessing Electronic Satellite Observations," NASA CR-1183, prepared by Ohio State University, Columbus, Ohio, November, 1968.

7. Lundquist, C. A., and Veis, G., "Geodetic Parameters for a 1966 Smithsonian Institution Standard Earth," SAO Special Report No. 200, Vol. 1, 1966.

8. Berbert, John H., and Parker, Horace C., "Comparison of C-Band, SECOR, and TRANET With a Collocated Laser on 10 Tracks of GEOS-2," Document No. X-514-68-458, November, 1968.

Appendix A

Optical and Doppler Data Used in the Analysis

The tables herein present the thirteen 2-day optical orbital solutions (Table A1) and the thirteen 2-day TRANET Doppler orbital solutions (Table A2) in detail. The number of observations from each station that were used to determine the orbit and the RMS of fit of the orbit to the data from each station is shown.

Table A1

2-Day Optical Orbital Solutions.

2-Day Arc	Station	Number of Observations Used	Number of Observations Rejected	RMS of Fit (secs. arc)
July 9-10	AUSBAK	14*		1.5
		14†		2.2
	1BPOIN	20		1.5
		19	1	2.3
	1COLBA	28		1.1
		28		1.3
	1CURAC	27	1	1.7
		27	1	2.3
	1DENVR	21		2.4
		21		1.3
	1EDINB	20	1	0.7
		21		1.3
	1GFORK	25		2.1
		25		2.0
	1GSFCP	6		-
		1	5	-
	1JOBUR	21		2.0
		18	3	2.5
	1JUPTR	35		1.8
		35		1.3
	1MAUIO	28		2.0
		28		1.5
	1OLFAN	14		2.0
		14		1.6

*First line is for declination observations.
†Second line is for right ascension observations.

Table A1 (Continued)

2-Day Arc	Station	Number of Observations Used	Number of Observations Rejected	RMS of Fit (secs. arc)
July 9-10 (continued)	1OOMER	21		2.0
		21		2.1
	1ORGAN	56		1.8
		56		1.6
	1QUIPA	14		1.2
		14		3.7
	1ROSMA	21		1.3
		20	1	2.5
	1SPAIN	14		1.2
		14		3.7
	1TANAN	7		-
		7		-
	ALL	775	13	1.8
July 11-12	AUSBAK	21		1.4
		21		2.4
	1BERMD	35		2.9
		35		2.7
	1BPOIN	25		1.2
		25		2.0
	1COLBA	65	1	1.4
		66		1.2
	1EDINB	49		0.7
		49		1.1
	1GFORK	48		1.8
		48		1.2
	1JAMAC	35		1.3
		34	1	1.9
	1JOBUR	14		1.6
		10	4	1.4
	1JUPTR	55		2.1
		55		2.4
	1MAUIO	3		-
		3		-
	1MOJAV	35		1.8
		35		1.5
	1NATOL	7		-
		6	1	-
	1OLFAN	21		1.7
		20	1	2.8

Table A1 (Continued)

2-Day Arc	Station	Number of Observations Used	Number of Observations Rejected	RMS of Fit (secs. arc)
July 11-12 (continued)	1OOMER	21		1.7
		20	1	2.2
	1ORGAN	35		1.5
		35		1.6
	1PURIO	7		-
		7		-
	1QUIPA	14		1.9
		14		3.1
	1ROSMA	12		1.2
		12		1.8
	1SHRAZ	14		2.2
		11	3	3.0
	1SPAIN	24	4	3.6
		28		2.1
	1SUDBR	46		2.0
		46		1.7
	1TANAN	14		1.8
		14		0.9
	1VILDO	17	4	3.8
		19	2	3.6
	ALL	1230	22	1.9
July 13-14	AUSBAK	20		1.8
		20		1.3
	1JOBUR	12	1	1.7
		10	3	1.8
	1JUPTR	105		1.7
		104	1	1.7
	1NATOL	25		1.4
		25		1.7
	1OLFAN	48	1	1.8
		47	2	2.0
	1OOMER	7		-
		7		-
	1ORGAN	59	2	1.9
		59	2	1.7
	1QUIPA	20		2.7
		20		2.0
	1SHRAZ	14		1.5
		14		2.8

Table A1 (Continued)

2-Day Arc	Station	Number of Observations Used	Number of Observations Rejected	RMS of Fit (secs. arc)
July 13-14 (continued)	1SPAIN	21		2.5
		21		1.2
	1TANAN	7		-
		7		-
	1VILDO	6		-
		0	6	-
	ALL	678	18	1.8
July 15-16	AUSBAK	14		1.9
		14		2.9
	1BERMD	14		1.8
		13	1	4.5
	1CURAC	6		-
		6		-
	1JOBUR	14		1.3
		14		2.2
	1JUPTR	110		1.5
		110		1.6
	1MAUIO	28		2.5
		28		1.2
	1OLFAN	49		1.6
		49		2.1
	1ORGAN	74		1.3
		74		1.4
	1PURIO	7		-
		7		-
	1QUIPA	21		1.6
		21		2.3
	1SPAIN	14		2.0
		14		1.4
	1SUDBR	14		1.8
		14		0.8
	1TANAN	7		-
		7		-
	1VILDO	14		1.9
		14		2.8
	ALL	771	1	1.8

Table A1 (Continued)

2-Day Arc	Station	Number of Observations Used	Number of Observations Rejected	RMS of Fit (secs. arc)
July 17-18	AUSBAK	49		1.7
		46	3	2.3
	1BERMD	42		2.9
		41	1	3.0
	1BPOIN	12		1.4
		12		2.7
	1COLBA	28		1.3
		28		1.5
	1EDINB	35		1.1
		35		1.8
	1GFORK	18		2.5
		17	1	2.1
	1JAMAC	13		1.2
		13		1.7
	1JOBUR	13		2.1
		13		1.5
	1JUPTR	112		1.9
		112		1.9
	1MAUIO	29		1.4
		29		1.6
	1MOJAV	14		2.0
		14		1.1
	1OLFAN	35		1.8
		35		1.9
	1ORGAN	71	2	1.6
		71	2	1.4
	1PURIO	13		1.0
		12	1	3.3
	1QUIPA	21		1.7
		21		2.8
	1SPAIN	47	2	1.9
		47	2	2.0
	1TANAN	14		2.3
		14		2.6
	1VILDO	14		1.4
		14		2.0
	ALL	1154	14	1.9

Table A1 (Continued)

2-Day Arc	Station	Number of Observations Used	Number of Observations Rejected	RMS of Fit (secs. arc)
July 19-20	AUSBAK	6		-
		6		-
	1BERMD	7		-
		7		-
	1BPOIN	33		1.7
		33		1.8
	1COLBA	43		1.0
		43		1.4
	1EDINB	56		1.0
		56		1.3
	1FTMYR	7		-
		7		-
	1GFORK	62		1.5
		62		1.3
	1GSFCP	7		-
		7		-
	1JAMAC	14		0.6
		14		2.6
	1JOBUR	32	3	1.9
		33	2	1.8
	1JUPTR	62	1	2.3
		62	1	2.3
	1MAUIO	12		2.6
		12		2.6
	1MOJAV	35		1.3
		35		1.9
	1OLFAN	21		1.6
		21		2.3
	1ORGAN	8		-
		8		-
	1QUIPA	27	1	3.0
		25	3	2.8
	1SPAIN	75	1	2.7
		75	1	1.9
	1SUDBR	42		2.1
		41	1	2.0
	1VILDO	7		-
		1	6	-
	ALL	1104	20	1.9

Table A1 (Continued)

2-Day Arc	Station	Number of Observations Used	Number of Observations Rejected	RMS of Fit (secs. arc)
July 21-22	AUSBAK	21		1.5
		21		2.6
	1COLBA	21		2.1
		21		1.5
	1EDINB	13		2.4
		13		1.3
	1FTMYR	7		-
		7		-
	1JOBUR	7		-
		7		-
	1JUPTR	31		1.7
		31		2.0
	1MAUIO	14		2.6
		14		1.1
	1OLFAN	42		1.8
		42		2.1
	1ORGAN	66		1.9
		66		2.5
	1QUIPA	47		1.7
		47		2.6
	1ROSMA	14		2.4
		14		1.2
	1SPAIN	62	1	2.7
		63		1.8
	1SUDBR	21		3.3
		21		2.0
	1VILDO	7		-
		7		-
	ALL	747	1	2.1
July 23-24	AUSBAK	49		1.4
		48	1	2.1
	1BERMD	18		1.3
		18		3.8
	1BPOIN	14		1.1
		14		1.9
	1DENVR	7		-
		7		-
	1EDINB	21	12	0.9
		21	12	1.3

Table A1 (Continued)

2-Day Arc	Station	Number of Observations Used	Number of Observations Rejected	RMS of Fit (secs. arc)
July 23-24 (continued)	1FTMYR	7		-
		7		-
	1GFORK	26		2.2
		26		1.5
	1GSFCP	7		-
		7		-
	1JAMAC	14		1.6
		14		2.2
	1JOBUR	21		1.1
		21		1.5
	1MAUIO	8		-
		8		-
	1MOJAV	14		1.5
		14		2.1
	1OLFAN	21		1.6
		21		2.0
	1ORGAN	132		1.7
		132		1.6
	1PURIO	14		1.9
		14		1.6
	1QUIPA	28		1.6
		28		2.8
	1ROSMA	38		1.0
		38		1.4
	1SPAIN	14		1.8
		14		1.7
	1SUDBR	21		2.3
		21		1.8
	1VILDO	21		1.7
		21		2.2
	ALL	989	25	1.8
July 25-26	AUSBAK	35		1.8
		33	2	2.3
	1BPOIN	7		-
		7		-
	1COLBA	21		0.8
		21		1.2
	1DENVR	19		1.4
		19		1.3

Table A1 (Continued)

2-Day Arc	Station	Number of Observations Used	Number of Observations Rejected	RMS of Fit (secs. arc)
July 25–26 (continued)	1EDINB	35		1.0
		35		1.2
	1GFORK	13		1.9
		11	2	1.6
	1MAUIO	49		1.8
		49		1.6
	1MOJAV	32	1	1.1
		33		1.7
	1ORGAN	73	1	1.4
		73	1	1.6
	1QUIPA	6	1	-
		3	4	-
	1ROSMA	7		-
		7		-
	1SPAIN	70	7	2.3
		77		1.6
	1SUDBR	14		2.3
		14		1.6
	ALL	763	19	1.7
July 31— August 1	1BPOIN	27	1	1.3
		26	2	1.8
	1COLBA	27		0.9
		27		1.4
	1EDINB	35		1.1
		35		1.4
	1FTMYR	7		-
		7		-
	1GSFCP	21		2.4
		21		3.0
	1JUPTR	25	3	2.9
		28		2.4
	1ORGAN	142	2	2.0
		144		1.8
	1PURIO	7		-
		7		-
	1SPAIN	67		1.9
		67		1.8
	1SUDBR	34		1.3
		34		1.9
	ALL	788	8	1.9

Table A1 (Continued)

2-Day Arc	Station	Number of Observations Used	Number of Observations Rejected	RMS of Fit (secs. arc)
August 2-3	JOHNST	0	2	-
		1	1	-
	1BERMD	7		-
		4	3	-
	1BPOIN	21		1.5
		21		1.9
	1COLBA	63		2.0
		63		1.2
	1FTMYR	28		1.7
		28		1.5
	1GFORK	42		1.9
		42		1.5
	1GSFCP	19		2.1
		17	2	3.8
	1JUPTR	56		1.6
		56		1.4
	1MAUIO	27		2.0
		27		2.6
	1MOJAV	14		2.4
		14		2.0
	1SPAIN	63		2.3
		63		2.5
	1SUDBR	53		2.1
		51	2	2.8
	ALL	780	10	2.1
August 4-5	AUSBAK	35		2.3
		35		1.7
	1BERMD	7		-
		0	7	-
	1COLBA	41		2.3
		41		2.9
	1EDINB	21		1.6
		21		1.9
	1GFORK	32		1.7
		32		3.4
	1JOBUR	21		1.5
		21		1.6
	1JUPTR	75		2.2
		74	1	1.9

Table A1 (Continued)

2-Day Arc	Station	Number of Observations Used	Number of Observations Rejected	RMS of Fit (secs. arc)
August 4-5 (continued)	1MAUIO	53		1.9
		53		1.7
	1MOJAV	27		2.0
		27		1.9
	1OLFAN	21		1.8
		21		2.8
	1ORGAN	56		1.5
		56		1.5
	1QUIPA	14		1.8
		14		1.6
	1SPAIN	90		1.8
		90		2.2
	1VILDO	7		-
		7		-
	ALL	992	8	2.0
August 6-7	AUSBAK	14		1.4
		14		1.8
	JOHNST	0	1	-
		1		-
	1BERMD	14		2.0
		11	3	3.3
	1BPOIN	28		1.7
		28		1.5
	1COLBA	35	7	1.1
		37	5	2.2
	1DENVR	7		-
		7		-
	1EDINB	14		1.7
		14		3.0
	1GFORK	7		-
		7		-
	1JAMAC	7		-
		7		-
	1JOBUR	13	1	1.9
		13	1	1.9
	1MOJAV	14		2.3
		14		1.6
	1OLFAN	14		1.3
		14		2.2

Table A1 (Continued)

2-Day Arc	Station	Number of Observations Used	Number of Observations Rejected	RMS of Fit (secs. arc)
August 6-7 (continued)	1ORGAN	7		-
		7		-
	1PURIO	4		-
		4		-
	1QUIPA	14		2.2
		14		2.1
	1SPAIN	63		1.8
		62	1	1.8
	1SUDBR	17		1.6
		17		2.0
	1VILDO	14		2.1
		14		1.9
	ALL	571	19	1.9

Table A2

2-Day TRANET Doppler Orbital Solutions.

2-Day Arc	Station	Number of Observations Used	Number of Observations Rejected	RMS of Fit (cm/sec)
July 9-10	ANCHOR	363	4	2.9
	WAHIWA	214	6	2.8
	LACRES	352	2	2.5
	APLMND	500	3	2.8
	LASHM2	548	3	2.3
	ALL	1977	18	2.7
July 11-12	ANCHOR	449	11	3.2
	WAHIWA	98	0	2.4
	LACRES	420	2	2.7
	APLMND	409	4	2.9
	LASHM2	515	5	2.5
	ALL	1891	22	2.8
July 13-14	ANCHOR	522	7	3.1
	WAHIWA	154	1	2.6
	LACRES	326	5	2.6
	APLMND	321	5	2.9
	LASHM2	535	5	2.6
	ALL	1858	23	2.8

Table A2 (Continued)

2-Day Arc	Station	Number of Observations Used	Number of Observations Rejected	RMS of Fit (cm/sec)
July 15-16	ANCHOR	494	3	2.9
	WAHIWA	182	3	2.9
	LACRES	274	3	3.0
	APLMND	487	7	2.9
	LASHM2	528	2	2.4
	ALL	1965	18	2.8
July 17-18	ANCHOR	429	25	3.1
	WAHIWA	227	3	2.5
	LACRES	387	5	2.9
	APLMND	423	0	2.4
	LASHM2	447	3	2.5
	ALL	1913	36	2.7
July 19-20	ANCHOR	522	13	2.8
	WAHIWA	234	3	2.7
	LACRES	307	2	2.7
	APLMND	483	5	2.6
	LASHM2	410	2	2.1
	ALL	1956	25	2.6
July 21-22	ANCHOR	440	11	2.8
	WAHIWA	192	0	3.0
	LACRES	429	3	2.6
	APLMND	520	2	2.8
	LASHM2	307	41	2.0
	ALL	1888	57	2.7
July 23-24	ANCHOR	440	11	3.2
	WAHIWA	287	2	2.7
	LACRES	328	2	2.6
	APLMND	467	3	2.6
	LASHM2	275	2	2.3
	ALL	1797	20	2.7
July 25-26	ANCHOR	375	15	3.2
	WAHIWA	284	1	2.5
	LACRES	208	7	2.9
	APLMND	494	31	2.6
	LASHM2	501	3	2.1
	ALL	1862	57	2.7
July 31 — August 1	ANCHOR	438	13	3.3
	WAHIWA	316	1	2.3
	LACRES	160	2	3.1
	APLMND	484	4	2.8
	LASHM2	471	4	2.1
	ALL	1869	24	2.8

Table A2 (Continued)

2-Day Arc	Station	Number of Observations Used	Number of Observations Rejected	RMS of Fit (cm/sec)
August 2-3	ANCHOR	517	6	3.3
	WAHIWA	268	1	2.5
	LACRES	158	2	2.6
	APLMND	519	3	3.1
	LASHM2	391	36	2.7
	ALL	1853	48	3.0
August 4-5	ANCHOR	491	20	3.1
	LACRES	407	5	2.8
	APLMND	392	0	2.9
	LASHM2	532	4	2.1
	ALL	1822	29	2.7
August 6-7	ANCHOR	442	13	3.1
	WAHIWA	180	0	2.4
	LACRES	174	40	2.8
	APLMND	511	4	2.8
	LASHM2	541	3	2.2
	ALL	1848	60	2.7

Appendix B

Position Differences Between Doppler and Optically Determined Orbits

Figures are presented for five of the thirteen 2-day orbital intercomparisons showing plots of the satellite position differences between the optically determined and Doppler determined orbits over the span of the arc.

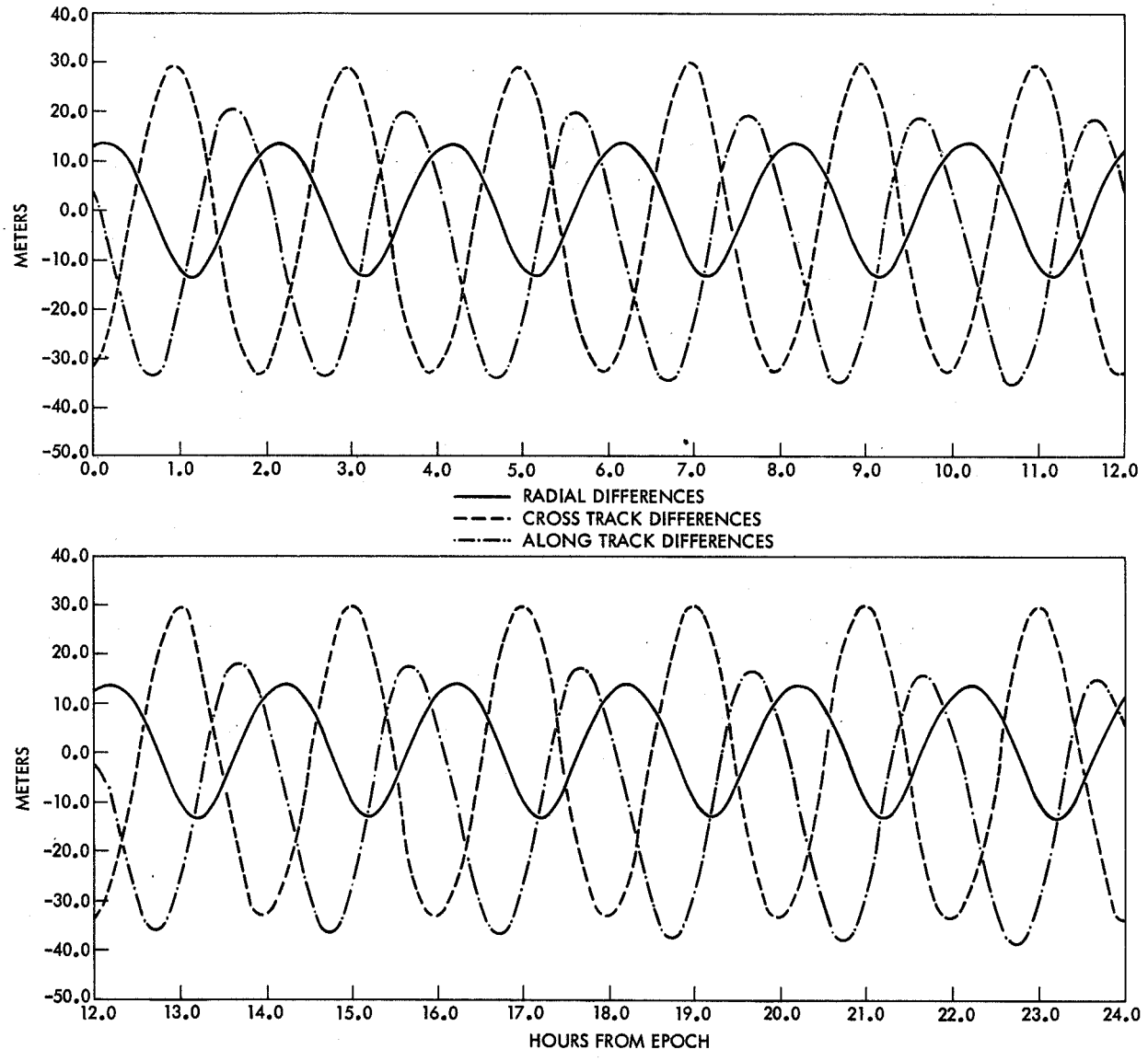

Figure B1—Position differences between TRANET Doppler orbit and optical orbit for the 2-day arc, July 15-16, 1966.

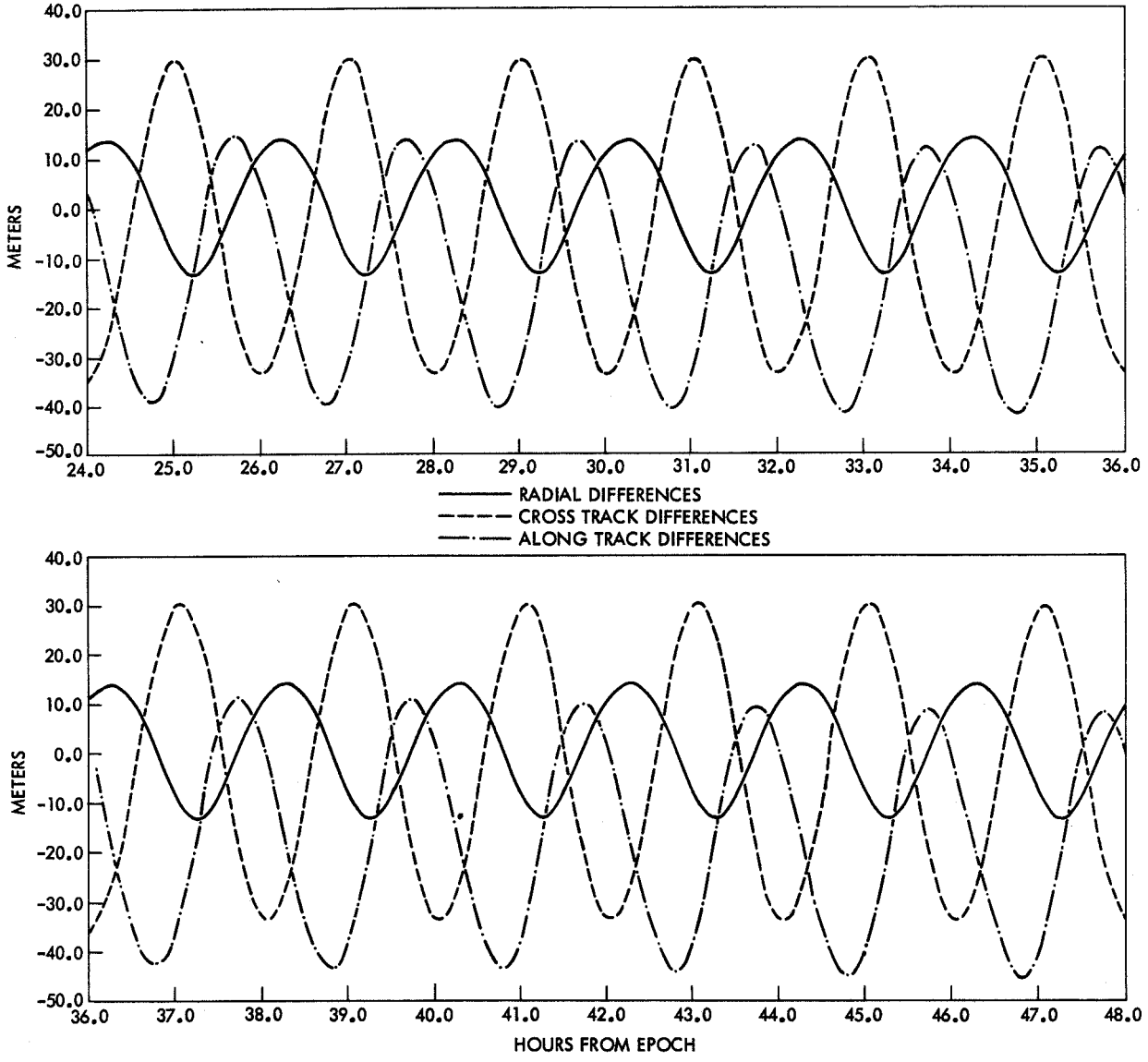

Figure B1 (continued)—Position differences between TRANET Doppler orbit and optical orbit for the 2-day arc, July 15-16, 1966.

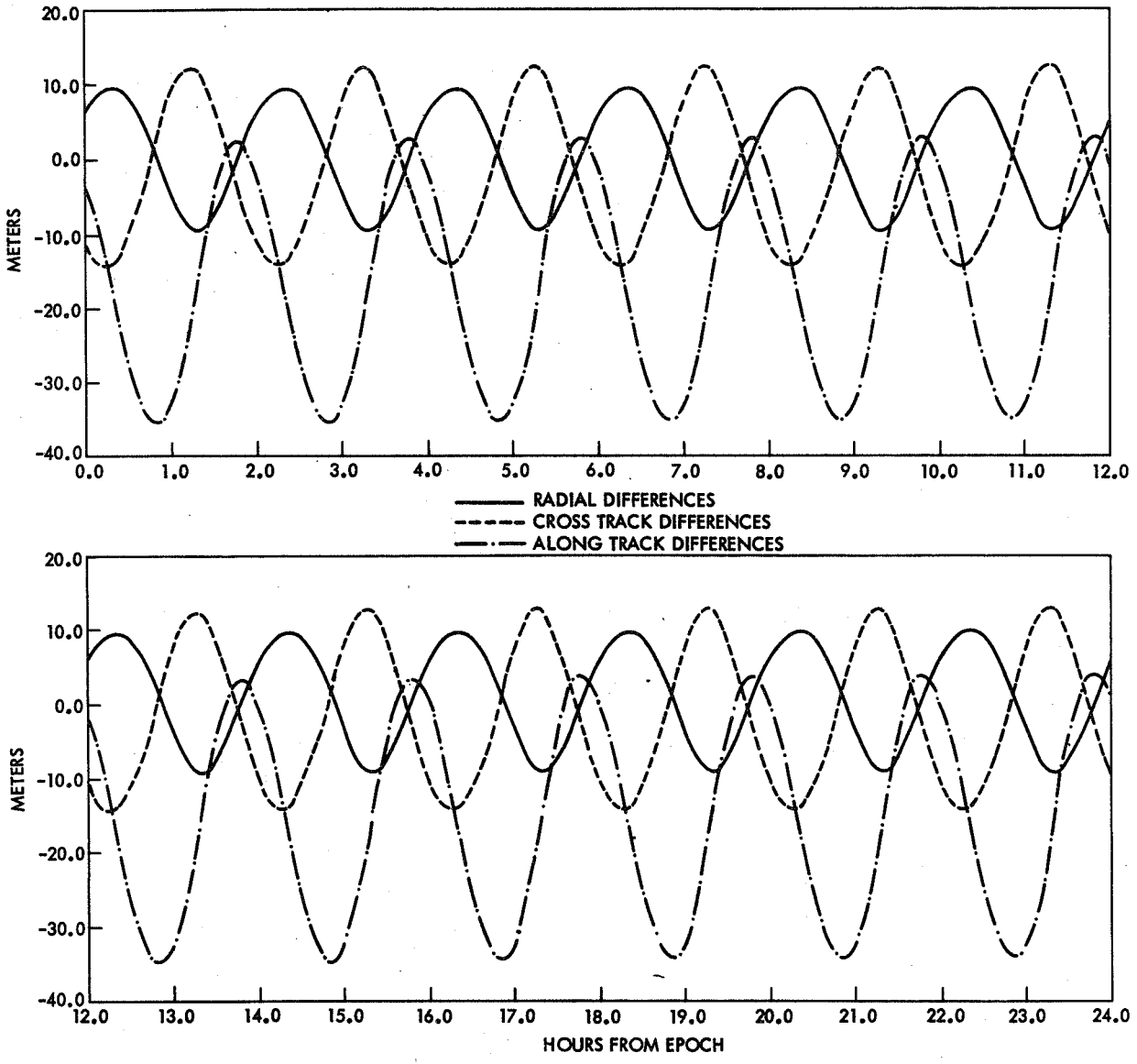

Figure B2—Position differences between TRANET Doppler orbit and optical orbit for the 2-day arc, July 17-18, 1966.

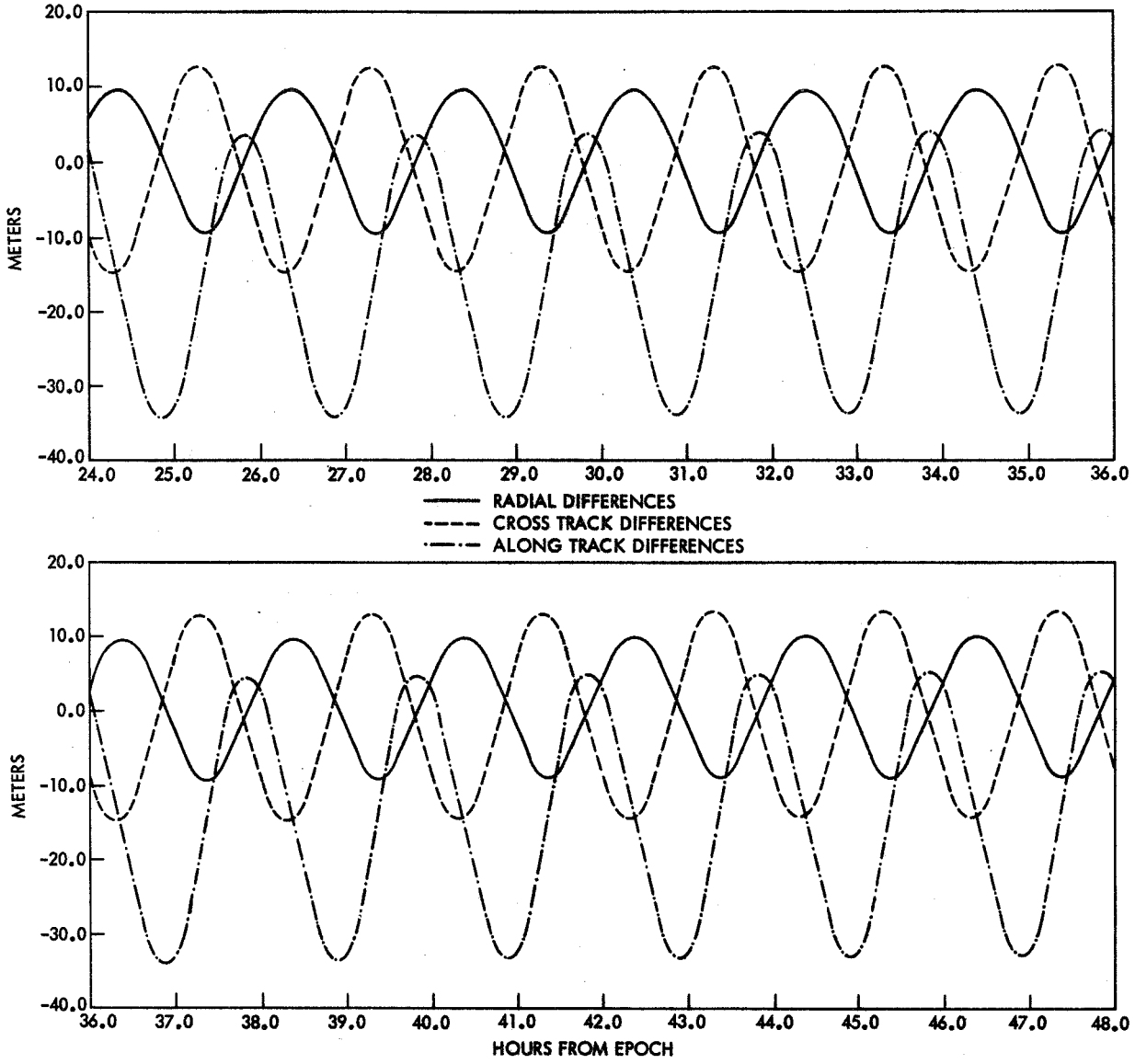

Figure B2 (continued)—Position differences between TRANET Doppler orbit and optical orbit for the 2-day arc, July 17-18, 1966.

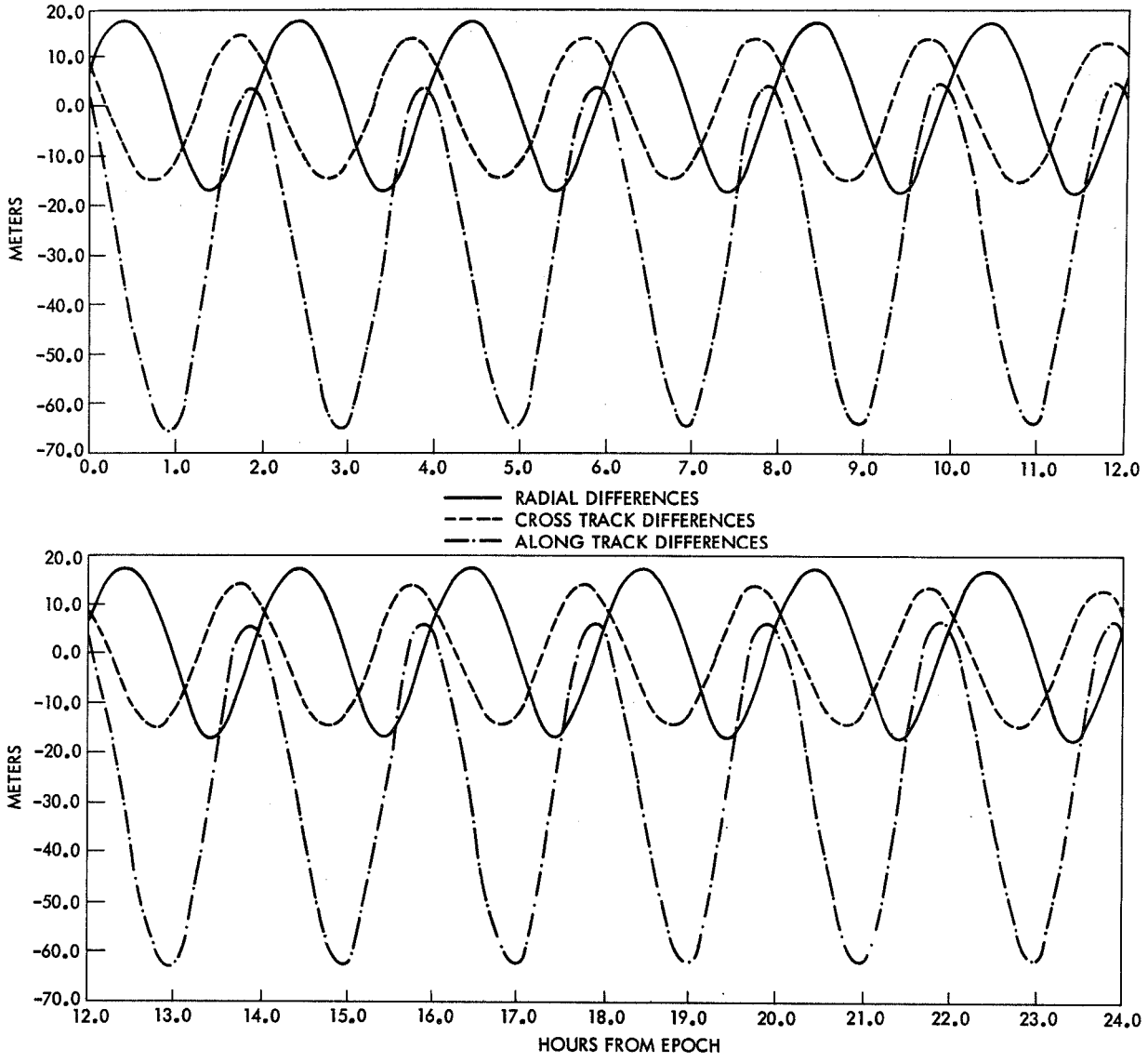

Figure B3—Position differences between TRANET Doppler orbit and optical orbit for the 2-day arc, July 19-20, 1966.

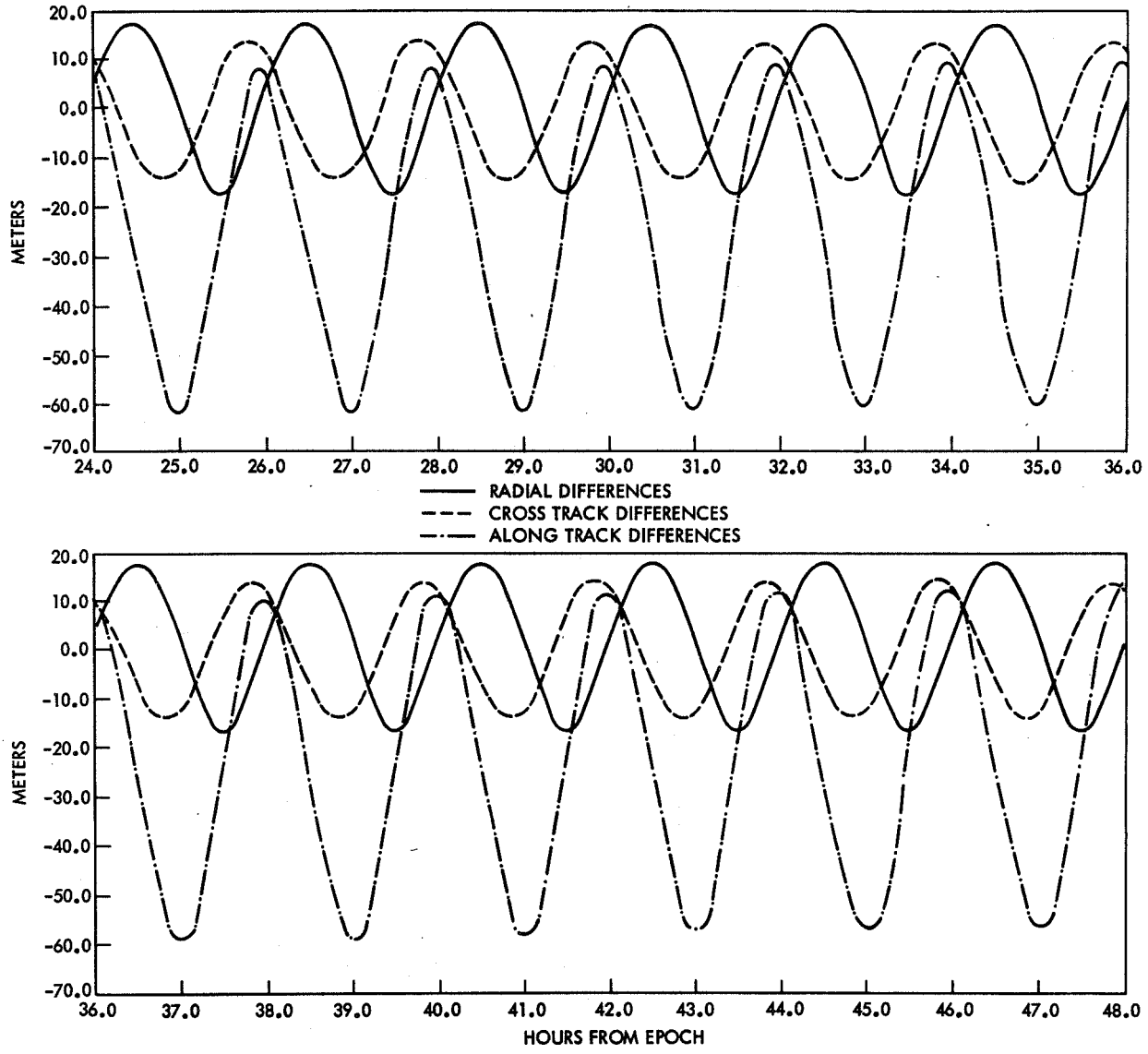

Figure B3 (continued)—Position differences between TRANET Doppler orbit and optical orbit for the 2-day arc, July 19-20, 1966.

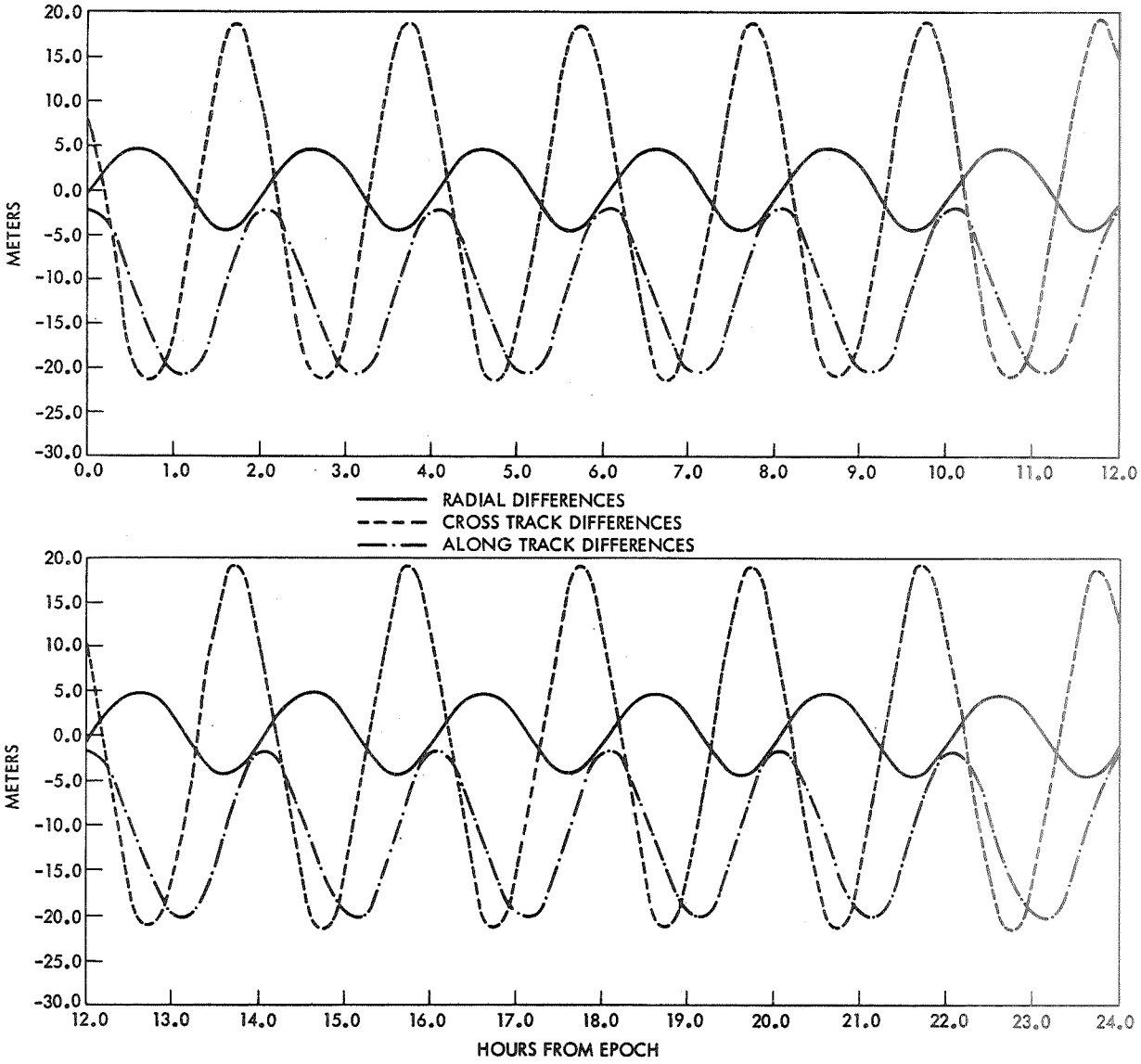

Figure B4—Position differences between TRANET Doppler orbit and optical orbit for the 2-day arc, July 23-24, 1966.

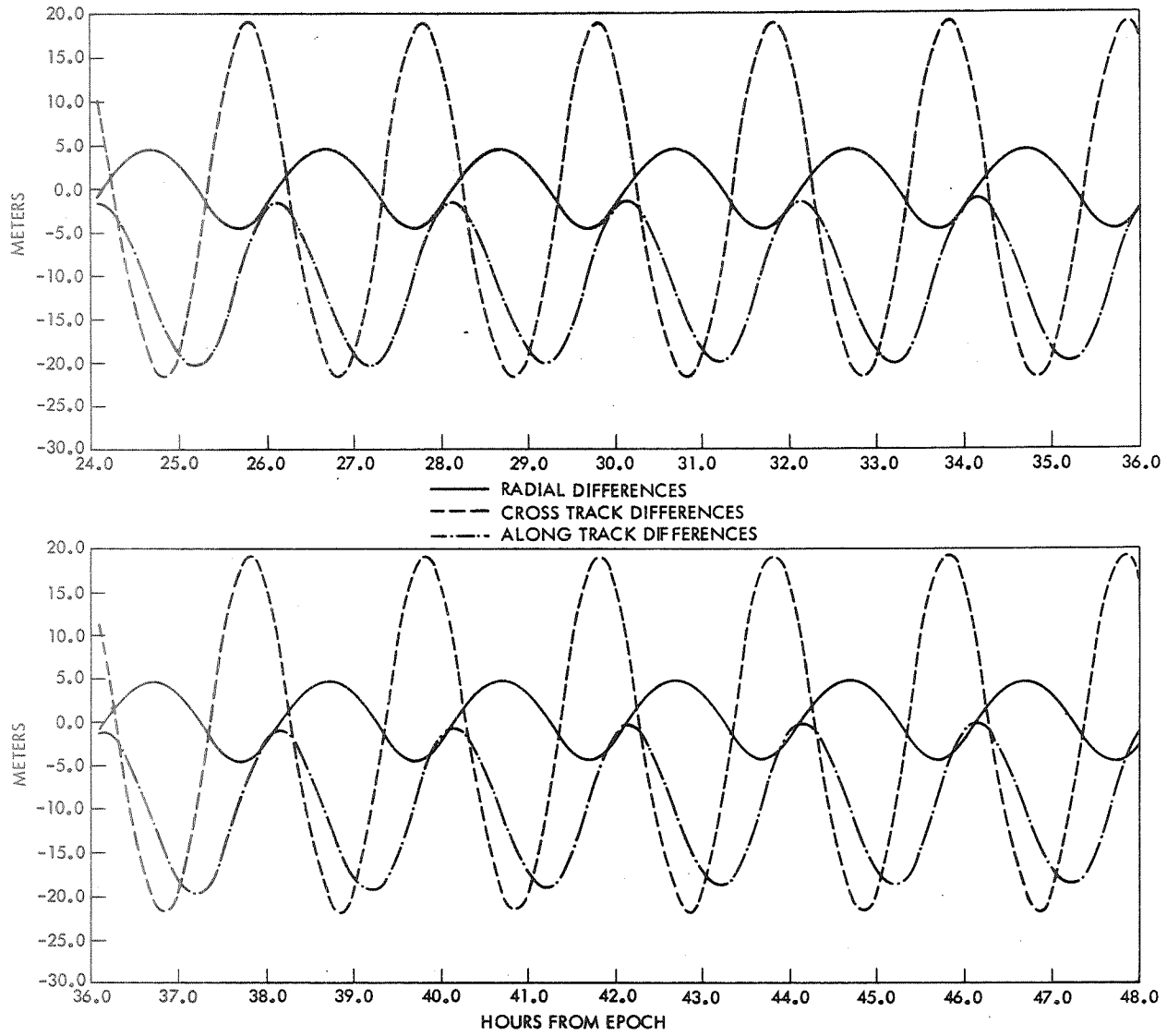

Figure B4 (continued)—Position differences between TRANET Doppler orbit and optical orbit for the 2-day arc, July 23-24, 1966.

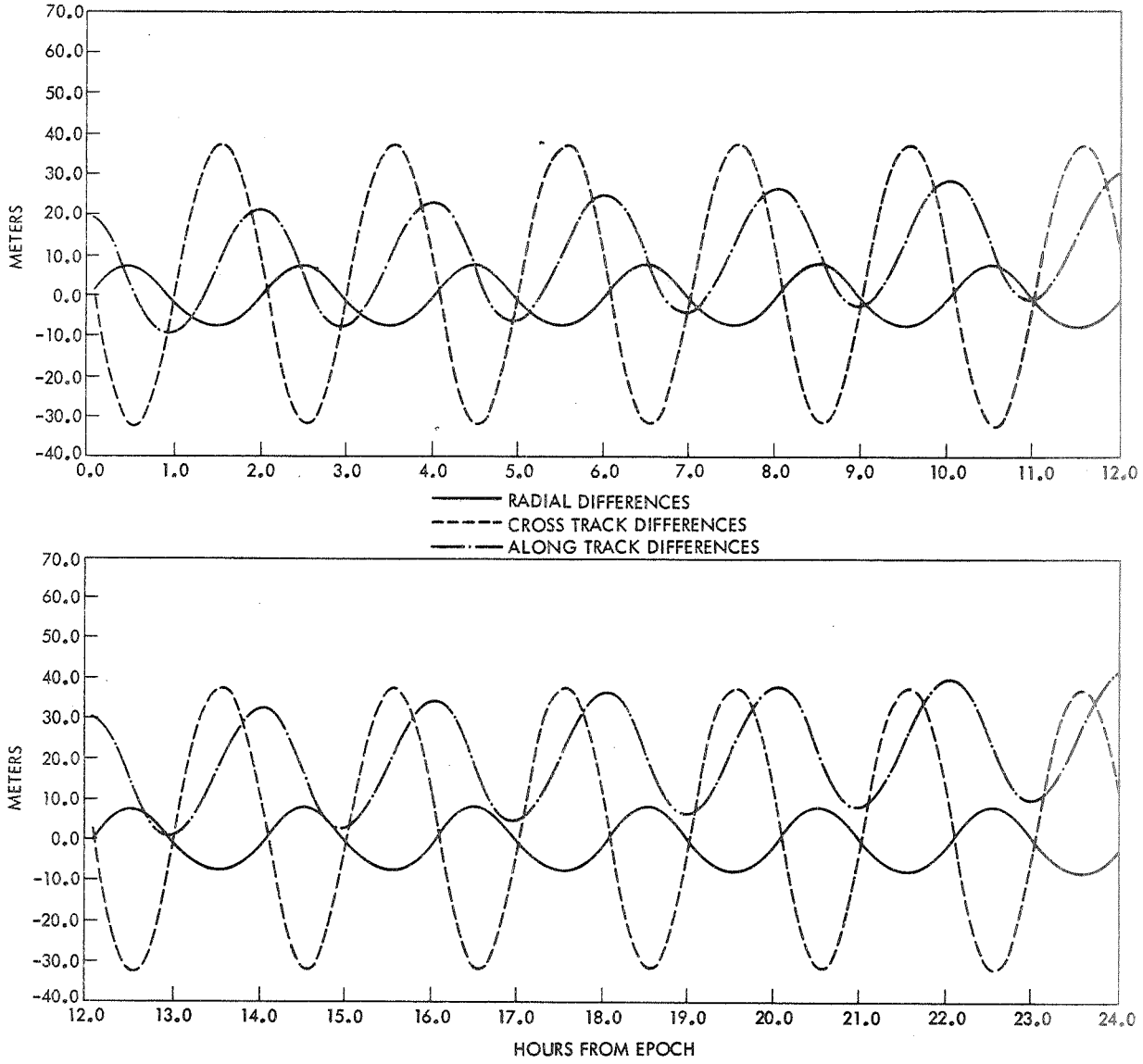

Figure B5—Position differences between TRANET Doppler orbit and optical orbit for the 2-day arc, August 4-5, 1966.

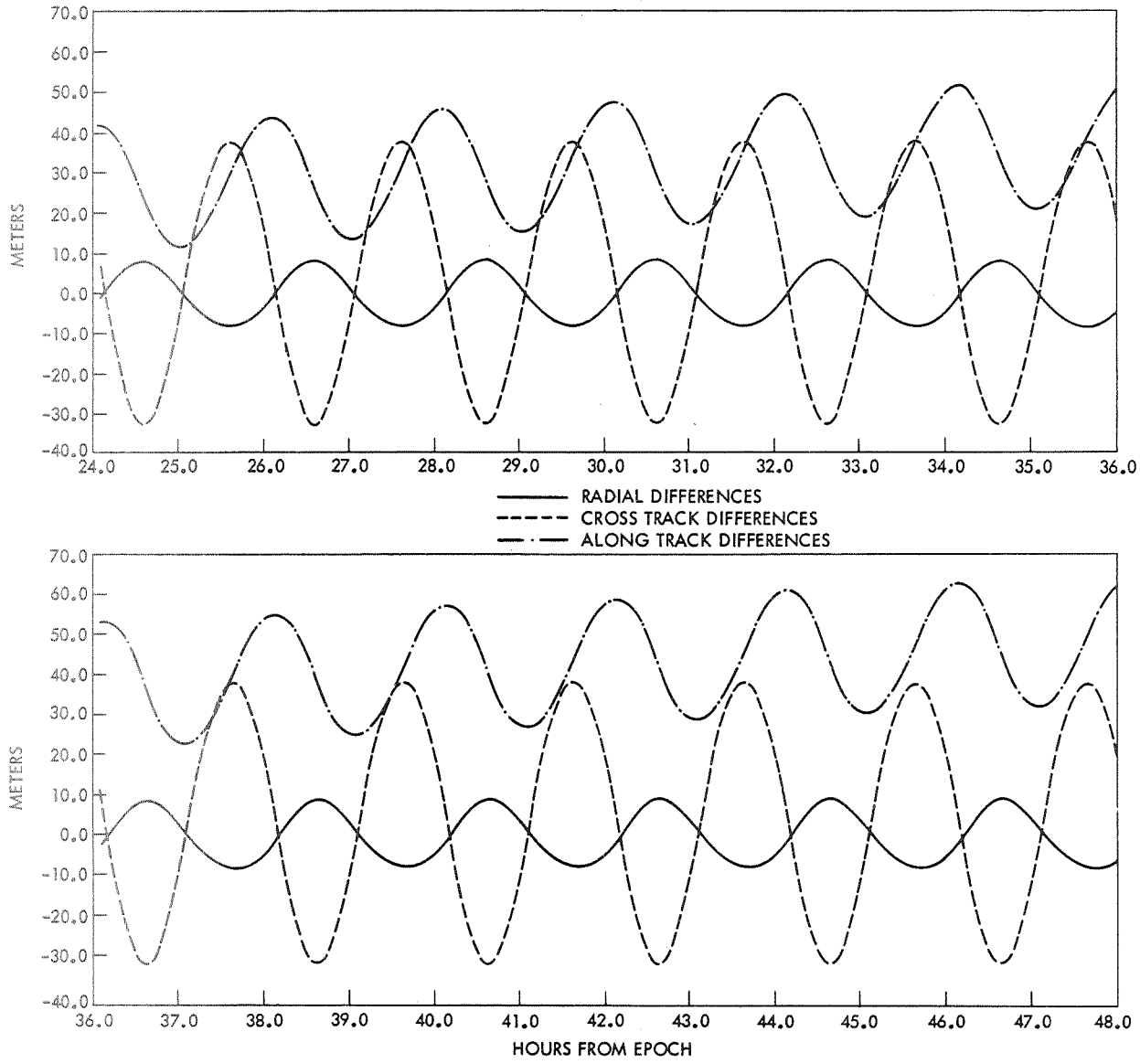

Figure B5 (continued)—Position differences between TRANET Doppler orbit and optical orbit for the 2-day arc, August 4-5, 1966.

Appendix C

Position Differences Between Doppler and Optically Determined Orbits for Selected Arc Lengths

Figures are presented for 9 selected arc lengths showing plots of the satellite position differences between the optically determined and Doppler determined orbits over the span of the particular arc.

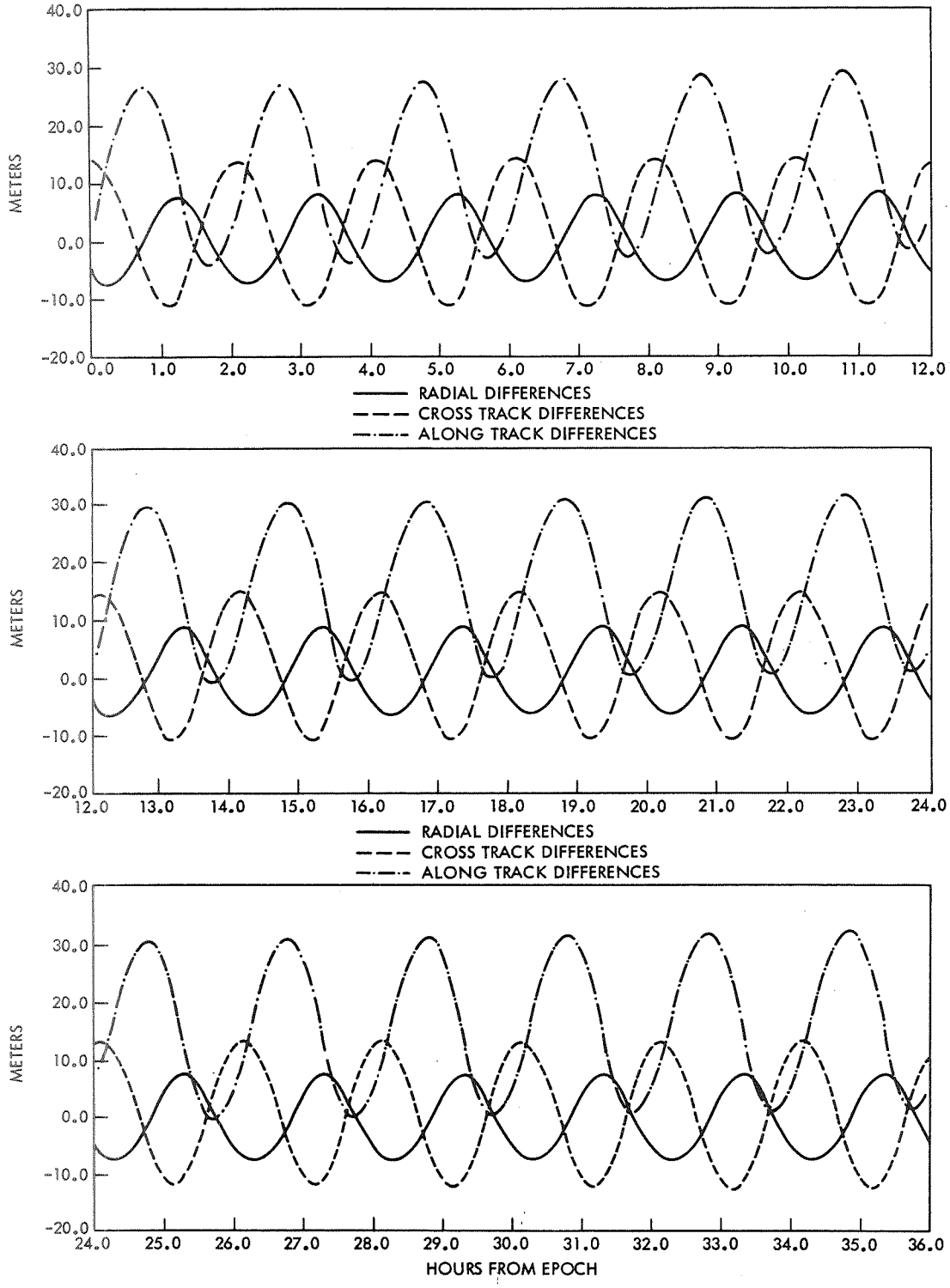

Figure C1—Position differences between TRANET Doppler orbit and optical orbit for the 1-1/2-day arc, July 17, 0 hrs—July 18, 12 hrs, 1966.

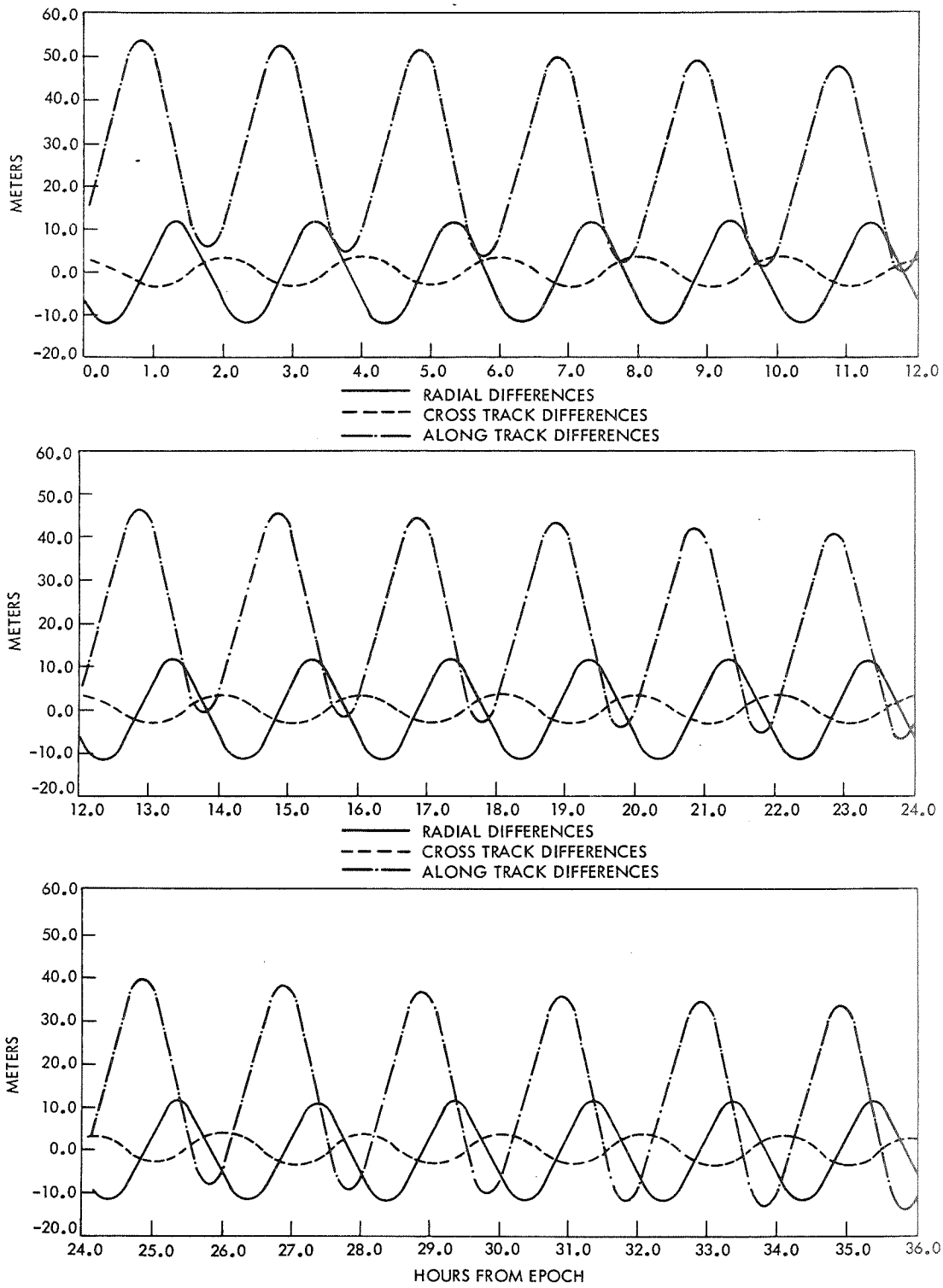

Figure C2—Position differences between TRANET Doppler orbit and optical orbit for the 1-1/2-day arc, July 17-12 hrs—July 19, 0 hrs, 1966.

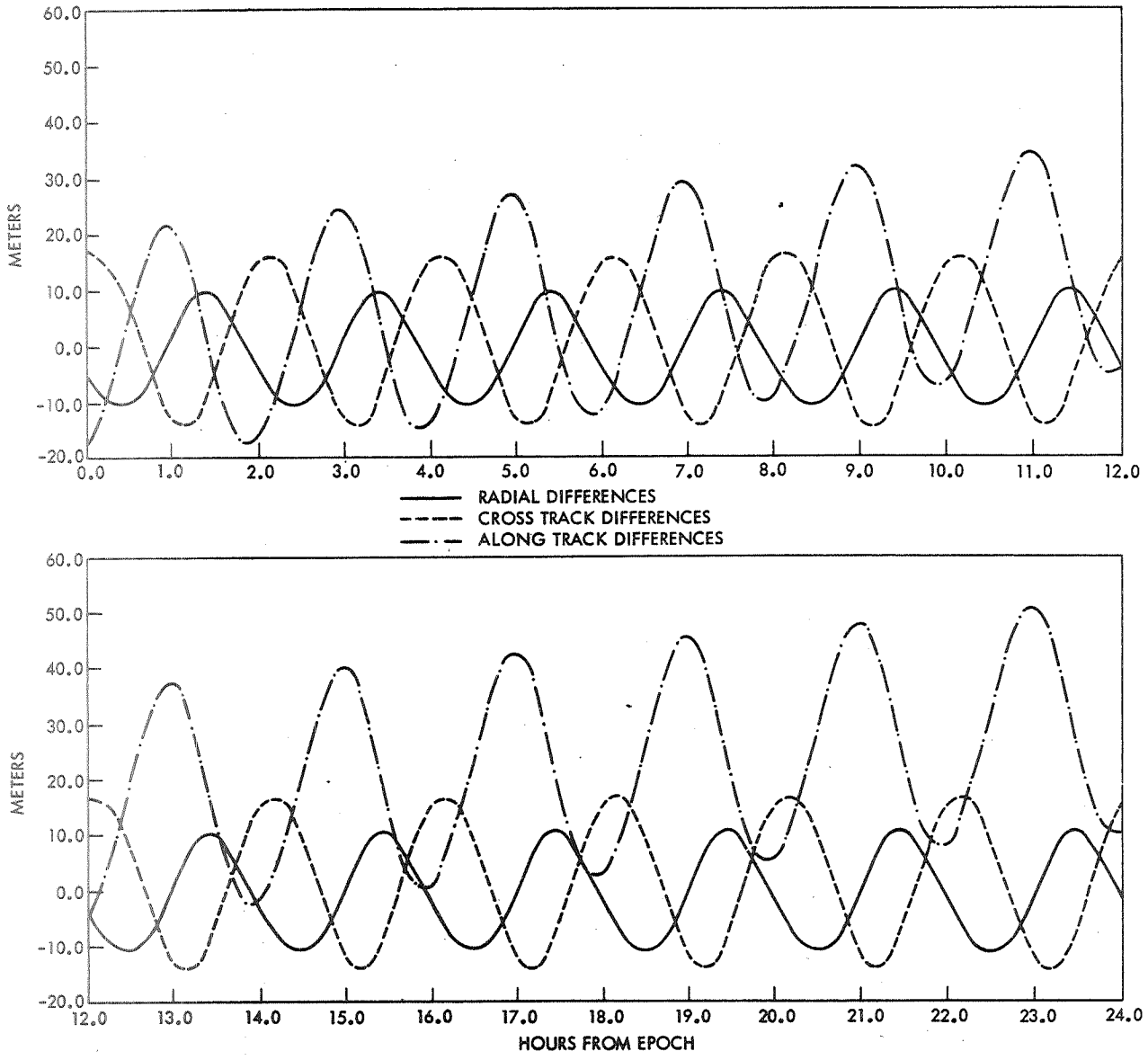

Figure C3—Position differences between TRANET Doppler orbit and optical orbit for the 1-day arc, July 17, 0 through 24 hrs, 1966.

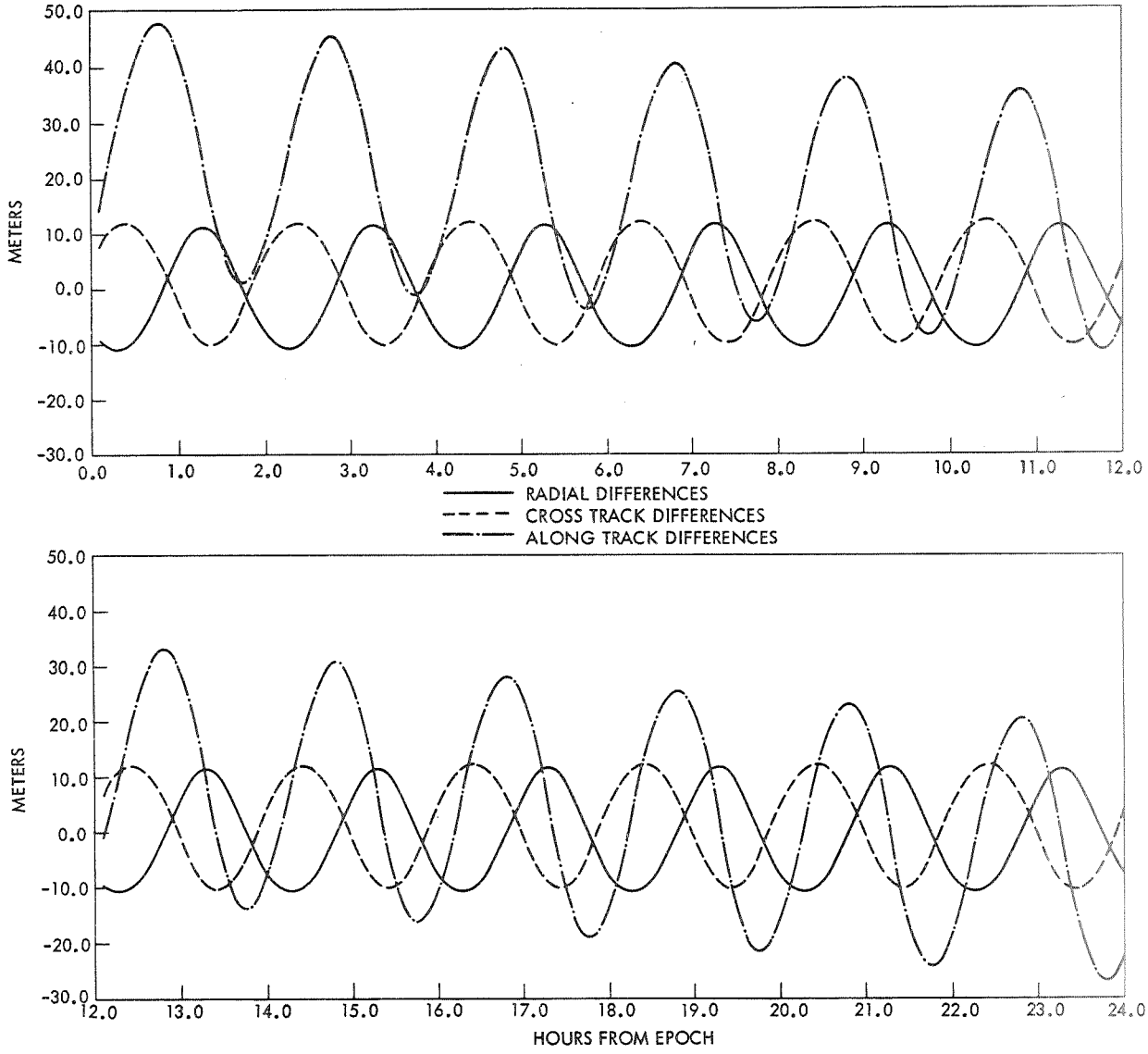

Figure C4—Position differences between TRANET Doppler orbit and optical orbit for the 1-day arc, July 18, 0 through 24 hrs, 1966.

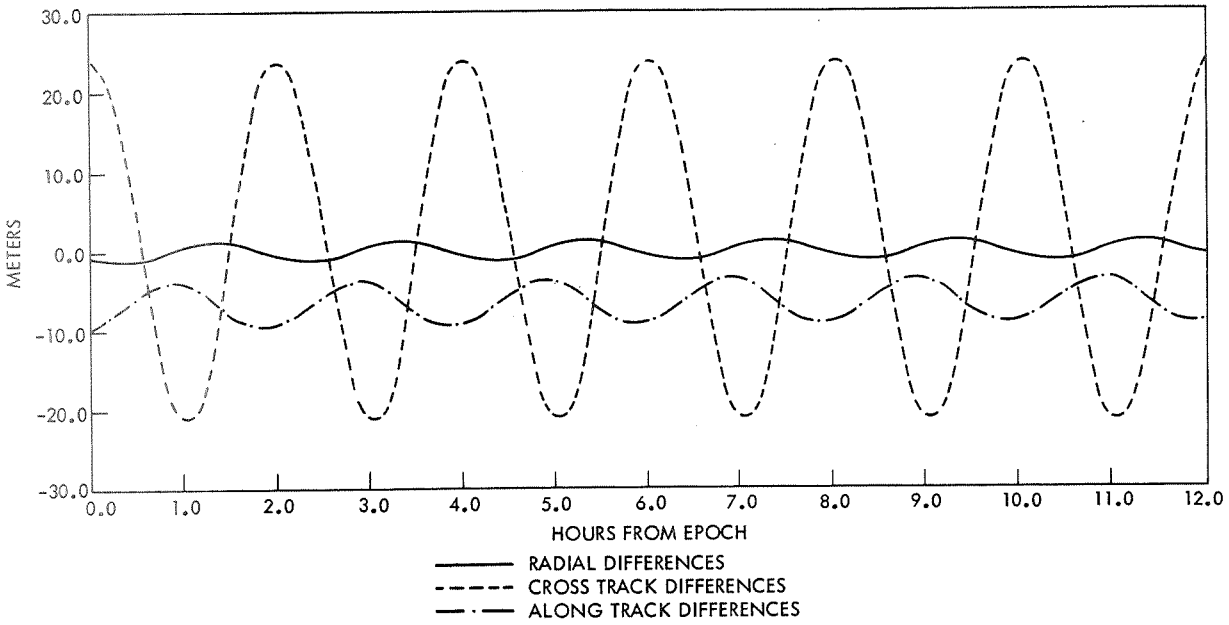

Figure C5—Position differences between TRANET Doppler orbit and optical orbit for the 1/2-day arc, July 17, 0 through 12 hrs, 1966.

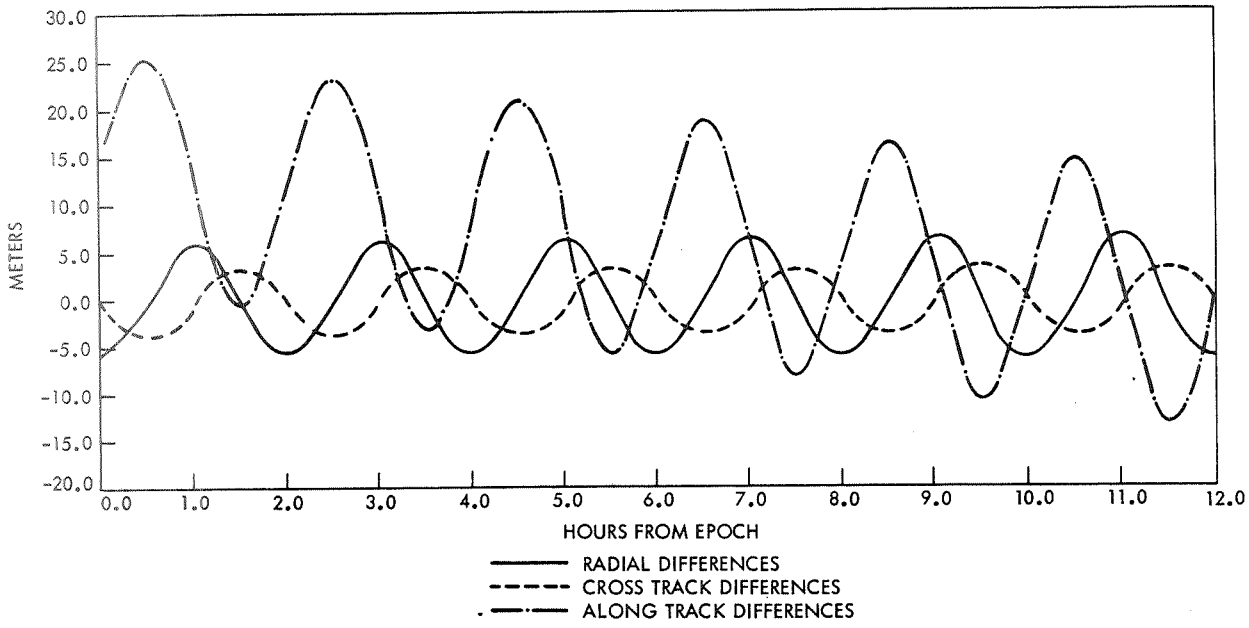

Figure C6—Position differences between TRANET Doppler orbit and optical orbit for the 1/2-day arc, July 18, 0 through 12 hrs, 1966.

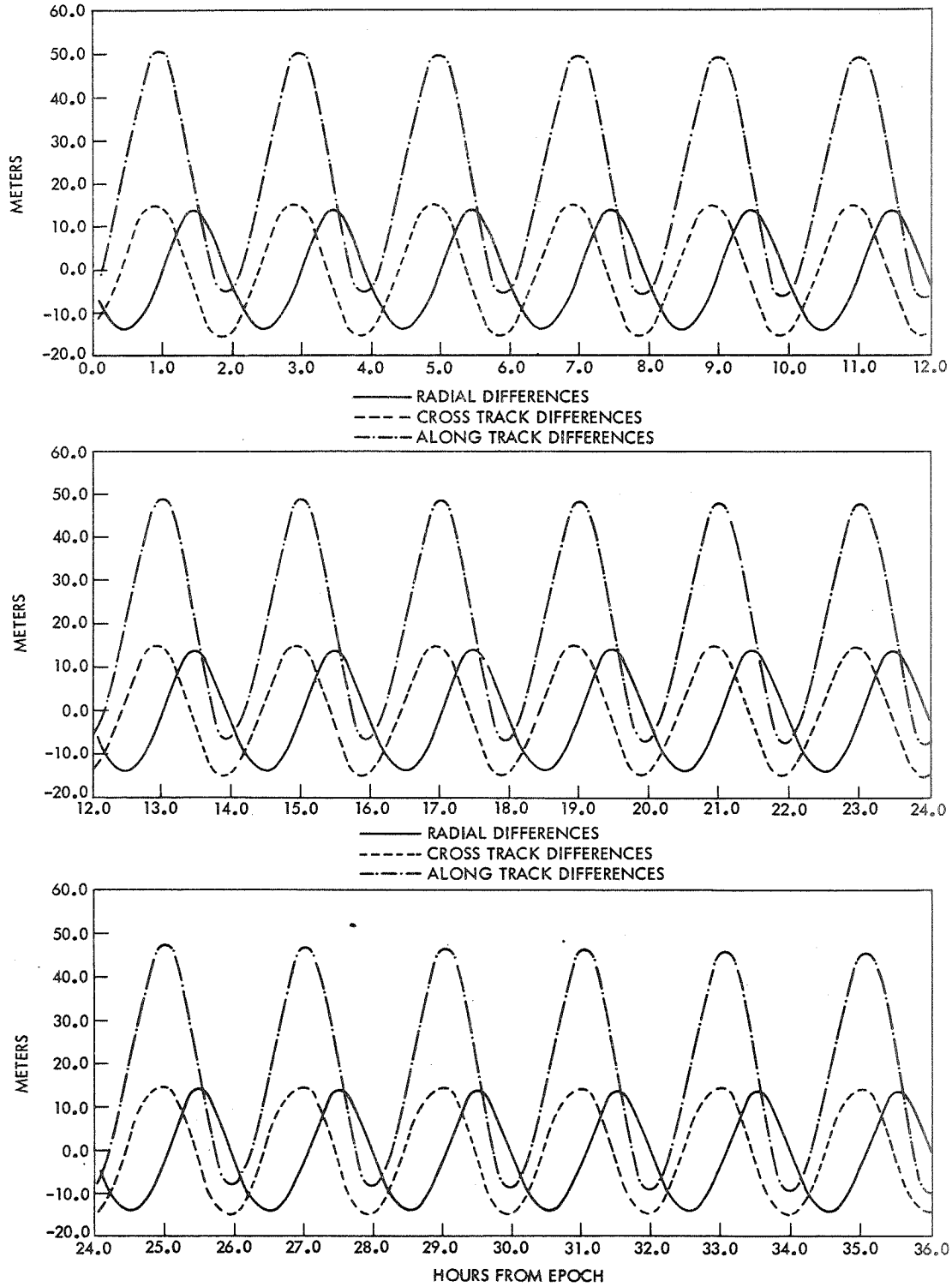

Figure C7—Position differences between TRANET Doppler orbit and optical orbit for the 1-1/2-day arc, July 19, 0 hrs—July 20, 12 hrs, 1966.

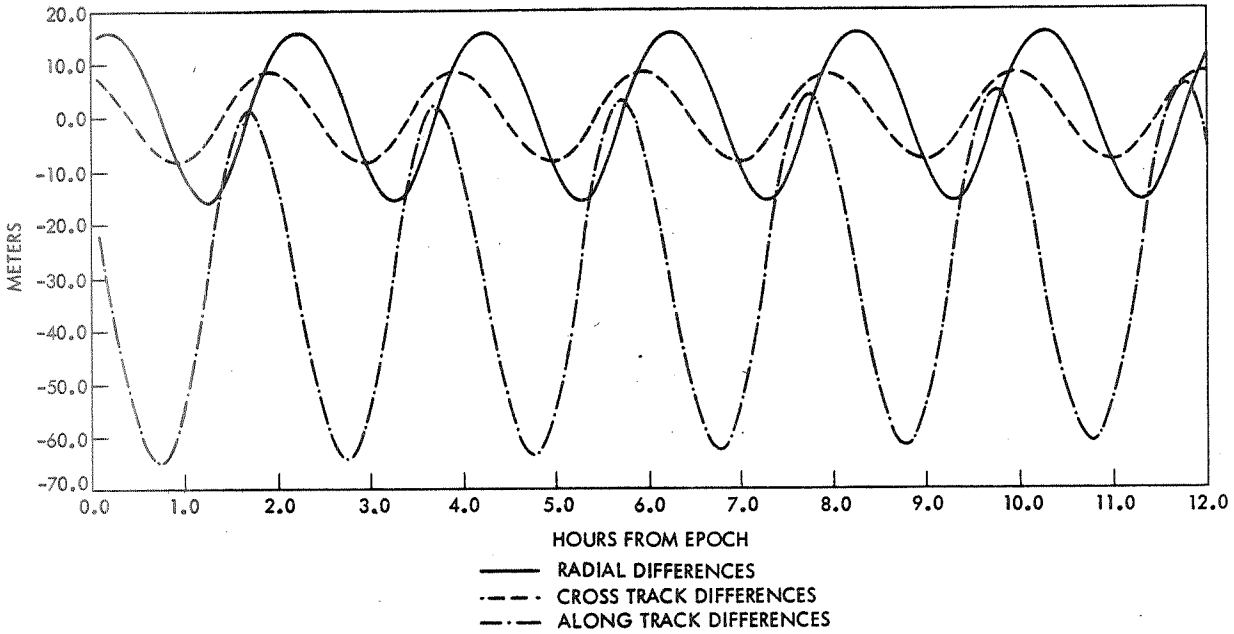

Figure C8—Position differences between TRANET Doppler orbit and optical orbit for the 1/2-day arc, July 19, 0 through 12 hrs, 1966.

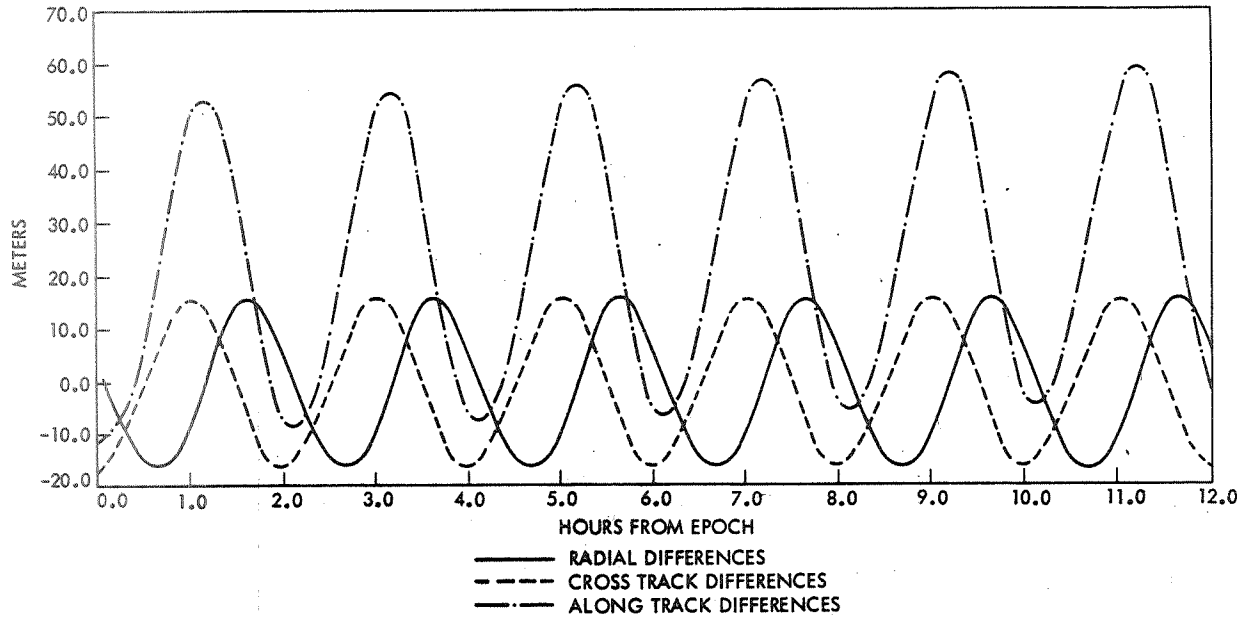

Figure C9—Position differences between TRANET Doppler orbit and optical orbit for the 1/2-day arc, July 20, 0 through 12 hrs, 1966.

Appendix D

Timing Biases and Range-Rate (Base Frequency) Biases in the Doppler Data

Table D1 presents timing biases,* calculated for each pass of TRANET Doppler data in the period July 17-20, 1966. The timing biases were determined by fitting the residuals from each pass to the formula:

$$\Delta\dot{R} = \Delta B + \Delta t\ddot{R} ,$$

where

$\Delta\dot{R}$ = residual (o-c)

ΔB = zero set bias

Δt = timing error

$\Delta\ddot{R}$ = rate of change of the observation.

Table D2 presents a summary of the (base frequency) range rate biases determined for each pass of TRANET Doppler data over the entire period of the study, July 9-26, July 31—August 7, 1966. In each 2-day Doppler orbital solution, the range rate biases for every pass were dynamically determined along with the state vector.

*These timing biases could possibly be attributed to hardware or to an orbital error or a combination of both.

Table D1

Timing Biases Found in the TRANET Doppler Data, July 17-20, 1966.

Station	Day (1966)	Pass		Timing Error (msecs.)	Mean Timing Error ± 1 Standard Deviation (msecs.)
		Start	End		
APLMND	July 17	3:28	3:47	-0.6	
		5:36	5:54	-1.5	
		7:40	8:03	1.8	
		9:49	10:14	-7.3	
		11:55	12:23	-4.1	
		14:02	14:26	4.1	0.6 ± 4.2
	July 18	3:30	3:52	1.2	
		5:38	5:59	1.4	
		7:45	8:08	4.4	
		14:06	14:28	6.6	
LASHM2	July 17	3:42	4:09	-2.2	
		5:48	6:16	-1.8	
		7:54	8:20	-1.8	
		21:33	21:51	4.4	
		23:34	23:58	5.5	
	July 18	1:40	2:05	1.9	0.0 ± 3.2
		3:49	4:14	-0.5	
		5:53	6:20	0.6	
		7:58	8:24	-5.0	
		21:38	21:56	-1.2	
ANCHOR	July 17	7:34	7:52	-1.7	
		9:35	9:58	3.8	
		11:40	12:04	-1.7	
		13:43	14:10	4.8	
		15:49	16:15	-1.0	
		17:53	18:17	-5.4	-0.8 ± 3.2
	July 18	9:39	10:03	-3.3	
		11:45	12:09	-0.4	
		13:48	14:15	0.6	
		15:53	16:19	-3.6	
LACRES	July 17	9:43	10:01	7.4	
		11:51	12:15	-3.1	
		13:57	14:25	5.6	
	July 18	5:29	5:50	1.6	
		7:37	7:57	1.9	-0.4 ± 5.5
		9:48	10:07	-0.1	
		11:56	12:21	-7.3	
		14:01	14:29	-0.6	
		16:08	16:32	-9.3	
WAHIWA	July 17	15:59	16:20	9.3	
		18:03	18:31	2.1	
	July 18	7:24	7:43	-3.9	2.7 ± 5.5
		16:03	16:26	7.0	
		18:07	18:35	-1.1	

Table D1 (Continued)

Station	Day (1966)	Pass		Timing Error (msecs.)	Mean Timing Error ± 1 Standard Deviation (msecs.)
		Start	End		
APLMND	July 19	3:34	3:57	2.2	
		5:41	6:03	0.5	
		7:50	8:14	1.6	
		9:58	10:25	-6.7	
		12:04	12:32	4.9	
		14:11	14:32	10.6	0.4 ± 5.8
	July 20	5:46	6:08	1.1	
		7:55	8:18	1.7	
		10:04	10:30	-9.3	
		12:08	12:35	4.0	
		14:16	14:35	-6.5	
LASHM2	July 19	3:55	4:18	0.1	
		5:58	6:25	-3.6	
		8:03	8:27	-4.8	
		21:40	22:00	2.0	
	July 20	1:49	2:15	-1.1	-2.1 ± 3.0
		3:55	4:23	-2.1	
		6:02	6:29	-4.4	
		8:07	8:31	-6.5	
		21:45	22:05	1.9	
LACRES	July 19	5:33	5:55	1.6	
		12:00	12:26	1.2	
		14:08	14:34	3.5	
	July 20	5:38	5:59	1.9	2.9 ± 1.5
		7:47	8:06	4.6	
		12:05	12:31	4.9	
		14:10	14:39	2.7	
WAHIWA	July 19	7:29	7:47	-3.1	
		16:07	16:31	11.3	
		18:12	18:40	2.4	3.5 ± 6.3
	July 20	16:11	16:36	8.5	
		18:12	18:44	-1.8	
ANCHOR	July 19	7:41	8:01	-2.6	
		9:43	10:07	-3.9	
		11:47	12:12	3.4	
		13:52	14:19	-0.5	
		15:57	16:24	-2.7	
		18:02	18:24	-4.4	
	July 20	7:45	8:05	-0.1	-1.7 ± 2.7
		9:48	10:11	-2.6	
		11:52	12:18	1.8	
		13:56	14:22	0.5	
		16:01	16:27	-5.1	
		18:07	18:28	-4.0	

Table D2

Summary of Range Rate Biases Found in the TRANET Doppler Data.

2-Day Arc (1966)	Station	Number of Passes	Mean Range Rate Bias ± 1 Standard Deviation (cm/sec)	2-Day Arc (1966)	Station	Number of Passes	Mean Range Rate Bias ± 1 Standard Deviation (cm/sec)
July 9-10	ANCHOR	8	8.0 ± 2.3	July 23-24	ANCHOR	11	7.9 ± 3.4
	WAHIWA	5	7.7 ± 2.2		WAHIWA	7	8.3 ± 3.1
	LACRES	8	6.0 ± 2.9		LACRES	8	7.3 ± 3.3
	APLMND	11	8.7 ± 3.1		APLMND	11	9.0 ± 3.3
	LASHM2	12	7.7 ± 3.2		LASHM2	7	7.0 ± 2.1
July 11-12	ANCHOR	11	8.2 ± 3.4				
	WAHIWA	2	11.1 ± 1.8	July 25-26	ANCHOR	9	8.7 ± 3.3
	LACRES	10	8.9 ± 2.1		WAHIWA	7	9.3 ± 2.6
	APLMND	10	10.6 ± 3.1		LACRES	5	10.5 ± 1.7
	LASHM2	11	9.3 ± 2.3		APLMND	12	11.5 ± 3.2
					LASHM2	11	8.8 ± 2.5
July 13-14	ANCHOR	12	7.8 ± 3.2				
	WAHIWA	4	9.7 ± 0.4				
	LACRES	8	7.5 ± 2.8	July 31 —	ANCHOR	11	9.1 ± 2.4
	APLMND	8	10.1 ± 5.3	August 1	WAHIWA	7	9.7 ± 2.7
	LASHM2	12	8.5 ± 2.9		LACRES	4	8.9 ± 3.1
					APLMND	11	10.8 ± 3.5
July 15-16	ANCHOR	11	8.3 ± 3.5		LASHM2	11	9.7 ± 3.5
	WAHIWA	4	9.2 ± 2.7				
	LACRES	6	7.7 ± 2.8				
	APLMND	11	10.4 ± 3.0	August 2-3	ANCHOR	12	8.7 ± 3.3
	LASHM2	12	8.0 ± 2.9		WAHIWA	6	9.2 ± 3.7
					LACRES	4	9.0 ± 2.4
	ANCHOR	10	9.3 ± 2.2		APLMND	12	11.3 ± 3.5
July 17-18	WAHIWA	5	9.9 ± 1.5		LASHM2	10	8.4 ± 2.7
	LACRES	9	8.6 ± 2.7				
	APLMND	10	10.2 ± 2.9				
	LASHM2	10	9.2 ± 2.6	August 4-5	ANCHOR	12	7.9 ± 5.1
					WAHIWA	0	
	ANCHOR	12	8.5 ± 2.3		LACRES	10	7.5 ± 4.5
July 19-20	WAHIWA	5	10.3 ± 2.0		APLMND	9	9.2 ± 3.1
	LACRES	7	11.1 ± 1.2		LASHM2	12	6.9 ± 2.5
	APLMND	11	10.4 ± 4.0				
	LASHM2	9	8.3 ± 1.5				
				August 6-7	ANCHOR	10	8.0 ± 2.9
	ANCHOR	9	7.7 ± 3.0		WAHIWA	4	8.5 ± 2.6
July 21-22	WAHIWA	4	9.3 ± 1.0		LACRES	5	6.6 ± 4.5
	LACRES	10	8.5 ± 3.6		APLMND	12	10.5 ± 3.4
	APLMND	12	9.9 ± 3.0		LASHM2	13	7.7 ± 2.5
	LASHM2	8	6.7 ± 0.5				

Appendix E

Range-Rate (Base Frequency) Biases in the Doppler Data as Determined in Varying Arc Length Solutions

The two tables of this appendix present the results of the study to determine the independence of the range rate bias adjustment on the TRANET Doppler data with respect to orbital arc length. Table E1 presents the 44 Doppler passes in the 2-day period of July 17-18, 1966 which were used in this report and the range rate biases that were dynamically determined for each pass in differing arc length solutions (2, 1-1/2, 1, and 1/2 day arcs). Table E3 presents the same information for the 44 Doppler passes used in the 2-day period of July 19-20, 1966.

Table E1

TRANET Doppler Range Rate Bias Adjustment as Determined in Various Arc Length Solutions Over July 17-18, 1966.

Pass for Which $\dot{R}$ Bias is Computed			Arcs Used			Adjusted $\dot{R}$ Bias (cm/sec)	Mean $\dot{R}$ Bias ± 1 Standard Deviation (cm/sec)
Station	Day		Epoch (July, 1966)		Length in Days		
	Start	End	Day	Hour			
ANCHOR	July 17		17	0	2	11.8	
	7:34	8:03	17	0	1-1/2	12.1	12.3 ± 0.5
			17	0	1	12.3	
			17	0	1/2	12.9	
	July 17		17	0	2	10.8	
	9:35	10:03	17	0	1-1/2	11.2	11.4 ± 0.7
			17	0	1	11.0	
			17	0	1/2	12.4	
	July 17		17	0	2	8.3	
	11:40	12:08	17	0	1-1/2	8.3	8.2 ± 0.1
			17	0	1	8.1	
	July 17		17	0	2	12.6	
	13:43	14:12	17	0	1-1/2	12.6	
			17	12	1-1/2	11.5	12.3 ± 0.5
			17	0	1	12.1	
			17	12	1/2	12.5	

Table E1 (Continued)

Pass for Which $\dot{R}$ Bias is Computed			Arcs Used			Adjusted $\dot{R}$ Bias (cm/sec)	Mean $\dot{R}$ Bias ± 1 Standard Deviation (cm/sec)
Station	Day		Epoch (July, 1966)		Length in Days		
	Start	End	Day	Hour			
ANCHOR (continued)	July 17 15:49	16:18	17	0	2	7.5	
			17	0	1-1/2	7.7	
			17	12	1-1/2	6.5	7.1 ± 0.5
			17	0	1	6.8	
			17	12	1/2	6.9	
	July 17 17:53	18:22	17	0	2	5.5	
			17	0	1-1/2	5.5	
			17	12	1-1/2	4.5	4.8 ± 0.6
			17	0	1	4.3	
			17	12	1/2	4.3	
	July 18 9:38	10:07	17	0	2	8.5	
			17	0	1-1/2	8.0	
			17	12	1-1/2	8.7	8.8 ± 0.7
			18	0	1	8.7	
			18	0	1/2	10.0	
	July 18 11:44	12:13	17	0	2	9.1	
			17	12	1-1/2	9.2	9.2 ± 0.1
			18	0	1	9.4	
	July 18 13:47	14:16	17	0	2	10.7	
			17	12	1-1/2	11.1	11.1 ± 0.3
			18	0	1	11.3	
			18	12	1/2	11.2	
	July 18 15:52	16:21	17	0	2	7.7	
			17	12	1-1/2	8.2	8.2 ± 0.3
			18	0	1	8.5	
			18	12	1/2	8.3	
WAHIWA	July 17 15:58	16:27	17	0	2	11.4	
			17	0	1-1/2	11.3	
			17	12	1-1/2	10.3	10.8 ± 0.6
			17	0	1	10.9	
			17	12	1/2	10.0	
	July 17 18:02	18:31	17	0	2	9.9	
			17	0	1-1/2	10.0	
			17	12	1-1/2	8.9	9.2 ± 0.8
			17	0	1	8.8	
			17	12	1/2	8.2	

Table E1 (Continued)

Pass for Which $\dot{R}$ Bias is Computed			Arcs Used			Adjusted $\dot{R}$ Bias (cm/sec)	Mean $\dot{R}$ Bias ± 1 Standard Deviation (cm/sec)
Station	Day		Epoch (July, 1966)		Length in Days		
	Start	End	Day	Hour			
WAHIWA (continued)	July 18 7:24	7:53	17	0	2	8.1	
			17	0	1-1/2	7.9	
			17	12	1-1/2	8.0	8.4 ± 0.7
			18	0	1	8.3	
			18	0	1/2	9.6	
	July 18 16:02	16:31	17	0	2	11.3	
			17	12	1-1/2	11.5	11.3 ± 0.3
			18	0	1	11.7	
			18	12	1/2	10.9	
	July 18 18:07	18:36	17	0	2	8.9	
			17	12	1-1/2	9.2	9.1 ± 0.3
			18	0	1	9.5	
			18	12	1/2	8.9	
LACRES	July 17 9:42	10:11	17	0	2	7.3	
			17	0	1-1/2	7.0	7.3 ± 0.3
			17	0	1	7.3	
			17	0	1/2	7.7	
	July 17 11:51	12:20	17	0	2	5.9	
			17	0	1-1/2	5.8	5.9 ± 0.1
			17	0	1	5.9	
	July 17 13:57	14:25	17	0	2	11.9	
			17	0	1-1/2	11.9	
			17	12	1-1/2	10.5	11.4 ± 0.6
			17	0	1	11.5	
			17	12	1/2	11.2	
	July 18 5:28	5:57	17	0	2	12.1	
			17	0	1-1/2	11.6	
			17	12	1-1/2	12.0	12.0 ± 0.3
			18	0	1	12.2	
			18	0	1/2	12.3	
	July 18 7:36	8:05	17	0	2	11.1	
			17	0	1-1/2	10.4	
			17	12	1-1/2	11.4	11.1 ± 0.4
			18	0	1	11.4	
			18	0	1/2	11.2	
	July 18 9:47	10:16	17	0	2	8.0	
			17	0	1-1/2	7.2	
			17	12	1-1/2	8.2	7.9 ± 0.4
			18	0	1	8.2	
			18	0	1/2	8.1	

Table E1 (Continued)

Pass for Which $\dot{R}$ Bias is Computed			Arcs Used			Adjusted $\dot{R}$ Bias (cm/sec)	Mean $\dot{R}$ Bias ± 1 Standard Deviation (cm/sec)
Station	Day		Epoch (July, 1966)		Length in Days		
	Start	End	Day	Hour			
LACRES (continued)	July 18 11:55	12:24	17	0	2	5.9	6.0 ± 0.1
			17	12	1-1/2	6.0	
			18	0	1	6.1	
	July 18 14:01	14:30	17	0	2	9.7	9.8 ± 0.3
			17	12	1-1/2	9.9	
			18	0	1	10.1	
			18	12	1/2	9.6	
	July 18 16:08	16:37	17	0	2	5.2	5.5 ± 0.2
			17	12	1-1/2	5.5	
			18	0	1	5.8	
			18	12	1/2	5.5	
APLMND	July 17 3:28	3:57	17	0	2	9.6	10.4 ± 0.7
			17	0	1-1/2	10.0	
			17	0	1	11.2	
			17	0	1/2	10.7	
	July 17 5:36	6:05	17	0	2	7.0	7.4 ± 0.5
			17	0	1-1/2	7.0	
			17	0	1	8.0	
			17	0	1/2	7.7	
	July 17 7:40	8:09	17	0	2	10.2	10.4 ± 0.3
			17	0	1-1/2	10.1	
			17	0	1	10.6	
			17	0	1/2	10.8	
	July 17 9:48	10:17	17	0	2	5.6	6.0 ± 0.5
			17	0	1-1/2	5.6	
			17	0	1	5.9	
			17	0	1/2	6.7	
	July 17 11:54	12:23	17	0	2	7.6	7.6 ± 0.1
			17	0	1-1/2	7.7	
			17	0	1	7.5	
	July 17 14:01	14:30	17	0	2	11.8	11.4 ± 0.6
			17	0	1-1/2	12.1	
			17	12	1-1/2	10.5	
			17	0	1	11.3	
			17	12	1/2	11.5	

Table E1 (Continued)

Pass for Which $\dot{R}$ Bias is Computed			Arcs Used			Adjusted $\dot{R}$ Bias (cm/sec)	Mean $\dot{R}$ Bias ± 1 Standard Deviation (cm/sec)
Station	Day		Epoch (July, 1966)		Length in Days		
	Start	End	Day	Hour			
APLMND (continued)	July 18 3:30	3:59	17	0	2	12.5	
			17	0	1-1/2	12.1	
			17	12	1-1/2	12.2	12.2 ± 0.2
			18	0	1	12.2	
			18	0	1/2	12.0	
	July 18 5:38	6:07	17	0	2	9.6	
			17	0	1-1/2	8.9	
			17	12	1-1/2	9.6	9.3 ± 0.3
			18	0	1	9.5	
			18	0	1/2	9.0	
	July 18 7:45	8:14	17	0	2	13.8	
			17	0	1-1/2	13.2	
			17	12	1-1/2	13.9	13.7 ± 0.3
			18	0	1	13.9	
			18	0	1/2	13.7	
	July 18 14:06	14:34	17	0	2	13.9	
			17	12	1-1/2	14.1	14.1 ± 0.2
			18	0	1	14.3	
			18	12	1/2	14.1	
LASHM2	July 17 3:41	4:10	17	0	2	8.0	
			17	0	1-1/2	8.1	8.6 ± 0.7
			17	0	1	9.3	
			17	0	1/2	8.9	
	July 17 5:47	6:16	17	0	2	8.0	
			17	0	1-1/2	8.2	8.5 ± 0.6
			17	0	1	8.9	
			17	0	1/2	9.2	
	July 17 7:54	8:23	17	0	2	8.8	
			17	0	1-1/2	9.1	9.4 ± 0.7
			17	0	1	9.4	
			17	0	1/2	10.4	
	July 17 21:32	22:01	17	0	2	13.9	
			17	0	1-1/2	13.8	
			17	12	1-1/2	12.9	12.5 ± 1.5
			17	0	1	10.9	
			17	12	1/2	10.9	
	July 17 23:34	24:03	17	0	2	13.0	
			17	0	1-1/2	13.0	12.9 ± 0.2
			17	12	1-1/2	12.6	

Table E1 (Continued)

Pass for Which $\dot{R}$ Bias is Computed			Arcs Used			Adjusted $\dot{R}$ Bias (cm/sec)	Mean $\dot{R}$ Bias ± 1 Standard Deviation (cm/sec)
Station	Day		Epoch (July, 1966)		Length in Days		
	Start	End	Day	Hour			
LASHM2 (continued)	July 18		17	0	2	9.2	
	1:39	2:08	17	0	1-1/2	8.7	
			17	12	1-1/2	8.7	8.5 ± 0.7
			18	0	1	8.3	
			18	0	1/2	7.4	
	July 18		17	0	2	8.3	
	3:48	4:17	17	0	1-1/2	7.8	
			17	12	1-1/2	8.0	7.8 ± 0.4
			18	0	1	7.7	
			18	0	1/2	7.3	
	July 18		17	0	2	10.4	
	5:52	6:21	17	0	1-1/2	10.0	
			17	12	1-1/2	10.1	10.2 ± 0.2
			18	0	1	10.0	
			18	0	1/2	10.5	
	July 18		17	0	2	7.8	
	7:58	8:27	17	0	1-1/2	7.6	
			17	12	1-1/2	7.7	7.9 ± 0.5
			18	0	1	7.6	
			18	0	1/2	8.8	
	July 18		17	0	2	5.1	
	21:37	22:06	17	12	1-1/2	6.4	6.6 ± 1.1
			18	0	1	7.5	
			18	12	1/2	7.3	

Table E2

TRANET Doppler Range Rate Bias Adjustment as Determined in Various Arc Length Solutions Over July 19-20, 1966.

Pass for Which $\dot{R}$ Bias is Computed			Arcs Used			Adjusted $\dot{R}$ Bias (cm/sec)	Mean $\dot{R}$ Bias ± 1 Standard Deviation (cm/sec)
Station	Day		Epoch (July, 1966)		Length in Days		
	Start	End	Day	Hour			
ANCHOR	July 19		19	0	2	9.7	
	7:41	8:09	19	0	1-1/2	9.7	10.0 ± 0.5
			19	0	1	9.9	
			19	0	1/2	10.8	
	July 19		19	0	2	7.7	
	9:42	10:11	19	0	1-1/2	7.7	8.1 ± 0.9
			19	0	1	7.6	
			19	0	1/2	9.5	
	July 19		19	0	2	11.9	
	11:46	12:15	19	0	1-1/2	11.9	11.8 ± 0.1
			19	0	1	11.8	
	July 19		19	0	2	9.5	
	13:51	14:20	19	0	1-1/2	9.6	
			19	12	1-1/2	8.6	9.0 ± 0.5
			19	0	1	8.9	
			19	12	1/2	8.4	
	July 19		19	0	2	7.1	
	15:56	16:25	19	0	1-1/2	7.3	
			19	12	1-1/2	6.3	6.7 ± 0.5
			19	0	1	6.6	
			19	12	1/2	6.2	
	July 19		19	0	2	5.0	
	18:02	18:31	19	0	1-1/2	5.3	
			19	12	1-1/2	4.2	4.7 ± 0.4
			19	0	1	4.6	
			19	12	1/2	4.4	
	July 20		19	0	2	11.1	
	7:45	8:14	19	0	1-1/2	12.0	
			19	12	1-1/2	10.6	11.4 ± 0.7
			20	0	1	11.0	
			20	0	1/2	12.4	
	July 20		19	0	2	6.4	
	9:47	10:16	19	0	1-1/2	7.4	
			19	12	1-1/2	6.2	6.9 ± 0.9
			20	0	1	6.1	
			20	0	1/2	8.3	

Table E2 (Continued)

Pass for Which $\dot{R}$ Bias is Computed			Arcs Used			Adjusted $\dot{R}$ Bias (cm/sec)	Mean $\dot{R}$ Bias ± 1 Standard Deviation (cm/sec)
Station	Day		Epoch (July, 1966)		Length in Days		
	Start	End	Day	Hour			
ANCHOR (continued)	July 20 11:52	12:21	19	0	2	9.9	
			19	12	1-1/2	10.1	10.1 ± 0.1
			20	0	1	10.1	
	July 20 13:56	14:25	19	0	2	11.0	
			19	12	1-1/2	11.3	10.9 ± 0.5
			20	0	1	11.1	
			20	12	1/2	10.1	
	July 20 16:01	16:30	19	0	2	6.3	
			19	12	1-1/2	6.6	6.3 ± 0.3
			20	0	1	6.3	
			20	12	1/2	5.9	
	July 20 18:06	18:35	19	0	2	5.9	
			19	12	1-1/2	6.2	6.0 ± 0.2
			20	0	1	5.8	
			20	12	1/2	6.0	
WAHIWA	July 19 7:29	7:57	19	0	2	8.3	
			19	0	1-1/2	8.2	8.9 ± 1.1
			19	0	1	8.8	
			19	0	1/2	10.5	
	July 19 16:06	16:35	19	0	2	12.4	
			19	0	1-1/2	12.7	
			19	12	1-1/2	11.9	11.8 ± 0.8
			19	0	1	11.3	
			19	12	1/2	10.7	
	July 19 18:11	18:40	19	0	2	9.9	
			19	0	1-1/2	10.2	
			19	12	1-1/2	9.1	9.4 ± 0.6
			19	0	1	9.3	
			19	12	1/2	8.6	
	July 20 16:11	16:39	19	0	2	12.5	
			19	12	1-1/2	13.0	12.5 ± 0.7
			20	0	1	12.8	
			20	12	1/2	11.5	
	July 20 18:16	18:45	19	0	2	8.4	
			19	12	1-1/2	8.6	8.4 ± 0.2
			20	0	1	8.3	
			20	12	1/2	8.1	

Table E2 (Continued)

Pass for Which $\dot{R}$ Bias is Computed			Arcs Used			Adjusted $\dot{R}$ Bias (cm/sec)	Mean $\dot{R}$ Bias ± 1 Standard Deviation (cm/sec)
Station	Day		Epoch (July, 1966)		Length in Days		
	Start	End	Day	Hour			
LACRES	July 19 5:33	6:02	19	0	2	12.7	12.9 ± 0.2
			19	0	1-1/2	12.6	
			19	0	1	13.1	
			19	0	1/2	13.0	
	July 19 12:00	12:29	19	0	2	9.6	8.9 ± 0.8
			19	0	1-1/2	9.7	
			19	12	1-1/2	9.0	
			19	0	1	8.5	
			19	12	1/2	7.8	
	July 19 14:07	14:36	19	0	2	10.0	9.4 ± 0.7
			19	0	1-1/2	10.2	
			19	12	1-1/2	9.0	
			19	0	1	9.2	
			19	12	1/2	8.4	
	July 20 5:37	6:06	19	0	2	12.0	12.0 ± 0.5
			19	0	1-1/2	12.8	
			19	12	1-1/2	11.4	
			20	0	1	11.9	
			20	0	1/2	12.0	
	July 20 7:46	8:15	19	0	2	10.1	10.7 ± 0.5
			19	0	1-1/2	10.7	
			19	12	1-1/2	10.4	
			20	0	1	10.7	
			20	0	1/2	11.5	
	July 20 12:04	12:33	19	0	2	11.9	11.9 ± 0.9
			19	12	1-1/2	12.5	
			20	0	1	12.7	
			20	12	1/2	10.6	
	July 20 14:10	14:39	19	0	2	11.2	11.1 ± 0.5
			19	12	1-1/2	11.5	
			20	0	1	11.4	
			20	12	1/2	10.3	
APLMND	July 19 3:34	4:03	19	0	2	14.3	14.0 ± 0.5
			19	0	1-1/2	13.9	
			19	0	1	14.5	
			19	0	1/2	13.4	
	July 19 5:41	6:09	19	0	2	11.0	10.7 ± 0.3
			19	0	1-1/2	10.7	
			19	0	1	10.6	
			19	0	1/2	10.3	

Table E2 (Continued)

Pass for Which $\dot{R}$ Bias is Computed			Arcs Used			Adjusted $\dot{R}$ Bias (cm/sec)	Mean $\dot{R}$ Bias ± 1 Standard Deviation (cm/sec)
Station	Day		Epoch (July, 1966)		Length in Days		
	Start	End	Day	Hour			
APLMND (continued)	July 19 7:50	8:18	19	0	2	11.2	10.8 ± 0.4
			19	0	1-1/2	11.0	
			19	0	1	10.3	
			19	0	1/2	10.9	
	July 19 9:58	10:27	19	0	2	4.9	4.9 ± 0.9
			19	0	1-1/2	4.9	
			19	0	1	3.8	
			19	0	1/2	6.1	
	July 19 12:03	12:32	19	0	2	11.7	11.1 ± 0.7
			19	0	1-1/2	11.8	
			19	12	1-1/2	10.7	
			19	0	1	11.1	
			19	12	1/2	10.3	
	July 19 14:10	14:39	19	0	2	17.9	17.5 ± 0.5
			19	0	1-1/2	18.1	
			19	12	1-1/2	16.9	
			19	0	1	17.6	
			19	12	1/2	17.0	
	July 20 5.45	6:14	19	0	2	12.0	12.3 ± 0.4
			19	0	1-1/2	12.6	
			19	12	1-1/2	11.7	
			20	0	1	12.6	
			20	12	1/2	12.7	
	July 20 7:54	8:23	19	0	2	9.3	10.1 ± 0.8
			19	0	1-1/2	9.9	
			19	12	1-1/2	9.7	
			20	0	1	10.1	
			20	12	1/2	11.3	
	July 20 10:03	10:32	19	0	2	4.3	5.4 ± 1.2
			19	0	1-1/2	5.3	
			19	12	1-1/2	4.8	
			20	0	1	5.0	
			20	12	1/2	7.3	
	July 20 12:08	12:37	19	0	2	11.5	11.4 ± 0.6
			19	12	1-1/2	11.6	
			20	0	1	11.9	
			20	12	1/2	10.4	

Table E2 (Continued)

Pass for Which $\dot{R}$ Bias is Computed			Arcs Used			Adjusted $\dot{R}$ Bias (cm/sec)	Mean $\dot{R}$ Bias ± 1 Standard Deviation (cm/sec)
Station	Day		Epoch (July, 1966)		Length in Days		
	Start	End	Day	Hour			
APLMND (continued)	July 20 14:16	14:44	19	0	2	6.5	6.4 ± 0.2
			19	12	1-1/2	6.5	
			20	0	1	6.6	
			20	12	1/2	6.2	
LASHM2	July 19 3:55	4:24	19	0	2	6.2	5.7 ± 0.5
			19	0	1-1/2	6.0	
			19	0	1	5.4	
			19	0	1/2	5.1	
	July 19 5:57	6:26	19	0	2	7.2	7.1 ± 0.4
			19	0	1-1/2	7.1	
			19	0	1	6.6	
			19	0	1/2	7.6	
	July 19 8:02	8:31	19	0	2	8.4	8.8 ± 0.9
			19	0	1-1/2	8.4	
			19	0	1	8.1	
			19	0	1/2	10.1	
	July 19 21:40	22:08	19	0	2	10.6	10.4 ± 0.7
			19	0	1-1/2	11.1	
			19	12	1-1/2	9.3	
			19	0	1	10.5	
			19	12	1/2	10.5	
	July 20 1:48	2:17	19	0	2	8.1	8.5 ± 0.5
			19	0	1-1/2	8.6	
			19	12	1-1/2	7.9	
			20	0	1	9.1	
			20	0	1/2	8.6	
	July 20 3:55	4.24	19	0	2	8.6	9.2 ± 0.6
			19	0	1-1/2	9.2	
			19	12	1-1/2	8.6	
			20	0	1	9.6	
			20	0	1/2	9.8	
	July 20 6:02	6:30	19	0	2	7.7	8.4 ± 0.9
			19	0	1-1/2	8.4	
			19	12	1-1/2	7.6	
			20	0	1	8.4	
			20	0	1/2	9.8	

Table E2 (Continued)

Pass for Which $\dot{R}$ Bias is Computed			Arcs Used			Adjusted $\dot{R}$ Bias (cm/sec)	Mean $\dot{R}$ Bias ± 1 Standard Deviation (cm/sec)
Station	Day		Epoch (July, 1966)		Length in Days		
	Start	End	Day	Hour			
LASHM2 (continued)	July 20 8:07	8:36	19	0	2	7.6	8.4 ± 1.2
			19	0	1-1/2	8.3	
			19	12	1-1/2	7.4	
			20	0	1	8.1	
			20	0	1/2	10.5	
	July 20 21:44	22:13	19	0	2	10.7	10.5 ± 0.9
			19	12	1-1/2	11.1	
			20	0	1	9.2	
			20	12	1/2	11.1	

GLOBAL C-BAND RADAR NETWORK CALIBRATION UTILIZING GEOS-II SATELLITE

by
RONALD L. BROOKS
Wolf Research and Development Corporation
Riverdale, Maryland

H. RAYMOND STANLEY
National Aeronautics and Space Administration
Wallops Station
Wallops Island, Virginia

Prepared for Presentation at
GEOS-II Review Conference
Goddard Space Flight Center
Greenbelt, Maryland
June 1970

GLOBAL C-BAND RADAR NETWORK CALIBRATION UTILIZING GEOS-II SATELLITE

by
Ronald L. Brooks
Wolf Research and Development Corporation

H. Raymond Stanley
National Aeronautics and Space Administration

ABSTRACT

A calibration project for the C-Band Radar Network is currently in progress at NASA/Wallops Station. The project objectives, unique data processing problems, and accomplishments are summarized. Recommendations are presented for future radar calibration projects.

1. GEOS-II C-BAND PROJECT

1.1 Introduction

Prior to the launch of the GEOS-II satellite, it was realized that data from the worldwide C-Band radars were potentially of great benefit to geodesy. The C-Band radar sites not only have good geographic distribution (Figure 1), but are capable of all-weather, horizon-to-horizon tracking at rates as high as 40 observations per second. Further, the majority of these radars provide unambiguous ranging to 32,000 nautical miles. However, the accuracy of these radars had not been established due to the lack of a suitable calibration target at satellite distances.

Since February of 1968, both land-based and shipborne C-Band radars have successfully tracked a C-Band transponder on board the GEOS-II satellite. The primary goals of this GEOS-II Project are:

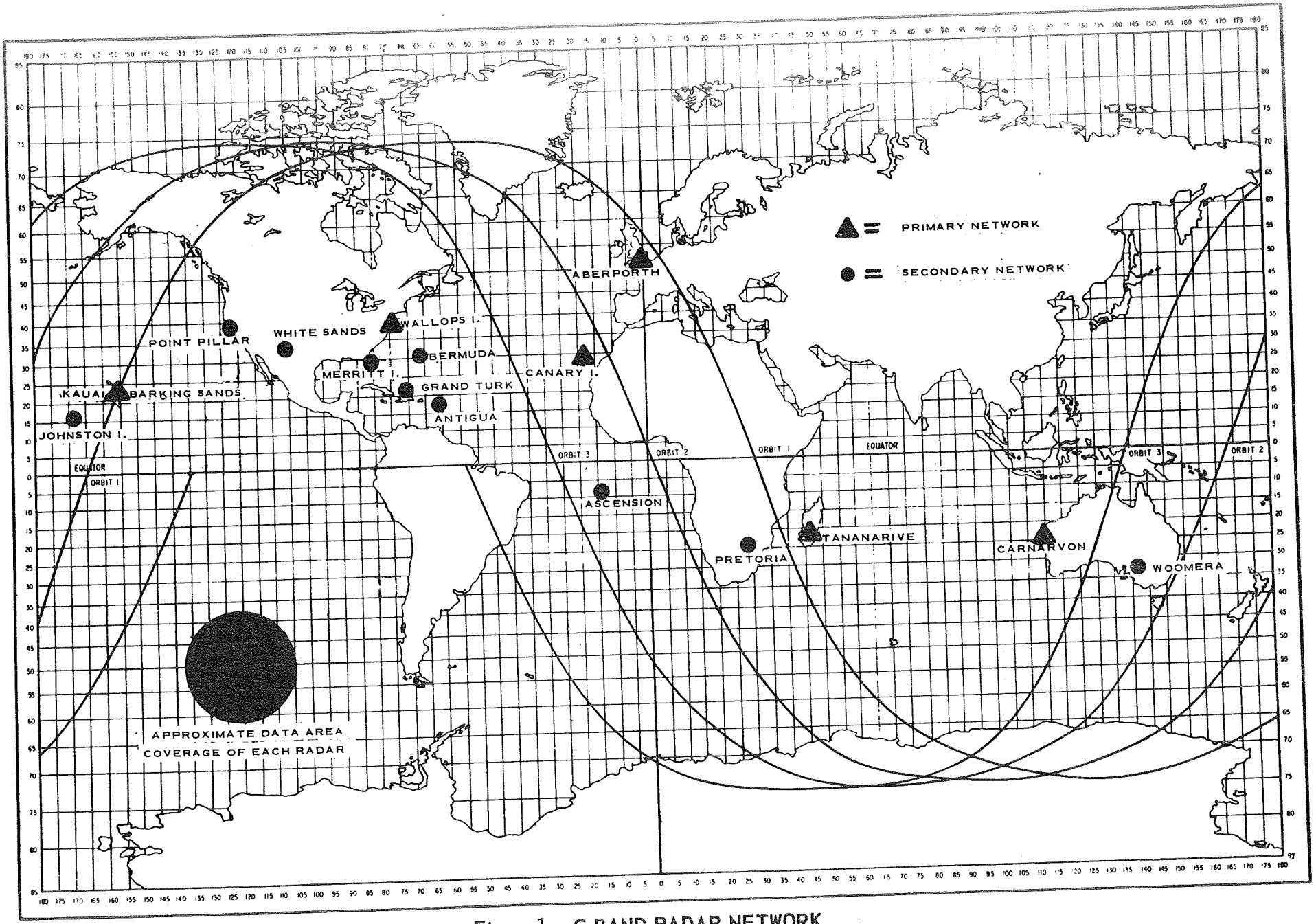

Figure 1 C-BAND RADAR NETWORK

a) To provide geodetic scale for the interim NASA unified network.

b) To better determine the absolute accuracy of instrumentation radar systems, develop refined methods of calibrating these systems, and improve the techniques employed in processing the associated data.

c) To better determine the geodetic location of the C-Band radar sites and their intersite distances.

d) To compare and correlate results obtained from other GEOS-B systems with those obtained by the C-Band system.

e) To make generally available the results of both the C-Band system calibration and geodetic investigations.

These objectives will assist specifically in meeting the GEOS Program objectives stated in the GEOS-A Mission Plan.

1.2 Accomplishments to Date

A team comprised of radar engineers and geodetic software specialists from NASA/Wallops Station, Wolf Research and Development*, and RCA/Moorestown**, has designed controlled radar studies involving data acquisition, reduction and analysis. The accomplishments to date include:

a) Ascertained the range accuracy of properly operated and ground calibrated C-Band radars. Wallops Station's results indicate that the AN/FPS-16 and AN/FPQ-6 radars are capable of providing range data at satellite distances with an accuracy of 1 - 4 meters, with an RMS noise of approximately one meter.[1,2]

b) Recovered a composite set of resonant geopotential coefficients for GEOS-II, from C-Band radar data alone, which improved orbital accuracies.[3]

---

* Contracts NAS6-1467 and NAS6-1628 with NASA/Wallops

** Subcontractor to Wolf Research and Development Corporation

c) Recovered geodetic positions of Apollo tracking ships utilizing data from ship-borne and land-based radars[4].

d) Utilized pulse doppler system of Wallops AN/FPQ-6 to generate range-rate-derived range measurements. The resulting ranges illustrate RMS noise values as low as 0.0006 meters from short arc orbital fits[5].

e) Improved procedures for radar calibrations which are applicable to all radar systems.

f) Recovered significant range, angle, and timing biases for several of the C-Band radars.

g) Determined improved geodetic coordinates and intersite distances for participating radars[6].

h) Filtered radar data to reduce storage requirements and computer time, but retains statistical content.

2. DATA PROBLEMS ENCOUNTERED AND RESOLVED

It was of course anticipated that each radar site could have time or measurement biases, or that the station coordinates may be in error. In the course of this study, several other problem areas have been encountered and resolved. The most significant of these have been

a) pulse-width mismatch

b) range calibration target refraction

c) radar operator/data analyst interface

2.1 Pulse-Width Mismatch

Since the radar can only be calibrated using its own transmitter's output pulse width, a transponder-generated return pulse will introduce some pulse-width dependent range bias error. The range bias, B_p, caused by the pulse-width mismatch is approximately[7,8]

$$B_p = 0.5(P_R - P_C)(150 \text{ meters}/\mu\text{sec})$$

where

P_R = pulse-width received from transponder, in μsec

P_C = radar calibration pulse-width, in μsec

The effect of the pulse-width mismatch was particularly brought to light when it was observed that a 15-meter range bias existed between the Bermuda AN/FPS-16 and AN/FPQ-6 radars with the AN/FPQ-6 measuring longer. Upon our request, Bermuda personnel measured the radars' pulse widths and found that their nominal 0.5 μsec pulse-widths actually were 0.38 μsec (AN/FPQ-6) and 0.55 μsec (AN/FPS-16)[9]. The pulsewidth mismatch, its cause and its effect, are discussed in considerably more detail in reference 7.

2.2 Range Calibration Target Refraction

Radar range measurements are made on a well-surveyed calibration target, both prior to and after each satellite track to obtain zero-set corrections for the track data. The multi-station reductions currently being performed have promoted the realization that significant range errors (range measurements are short) will result if refraction effects are not taken into account during the range target calibration. This error is nominally as large as 13 meters (Table 1) for the Carnarvon AN/FPQ-6 radar, due to the fact that their range calibration target is approximately 30 miles distant. For other radars, this error is normally 1 - 2 meters.

2.3 Radar Operator/Data Analyst Interface

As a result of the data used in the Network evaluation coming from many different radars and agencies, a communication problem developed. Information pertinent to the data reduction and analysis such as detailed calibration procedures at individual sites was not readily available.

TABLE 1

GEOS-II Rev	Date	Time	NCARNV Timing Bias	NCARNV Range Bias	Transponder
5191	690219	10^h 09^m	.010 sec	-16.3	2
5204	690220	10 30	.000	-13.5	2
5268	690225	10 13	.040	-14.9	1
5275	690225	23 59	.030	- 8.1	2
5281	690226	10 36	.010	-10.0	1

CARNARVON COLLOCATION

Preliminary results concerning the individual radars have been sent to the participating radar sites and the radar system operators are now more cognizant of the objectives of the study being performed at NASA/Wallops Station. More information concerning on-site data corrections, radar timing systems, and site operating procedures is being provided.

3. EXPERIMENT DESCRIPTIONS

3.1 Achievable Range Accuracy

Generally speaking, the C-Band radars are unmatched as geodetic instrumentation in terms of dependability, consistency, or precision. The calibration project personnel at Wallops Island have been concerned with assessing or achieving accuracy. To achieve this goal, the following studies have been performed:

a) Radar parameters have been varied during tracks of GEOS-II. After short-arc orbital reductions, the residuals show effects on the range measurements of changing parameters such as pulsewidth, bandwidth and prf (Figure 2).

b) Collocated radar range residuals have been compared to assess relative accuracies. Five meters of the observed Wallops FPS-16 minus FPQ-6 range differences (shown in Figure 3) are attributable to the FPS-16's use of a water tank for calibration, rather than a point source.

c) Collocated laser and radar range residuals have been compared as an independent accuracy check (Table 2). The average Wallops Island Collocation Experiment (WICE) Laser/FPQ-6 range difference was only 0.5 meters.

d) Unweighted WICE radar and laser range measurement were compared with an optically-determined orbit. The results are shown in Table 3.

FIGURE 2

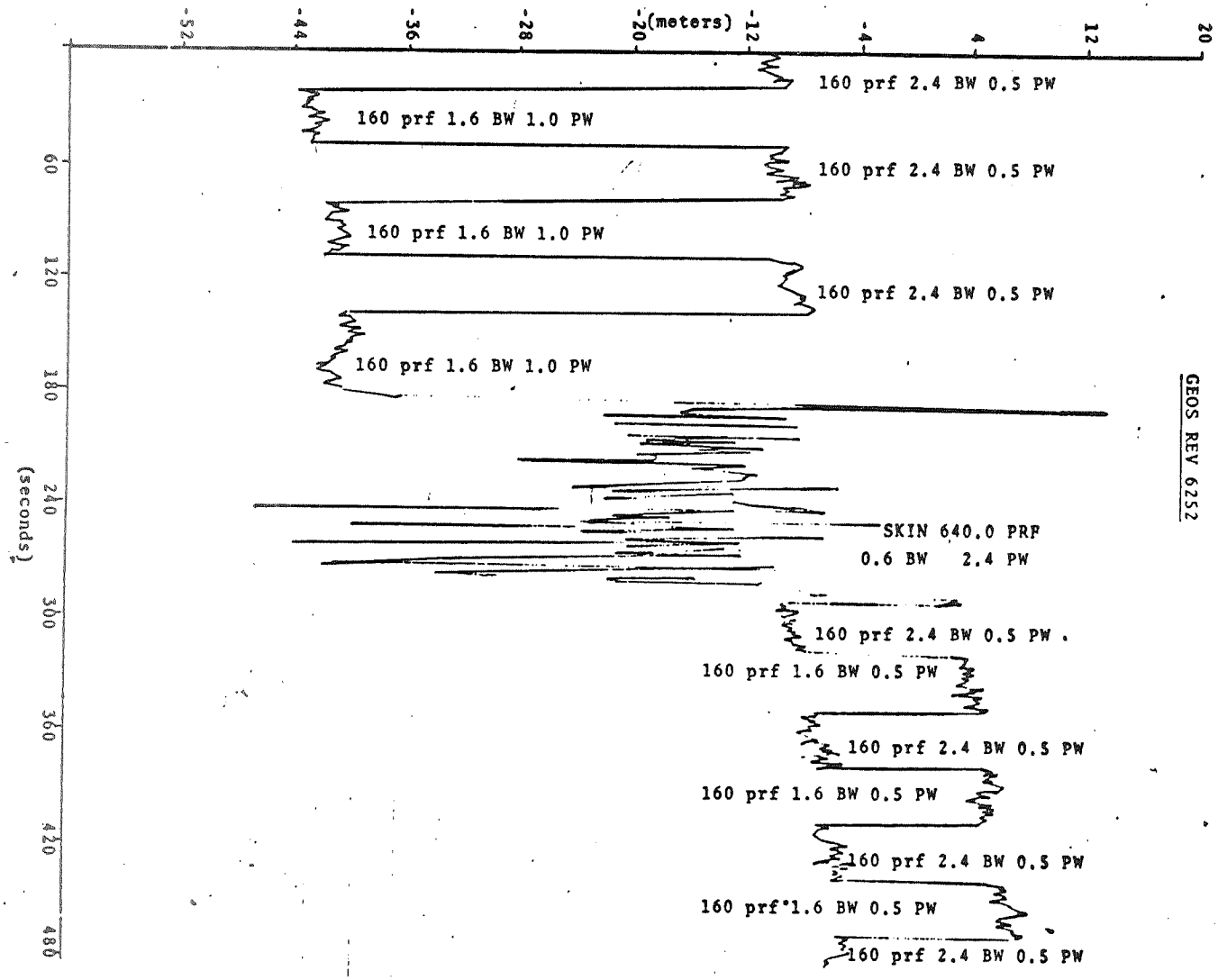
-52
-44
-36
-28
-20
(meters)
-12
-4
4
12
20
60
120
180
240
300
360
420
480
(seconds)
160 prf 2.4 BW 0.5 PW
160 prf 1.6 BW 1.0 PW
160 prf 2.4 BW 0.5 PW
160 prf 1.6 BW 1.0 PW
160 prf 2.4 BW 0.5 PW
160 prf 1.6 BW 1.0 PW
SKIN 640.0 PRF
0.6 BW 2.4 PW
160 prf 2.4 BW 0.5 PW
160 prf 1.6 BW 0.5 PW
160 prf 2.4 BW 0.5 PW
160 prf 1.6 BW 0.5 PW
160 prf 2.4 BW 0.5 PW
160 prf 1.6 BW 0.5 PW
160 prf 2.4 BW 0.5 PW
GEOS REV 6252

FIGURE 3

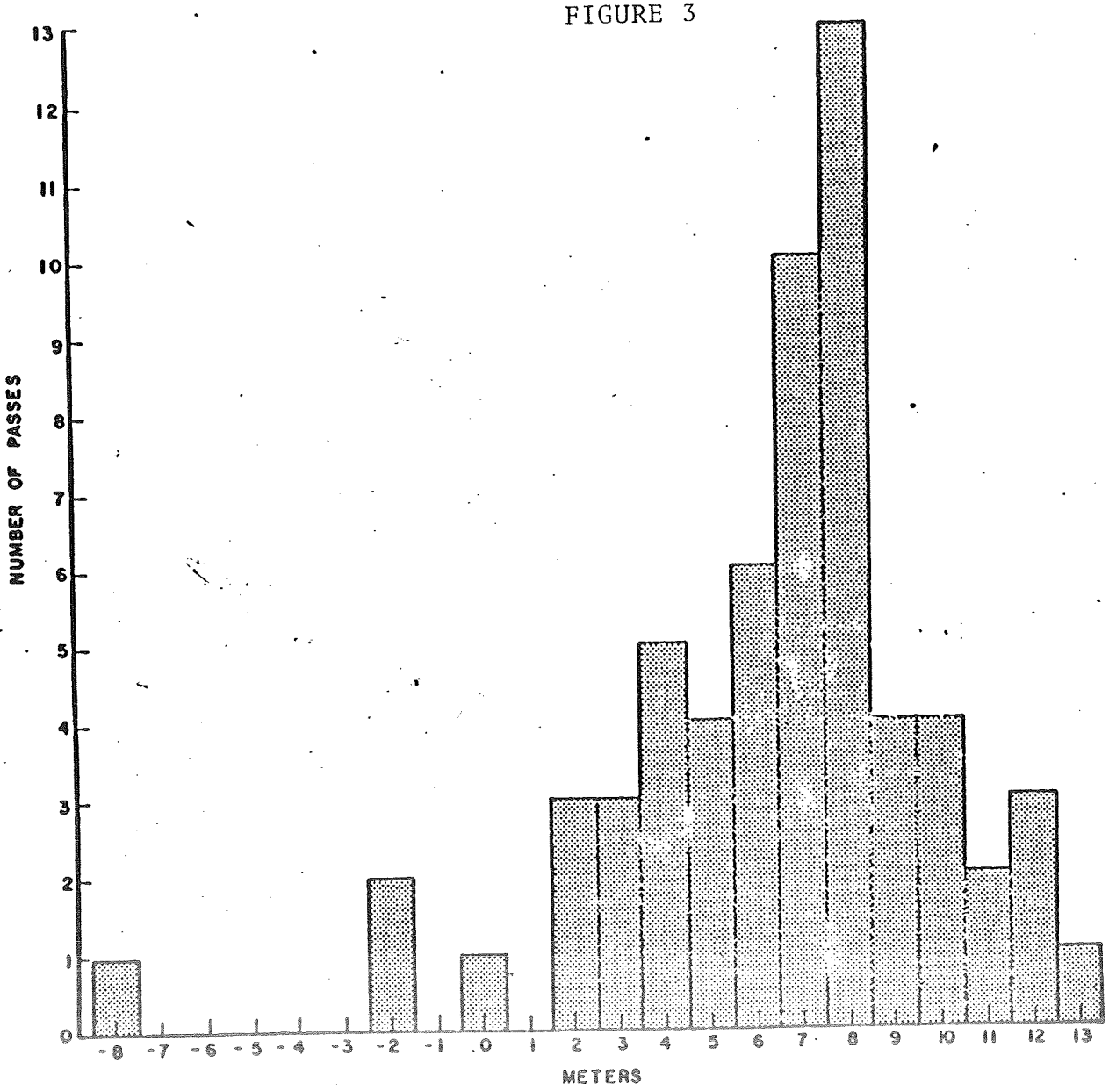

RANGE DIFFERENCES FPS-16 - FPQ-6 WICE COLOCATION

TABLE 2

DIFFERENCES BETWEEN AN/FPQ-6 RANGE & LASER RANGE

DATE	GEOS-II REV NUMBER	WICE TEST NUMBER	RANGE DIFFERENCE in meters	REMARKS
680403	1057	3	0.	
680405	1083	5	-1.	
680410	1147	9	+2.	
680412	1173	11	-5.	trended
680413	1186	12	-1.	
680418	1250	16	+4.	37 Laser pts.
680420	1275	18	+2.	
680426	1352	26	+2.	
680426	1353	27	+3.	
680503	1442	34	0.	
680507	1494	38	+1.	
680508	1507	40	-2.	
680521	1673	47	0.	
680522	1686	49	0.	
680523	1699	52	+4.	trended
680614	1982	77	-2.	

WALLOPS ISLAND COLLOCATION

TABLE 3

OPTICAL SOLUTION
5 1/2 DAY ARC
28 APRIL 1968 TO 4 MAY 1968

SITE	MEASUREMENT TYPE	NO. OF OBSERVATIONS	RMS SECONDS OF ARC
Tananarive, Malagasy	Declination Right Ascension	20 21	2.9 2.8
Johannesburg, S. Africa	Declination Right Ascension	23 22	5.9 5.0
Santiago, Chile	Declination Right Ascension	25 19	1.6 6.6
Columbia, Missouri, U.S.A.	Declination Right Ascension	28 26	3.4 8.4
Mojave, California, U.S.A.	Declination Right Ascension	68 63	4.6 4.9
Fort Myers, Florida, U.S.A.	Declination Right Ascension	63 55	5.3 4.7
Rosman, N. Carolina, U.S.A.	Declination Right Ascension	53 53	1.4 3.9
Edinburg, Texas, U.S.A.	Declination Right Ascension	14 9	5.1 8.4
	TOTAL MEASUREMENTS	562	4.7

MEAN RESIDUALS (UNWEIGHTED)
RANGE MEASUREMENTS WERE THROUGHOUT 5 1/2 DAY PERIOD

SITE	MEASUREMENT TYPE	NO. OF OBSERVATIONS	MEAN (METERS)
WALLOPS AN/FPQ-6 RADAR	RANGE	776	- 1.6
NASA/GSFC LASER	RANGE	248	- 0.6

3.2 Recovery of Resonance Coefficients

A composite set of 13^{th} order resonance coefficients have been recovered for GEOS-II using only radar data. Table 4 lists these recovered coefficients, along with a residual fit comparison for orbital solutions before and after coefficient recovery.

3.3 Ship Radar Calibration and Position Recovery

Dr. Martin is presenting a separate paper at this conference on this subject.

3.4 Coherent Signal Processing (CSP) Ranges

The CSP range-rates from the Wallops AN/FPQ-6 radar have been integrated to CSP ranges. Not only do these CSP ranges provide very low noise ranges, but even short bursts of CSP range data provide relatively accurate orbits.

In a recent experiment, three different determinations of an orbit were made, each using only data from the same 20 second time span, including PCA. The first orbit was determined using the normal range, azimuth, and elevation measurements from the skin-track data. The second orbit determination was made using CSP ranges in place of the normal ranges used on orbit 1. The third orbit was computed using filtered CSP ranges. The RMS of fit for each solution is shown in Figure 4.

Unweighted collocated laser data was used to assess the orbital accuracies of each solution. The laser residuals plotted in Figure 4 clearly show a marked improvement in orbital determination with the use of CSP ranges.

3.5 Improved Radar Site Geodetic Coordinates

Improved station coordinates on a common datum have been determined for many of the C-Band sites. Mr. Leitao is presenting a separate

TABLE 4

STATION	NO. OF WEIGHTED MEASUREMENTS	RSS BEFORE ADJUSTMENT	RSS AFTER ADJUSTMENT
WALLOPS	144	58.7 m	14.8 m
CARNARVON	84	44.2 m	26.5 m
TANANARIVE	46	72.2 m	14.8 m
KAUAI	65	86.4 m	49.4 m
TOTAL	339	64.2 m	27.8 m

RESIDUAL FIT BEFORE AND AFTER RECOVERY OF
13TH ORDER RESONANCE COEFFICIENTS

4 1/2 DAY SOLUTION
NOVEMBER 1968

C(14,13)	1.176×10^{-21}
S(14,13)	6.549×10^{-21}

RECOVERED VALUES OF LUMPED 13TH
ORDER RESONANCE COEFFICIENTS

FIGURE 4

RANGE RESIDUALS VS. TIME

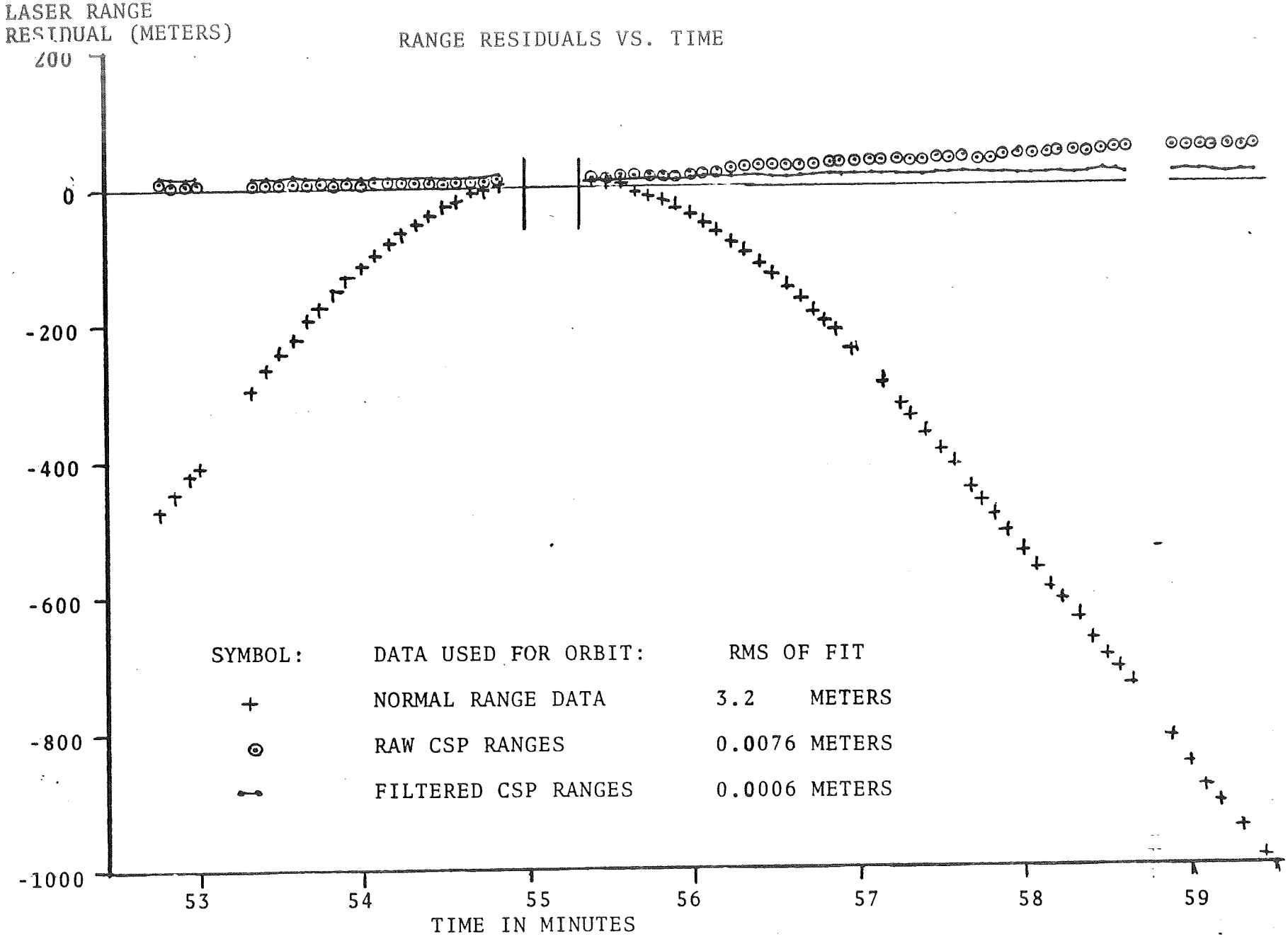

paper on this subject at this Conference.

3.6 Data Filtering

Due to the data gathering ability fo the C-Band radars, filtering programs have been developed to reduce the data storage requirements and computer time for orbital solutions; however, the statistical content of the data is retained.

Figure 5 compares filtered and unfiltered range residuals. A time-tag truncation problem in the NGSP data format is revealed.

4. CONCLUSIONS AND RECOMMENDATIONS

4.1 Software Development

The radar hardware provides data with excellent inherent precision. The proper software development and data analysis is necessary, however, to assess and achieve accuracy.

4.2 Future C-Band Satellite Transponders

It would not have been possible to recover the radar calibration information without a satellite such as GEOS-II. Due to the installation of new radars and the modification of existing radars, future satellites with C-Band transponders are required. It would be very desirable if these transponders could be manufactured such that they were pulse-width sensitive; that is, they would respond with the same pulsewidth as the interrogation pulsewidth from the radar. It would be of benefit also, if future satellite transponders were coherent so that valid range-rate measurements would not have to be restricted to relatively low-signal skin tracking.

4.3 Radar Site Operations

The C-Band radars have all been built to government specifications; these specifications include multiple switches for the radar operator to change to allow for a wide dynamic range of tracking conditions.

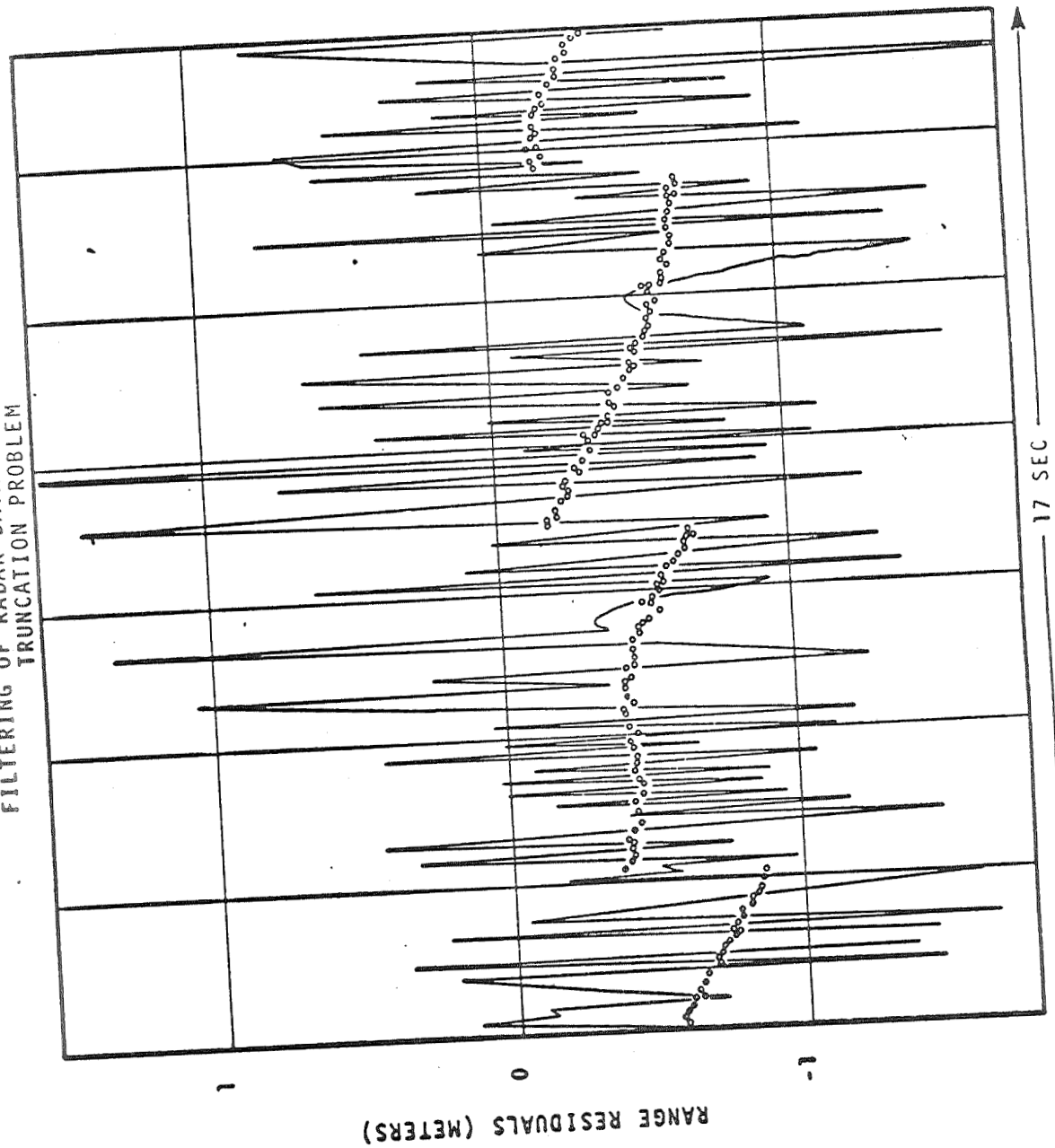

FIGURE 5
FILTERING OF RADAR DATA REVEALS TIMING
TRUNCATION PROBLEM

However, the calibrations performed at Wallops Island illustrate clearly that the majority of these switches affect the measurements. It is a pre-requisite to all radar calibration that all satellite tracking be performed in a consistent manner.

4.4 Radar Data

Steady progress has been made during this radar calibration project. We have become increasingly aware of the factors which affect the radar measurements, such as pulsewidth mismatch, configuration of the range calibration target, and calibration techniques. In view of this increased knowledge, we offer to provide fine-grain data corrections, where necessary, for that C-Band radar data which has been earlier distributed to others in the geodetic community. We also invite other geodetic investigators to utilize our data.

REFERENCES

1. Leitao, C.D., and Brooks, R.L., C-Band Radar Measurements: An Assessment of Accuracy. Presented at International Association of Geodesy Symposium on Electronic Distance Measuring; Boulder, Colorado, June 1969.

2. Moss, S.J., C-Band Radar Accuracy Estimates from the Wallops Island Collocation Experiment. Presented at GEOS-B C-Band Technical Conference at Goddard Space Flight Center, June 1969; published in Conference Proceedings.

3. Martin, C.F., and Roy, N.A., Effective GEOS-II Resonant Geopotential Coefficients as Determined from C-Band Radar Tracking. Presented at GEOS-B C-Band Technical Conference at Goddard Space Flight Center, June 1969; published in Conference Proceedings.

4. Martin, C.F., Roy, N.A., Stanley, H.R., and Krabill, W.B., The Use of Ship-borne C-Band Radar Satellite Ranging Data for Accurate Position Determinations in Broad Ocean Areas. Presented at Marine Geodesy Symposium, November 1969; published in Conference Proceedings.

5. McGoogan, J.T., Mitchell, R.D., and Wells, W.T., Further Results on Coherent Signal Processor Range Measurements. Presented at GEOS-B Technical Conference at Goddard Space Flight Center, June 1969; published in Conference Proceedings.

6. Brooks, R.L., and Leitao, C.D., C-Band Radar Network Intersite Distances. Presented at American Geophysical Union National Fall Meeting; San Francisco, California, December 1969.

7. Dempsey, D.J., An Evaluation of the Wallops Island C-Band Radar Experiment (WICE) Radar Range Errors. Prepared for Wolf Research and Development by Radio Corporation of America, Moorestwon, N.J., September 1969.

8. Leitao, C.D., McGoogan, J.T., Stanley, H.R., Moss, S.J., Roy, N.A., and Wells, W.T., Calibration and Evaluation of the Wallops AN/FPQ-6 Radar Utilizing the GEOS-II Satellite. NASA/Wallops Station Document X-16-68-1.

9. Memorandum to H.N. Hoge from J.T. Macomber of Bendix Engineering Corporation on subject of Bermuda FPQ-6/ FPS-16 Range Differences. October 7, 1969.

THE JUPITER CAMERA INTERCOMPARISON TEST

by

Frank G. Rawlinson
David W. Harris
John H. Berbert
John D. Oosterhout
Goddard Space Flight Center

From November, 1965 to May, 1966, a test was conducted at Jupiter, Florida to compare the various cameras used in the tracking of GEOS-I.

The cameras used in this test were:

Camera	Focal Length
1) SAO Baker-Nunn	500 mm
2) SAO K50	914 mm
3) PC-1000	1000 mm
4) MOTS-40	1000 mm
5) PTH-100	1000 mm
6) MOTS-24	610 mm
7) BC4	305 mm

Three of these cameras, the MOTS-40, the PC-1000, and the PTH-100 have identical lens systems.

The SAO cameras were operated by Smithsonian Astrophysical Observatory (SAO) personnel, the PC-1000 was operated by Air Force personnel and the remaining four cameras were operated under contract from GSFC by Bendix Field Engineering personnel.

All of these cameras were located within thirty meters of each other to minimize ground parallax. The GEOS-I satellite was tracked by all of the cameras for a period of several months in order to accumulate a set of simultaneous observations for the intercomparison study.

The data taken was reduced by the various agencies using the techniques described in the "Preprocessing of Optical Satellite Observations" by Frank Donald Hotter. This is the Ohio State University Department of Geodetic Science Report No. 82 as revised in May, 1968.

The data from the four cameras operated for GSFC was reduced by New Mexico State University under a contract from GSFC. The technique described in the above report for the MOTS-40 reduction was used on all of these cameras with appropriate modification for the two ballistic cameras.

Operational problems were encountered with the four cameras operated for GSFC which increased the difficulty of the reduction and led to a delay in reporting of the results. These problems will be detailed more fully in a report to be issued on the Jupiter experiment in the near future.

A special problem occurred with the BC4 camera. Due to operator error a possible time error may have been introduced into the star calibration times of the plates taken by this camera. This error is in the range of 0 to 300 milliseconds and varies from plate to plate. This leads to a varying bias in Right Ascension and is probably not recoverable.

The data from this experiment did not provide as high a degree of simultaneous observations as was desired. Currently there are 65 passes in the Data Center from Jupiter which have two or more cameras observing the same pass. Of these 65 passes about 50 percent consist of two or three simultaneous camera sets.

The results presented in this paper are preliminary as all of the 65 passes have not been analyzed. A more complete paper will be published in the near future giving a more extensive analysis of the Jupiter experiment. Forty-two (42) passes have been analyzed in part and the results are reported here. The data in this set for the two SAO cameras is the current data in the Data Center. The corrections for parallactic refraction and diurnal aberration were not applied to the SAO data in this preliminary analysis. These corrections are small. Paralactic refraction is on the order of 0.150 seconds of arc and diurnal aberration is a maximum of 0.290 seconds of arc. These corrections will be applied to the SAO data in the final report. The data in this set for the PC-1000 was obtained from the Data Center in December, 1969. Since that time the Aeronautical Chart and Information Center (ACIC) has resubmitted their Jupiter data to the Data Center. In this recent submission the total number of passes was markedly reduced. It was decided to use the data from the earlier set for this initial investigation in order to obtain a reasonable number of passes. A preliminary comparison was done with the two submissions (on four of the passes in both) and the changes were found to be small. The Right Ascension did not change. The change in Declination was about 0.003 seconds of arc.

The data included for the four cameras operated for GSFC consists of passes that are in the Data Center currently. However, for this preliminary investigation they were re-reduced using a reduction program which solves for the elements of interior orientation separately on each plate. In this reduction the correction for decentering distortion is not included. This was done as a special test to investigate some of the operational problems that occurred with these cameras. This will be discussed in the final report.

The initial approach adopted to compare the various cameras was to fit the observations from each pass to a common trajectory. All the cameras were given a weight of one in this curve fitting except the BC4 which was given a weight of zero because of the possible timing problem. The Noname orbit generator program was used to do the curve fitting and produce the residuals.

The table included presents the results of this effort. The residuals given are in Right Ascension and Declination. The statistic quoted in the table is the RMS of the residuals for each coordinate of the flash images on the plate. In most cases there were seven images present. The Right Ascension values are in seconds of arc and had been modified by the usual cosine of Declination factor. The Declination values are also in seconds of arc. At the bottom of the second page of the table the averages of each column in the table are given.

As can be seen from the table, three of the cameras produced a larger number of observations for the 42 passes then the others. The breakdown is as follows:

1) SAO Baker-Nunn	32 passes
2) MOTS-40	26 passes
3) PC-1000	20 passes
4) SAO K50	10 passes
5) MOTS-24	10 passes
6) PTH-100	9 passes
7) BC4	8 passes

The data contained in the table indicates the presence of three basic camera groupings. This can be seen from the average values given at the end of the table. There is a four camera group consisting of the K50, the Baker-Nunn, the MOTS-40, and the PC-1000 whose average values are slightly smaller than those of the other groups. This group's average values are on the order of 1.5 seconds of arc. The two camera group, consisting of the MOTS-24 and the PTH-100, has average values on the order of 2.0 seconds of arc.

The BC4 camera's average values are higher than those of the other two groups being on the order of 3.3 seconds of arc. This is due in part to the possible timing problem. What part, if any, is due to the characteristics of the camera is being investigated.

The analysis of the results of the Jupiter experiment is still in process. As was stated earlier a more detailed report will be published in the near future.

JUPITER INTERCOMPARISON TEST

All Values are RMS in Seconds of ARC
Right Ascension Corrected by COS (declination)

Date	Time	K50		Baker-Nunn		MOTS 40		PC-1000		MOTS 24		Pth-100		BC4	
YYMMDD	HHMM	RMSΔα	RMSΔδ	RMSΔα	RMSΔδ	RMSΔα	RMSΔδ	RMSΔα	RMSΔδ	RMSΔα	RMSΔδ	RMSΔα	RMSΔδ	RMSΔα	RMSΔδ
651126	0523			0.617	1.245	0.947	1.095								
651221	0928			1.385	1.874					1.365	1.562				
651222	0932			1.055	1.473	2.305	1.171			2.078	1.395				
651224	0942			2.751	1.567					1.518	2.182	2.529	2.746		
651227	0750			0.442	1.334	1.395	1.492			1.318	1.272				
651227	0755			1.508	1.693	1.637	1.724								
651227	0955			1.731	1.593	1.200	1.345								
651228	0758			1.984	2.196					2.169	1.584	1.770	3.166		
660113	0452			1.628	2.056			1.133	1.055	3.093	1.338			3.718	2.095
660116	0301			1.511	1.312			3.999	0.824	2.804	1.620				
660116	0506							0.599	1.010	1.134	1.495				
660117	0512			2.157	1.398					2.106	1.883				
660118	0310			2.819	0.979					2.654	1.931			3.341	2.856
660119	0314			1.082	2.051			0.929	2.151						
660201	0207			0.499	0.451	2.469	1.680	2.188	1.520			2.628	2.200		
660203	0017							1.988	2.639			1.781	1.613		
660205	0016					1.375	0.576	1.696	1.027						
660206	0025			1.469	1.038			1.436	0.929						
660209	0037	3.890	2.852	0.758	1.222	2.072	0.892	2.096	1.095			1.296	1.613	2.464	3.779
660217	1018			1.198	0.961	0.550	1.086	1.398	1.191					1.883	3.792
660220	1030			0.938	1.611			2.039	1.355					2.672	3.719
660220	1041			1.869	1.623			1.104	1.320					5.754	3.610
660221	1033					2.418	2.013	1.472	2.072			1.159	0.790	3.379	3.542
660221	1038							1.375	3.348					1.419	4.793
660226	0852					2.012	1.783	1.040	0.945						
660226	0857							2.281	0.993			2.295	1.135		
660227	0906					1.794	0.929	2.367	1.708						
660302	0907	1.102	1.095	1.144	1.356	2.615	1.545	1.071	1.271			1.699	2.064		
660302	0912					1.035	0.951	1.348	1.135						
660302	0917					0.954	0.886	1.236	0.672						
660312	0540	1.353	1.298	1.805	1.030							3.297	1.645		
660312	0545	0.846	1.482	1.394	1.096	1.050	1.004								
660320	0416	1.615	1.030	1.370	1.190	1.144	1.728								

Date	Time	K50		Baker-Nunn		MOTS 40		PC-1000		MOTS 24		Pth-100		BC4	
YYMMDD	HHMM	RMS Δ∠	RMS Δ∫	RMS Δ∠	RMS Δ∫	RMS Δ∠	RMS Δ∫	RMS Δ∠	RMS Δ∫	RMS Δ∠	RMS Δ∫	RMS Δ∠	RMS Δ∫	RMS Δ∠	RMS Δ∫
660402	0103	1.987	1.272	1.671	1.581	2.389	1.111								
660409	0125			1.388	0.693	1.136	1.914								
660413	0149	0.644	2.627	1.573	0.963	1.345	0.981								
660413	0825			0.748	0.900	1.273	0.632								
660426	0711			1.609	0.923	1.246	0.624								
660502	0535			1.125	1.214	0.578	0.365								
660503	0336	1.696	0.892	1.903	1.773	2.503	1.343								
660503	0536	1.131	1.318	1.340	1.168	1.116	0.948								
660503	0541	1.300	0.619	0.799	1.455	1.076	0.633								
MEAN (All Passes)		1.556	1.449	1.415	1.344	1.525	1.171	1.654	1.311	2.024	1.626	2.050	1.886	3.316	3.342

NOTE: The pass on 660221 at 1038 was deleted from the calculation of the mean values because the BC4 was given a weight of 1 in its Noname run.

Geos-I and Geos-II MOTS Camera Operations, Data Analysis and Experiments

David W. Harris
Goddard Space Flight Center

Operations

MOTS camera operations on Geos-II were concluded December 22, 1969. By that time, the 40-inch focal length, 8-inch aperture cameras had compiled a substantial amount of data on both Geos-I and Geos-II. The percentage of successes to attempted operations and assignments for each MOTS station is provided in Table 1.

Table 1
Geos Results

		Geos-I		Geos-II	
STATION NUMBER	MOTS STATION	OPERATIONS/ ASSIGNMENTS	SUCCESSES/ OPERATIONS	OPERATIONS/ ASSIGNMENTS	SUCCESSES/ OPERATIONS
1021	BPOINT	53%	45%	–	–
1022	FTMYRS	72%	65%	51%	79%
1024	WOOMRA	72%	56%	–	–
1038	ORORAL	–	–	50%	76%
1025	QUITOE	6%	15%	3%	15%
1026	LIMAPU	1%	0%	0%	0%
1028	SNTAGO	47%	43%	53%	70%
1030	MOJAVE	70%	77%	71%	88%
1031	JOBURG	74%	78%	66%	82%
1043	MADGAR	33%	69%	27%	67%
1032	NEWFLD	19%	23%	6%	33%
1033	COLEGE	50%	41%	–	–
1036	ALASKA	–	–	57%	44%
1035	WNKFLD	22%	43%	15%	61%
1042/1037	ROSMAN	49%	54%	57%	71%
7036	EDINBG	60%	76%	54%	86%
7037	COLMBA	49%	74%	46%	79%
7039	BERMDA	48%	49%	35%	78%
7040	PURICO	67%	59%	52%	79%
7043	GSFCPO	35%	50%	–	–
7077	GSFCNF	–	–	22%	75%
7045	DENVER	56%	52%	55%	88%
7044	CKVLLE	18%	1%	–	–
7072	JUPTER	59%	38%	–	–
7075	SUDBRY	43%	75%	23%	69%
7076	JAMACA	48%	75%	42%	75%
1034/7034	UNDAKA	53%	67%	35%	70%
7078	WALMOT	–	–	31%	65%
7079	CARVON	–	–	43%	62%
	TOTALS	48%	59%	40%	72%

For Geos-I, 9,500 plates were exposed and 5,576 were found to contain the satellite flashes. Results from more than 3,300 of these plates, representing more than 21,000 flashes are now on tape in the Data Center. Results for Geos-II show that 7,891 plates were exposed, 5,714 of them containing flashes. By June 15, 1970, reductions of more than 2,500 Geos-II plates were submitted to the Data Center. Approximately 1,000 more plates are to be reduced. It is anticipated that all the MOTS data for these two spacecraft will be supplied to the Data Center prior to January, 1971.

Validation

Prior to submission to the Data Center, the reduced optical observations are processed through a validation program. The right ascensions and declinations from the reductions are compared to a reference orbit obtained from an independent tracking system. The gates applied, which determine whether or not an observation has passed the validation routine, is purposely set wide enough to remove only obvious outliers. A comprehensive report on the validation procedure is presented in the Goddard Space Flight Center (GSFC) document, NASA-GSFC GEOS-I MOTS Optical Validation Report, X-514-69-83.

In January 1969, while analyzing the Geos-I validation results, it became apparent that a subtle error existed in the MOTS reduction routine as employed by the reduction group at New Mexico State University (NMSU). The error, occurring only when the camera was pointed at or near the station's local meridian (i.e. an azimuth at or near 0 or 180 degrees), varied in magnitude from only hundredths of an arc second to nearly 50 seconds of arc depending upon the azimuth-elevation angles of the camera axis. The data containing the larger errors were flagged by the validation routine and were never submitted to the Data Center. However, more than 300 plates containing smaller errors of less than 10 arc seconds were provided to the Data Center before the problem was detected. Re-reductions, using corrected formulations were conducted and the new results submitted to the Data Center in June 1969. MOTS observation tapes provided by the center after October 9, 1969, contain the correct information and should be used in lieu of the earlier data. A list of the MOTS plates affected by this problem is provided in the above mentioned GSFC document X-514-69-83.

As is so often the case, the error was inadvertently introduced while attempting to remove a nearly insignificant source of bias. It was realized that during a Geos operation, the sidereally driven MOTS camera images the reference stars at very slightly different positions due to differential atmospheric refraction during the 24 seconds of plate exposure. The method introduced to handle this condition was to compute the camera orientation angles, azimuth, elevation and tilt for the center flash of the sequence (equivalent to the measured center of the stellar images) and by differential form obtain the orientation angles to the earlier and later flashes. In this technique, when the camera had certain angles (near the local meridian), the trigonometric functions used in the computations rapidly approached

infinity and accuracy was lost. The program has been corrected by exchanging the differential form of orientation angle computation for an exact computation for each desired flash time.

MOTS Camera Sensitivity

During the active tracking period of Geos-I, a camera sensitivity and tracking accuracy experiment was conducted at Jupiter, Florida. Six cameras were placed within 30 meters of the Baker-Nunn camera located there. By simultaneously observing the satellite flashes, the reduced observations may be compared and the relative accuracies of the cameras determined. A comprehensive report on this phase of the experiment is expected to be published by the GSFC shortly.

A photometer was also situated at the Jupiter station during the experiment. By observing the stars in the region of the satellite passage with the photometer, a value for the atmospheric attenuation may be computed. Measurement of the diameters of the recorded flash images then allow for a determination of the sensitivity of the camera system. The results were published in the GSFC document, GEOS Tracking Camera Sensitivity Report, X-514-69-533.

Briefly, the MOTS-40 camera results from Jupiter indicate that the camera-emulsion combination used appears to be more sensitive providing larger diameter images, than estimated prior to the launch of Geos-I. However, because of operational difficulties and changes made at the Jupiter station during the test period, it is possible that the larger images are due to focus problems and therefore the results may not be truly representative of all the MOTS cameras. Until such time when another test can be conducted under more uniform operational conditions, the a priori values used to determine the amount of illumination needed to obtain a reducible flash image should continue to be used.

MOTS Camera Drive Evaluation

The accuracy of a sidereally driven camera system has been an unanswered question. In connection with the evaluation of the accuracy of the MOTS camera data, an analysis of the camera drive system was undertaken. A report covering this subject has been prepared under the title Analyses of the MOTS Camera Drive, X-514-69-482. The report describes the tests conducted and presents the results for a number of individual MOTS cameras. In general, the conclusions reached for the "average" MOTS camera reveals that;

1. The camera exhibits a periodic drive oscillation on the order of nearly 90 seconds of time.
2. For a short Geos type exposure, depending upon the position of the drive gear in its oscillation, the error in the flash positions will vary from nearly 0 arc seconds to a maximum of ± 2 arc seconds in right ascension.
3. The error in declination caused by drive oscillations will be less than ± 1 second of arc.

Before any operations are conducted on Geos-C, it is anticipated that a technique for smoothing out the drive oscillations will be incorporated into the camera system. By this means, errors in the reduced data due to the sidereal drive will be reduced to the order of ± 1 arc second in both coordinates.